UNIVERSITY
OF TRENTO - Italy

DEPARTMENT OF INDUSTRIAL ENGINEERING

XXIX cycle

Doctoral School in Materials, Mechatronics

and Systems Engineering

Synthesis and Characterization of Sol-Gel Derived ZnO Thin Films for Memristive Applications

Dawit Gemechu Ayana

Advisor: Prof. Sandra Dirè

May 2017

May 2017

SYNTHESIS AND CHARACTERIZATION OF SOL-GEL DERIVED ZNO THIN FILMS FOR MEMRISTIVE APPLICATIONS

Dawit Gemechu Ayana

E-mail: dawitgemechu.ayana@unitn.it

Approved by:

Prof. Sandra Dirè, Advisor
Department of Industrial Engineering
University of Trento*, Italy.*

Ph.D. Commission:

Prof. Roberto Scotti,
Department of Materials Science
University of Milano-Bicocca*, Italy.*

Prof. Flavio Deflorian
Department of Industrial Engineering
University of Trento*, Italy.*

Prof. Luigi Torre,
Department of Civil and Environmental Engineering
University of Perugia*, Italy.*

University of Trento,
Department of Industrial Engineering

May 2017

University of Trento - Department of
Industrial Engineering

Doctoral Thesis

Dawit Gemechu Ayana - 2017
Published in Trento (Italy) – by University of Trento

ISBN: - - - - - - - - -

Abstract

The sol-gel route is a versatile wet chemistry method suitable for the preparation of multi-layer thin films with defined thickness and surface roughness. In this thesis work, sol-gel derived undoped and doped ZnO multi-layers were prepared by spin coating technique on different substrates for a memristive application. The curing and annealing conditions for the ZnO films were adjusted based on the study performed on the ZnO xerogel powders, and taking into account the thermal stability of the engineered substrate used as a bottom electrode for the fabrication of the memristive building block. Chemical, structural and morphological features of the samples were investigated by complementary techniques including electron microscopy, Fourier transform infrared spectroscopy, micro-Raman, X-ray photoelectron spectroscopy and X-ray diffraction analysis. The combined characterization techniques assessed that uniform, dense and flawless films were obtained on the platinum substrate, i.e. the bottom electrode of the memristive cell. In particular, Al-doping was found to significantly affect the surface morphology, grain sizes and overall porosity of the films. According to the electrical measurements performed on undoped and Al-doped ZnO thin films sandwiched between Pt/Ti/SiO_2 bottom electrode and different top electrodes including Ag and Pt-dishes, the selected fabrication conditions were suitable for fulfilling the requirements of active layers for the memristive development. The modification approach exploited toward the improvement of the memristive switching performances resulted in memristive responses with low compliance current in absence of electroforming steps. Furthermore, the resistance values at high resistance and low resistance states were reduced in the case of Al-doped films compared to the results obtained from undoped ZnO thin films.

Table of Contents

Preface and Objectives……………………………………………………………10

Chapter I

Introduction ……………………………………………………………………….…13

1.1 Background: Introduction to memristor……………………………….……13

1.2 Description of the memristive switching phenomena………………..…14

1.3 Memristive switching mechanism…………..16

1.3.1 Cation migration/Electrochemical metallization memory ……….17

1.3.2 Anion migration/Valence change memory……………..…………...18

1.4 Characteristics of memristive switching responses…………………....20

1.5 Metal oxide-based memristive devices…………………..…………..……21

1.5.1 General properties of ZnO……………………………………………..22

1.5.2 ZnO-based memristive switching ……………………………….....24

Chapter II

Fabrication Techniques of Thin Films…………………………….………….…29

2.1 Molecular Beam Epitaxy……………………………………………….….…29

2.2 Sputter Deposition…………………………………………………………..…30

2.3 Pulsed Laser Deposition………………………………………………….……30

2.4 Atomic Layer Deposition…………………………………………………….…31

2.5 Spray pyrolysis ………………………………………………………………..…32

2.6 Sol-gel Deposition……………………………………………………….....…..33

2.6.1 Sol-gel preparation of ZnO…………………………………………….…35

2.6.1.1 Selection of Zn precursor……………………………………..…….…35

2.6.2 Over-view of ZnO based sol-gel mechanism………………………35

2.6.3 Film deposition by spin coating………………………………………38

Chapter III

ZnO based memristors……………………………………………………………41

3.1 Sol-Gel based ZnO memristors…………………………………………….43

Chapter IV

Chemical Synthesis and Processing…………………………………………46

4.1 Preparation of ZnO sol……………………………………………………46

4.1.1 Xerogel powders preparation………………………………………48

4.1.2 Preparation of ZnO thin films……………………………………….48

4.1.2.1 Substrate cleaning and chemical treatment……………………….48

4.1.2.2 Thin film production and spin coating……………………………..49

4.1.2.3 Curing and annealing conditions…………………………..........50

4.2 Preparation of doped ZnO sol…………………………………………….51

4.2.1 Mg-doped ZnO…………………………………………………………51

4.2.2 Al-doped ZnO…………………………………………………...…..52

Chapter V

Characterization Techniques and Instruments……………………..…………54

5.1 Surface and compositional analysis…………………………………..…54

5.1.1 SEM and Field Emission-SEM………………………………….……..54

5.1.2 Atomic Force Microscopy (AFM)……………………………………..…55

5.1.3 X-ray photoelectron (XPS) and UV-photoelectron spectroscopy (UPS) analysis…………………………………………………………55

5.2 Structural Analysis…………………………………………………………57

5.2.1 X-Ray Diffraction Analysis……………………………………..……57

5.2.2 Fourier-Transform Infrared Spectroscopy ………………………......59

5.2.3 Micro-Raman spectroscopy …………………………………………..60

5.2.4 Optical Transmittance measurements…………………..…………61

5.3 Thermal Analysis……………………………………………………………61

5.3.1 Thermogravimetric/differential thermal analysis (TG/DTA)……...61

5.4 Memristive building blocks fabrication and Electrical Measurements…………………………………………………………….....62

Chapter VI

Results and Discussions (I): Undoped ZnO samples………………………...65

6.1 Preliminary Experiments ……………………………………………….65

6.2 Characterization of ZnO powders…………………………………….….69

6.3 Characterization of multilayer ZnO films…………………………….…77

6.4 Electrical characterization of the ZnO-based memristive building blocks…………………………………………………………………....92

Chapter VII

Results and Discussions (II): Doping of ZnO…………………………….……98

7.1 Mg-doped ZnO samples…………………………………………………...99

7.2 Al-doped ZnO samples……………………………………………...…107

7.2.1 Effect of dopant precursor…………………………………...…107

Chapter VIII

Conclusions……………………………………………………………..……125

List of abbreviations and acronyms ………………………………………..128

References ………………………………………………………………………129

Scientific production…………………………………………………….…142

Participation to Congresses, Schools and Workshops……………………142

Acknowledgements……………………………………………………………144

Preface and Objectives

Modern electronics require strongly innovative solutions that could comply, and possibly overcome, Moore's law predictions. The new electronics is being developed with the aim of getting over the physical, technological, and economical limits of circuit integration. Moreover, computers will be soon required to accomplish tasks in which the brain of human, and even of animals, is skilled.

In the emerging field of bio-electronics, the main demand is for devices and interfaces that could effectively exchange data information, overcoming the limits of the present approach essentially based on implantable electrodes.

Therefore, the research towards devices and systems that will mimic the adaptive response of natural brain elements by combining information storage and processing is of primary interest. The state of the art in material science, fabrication methods and nanotechnologies can hardly fulfill those expectations in terms of robust and reliable processes.

In accordance with these objectives, this doctoral thesis has been framed in a research project (supported by the Province of Trento, MaDEleNA - Grandi Progetti PAT, 2012-2017) aimed at the development of nanomaterials and devices towards adaptive electronics and neuroscience applications, by exploiting systems performing logic operations with intrinsic learning capacities.

Modern computing is based on separated processor and memory units so that learning occurs at software level only. On the contrary, system architectures able to perform both storage and processing of data at the hardware level, thus allowing adaptation and learning, can be obtained by exploiting the features of memristive devices.

The memristor is the missing electronic element predicted in 1971 by Chua [1] and its essential property is the dependence of resistance on the total charge that has passed through it [2].

The first example of metal oxide-based memristor was provided by Hewlett Packard [3] in 2008, and at present the majority of available patents on inorganic memristive devices belong to HP.

A great effort is required to develop inorganic based devices to a stage where optimization of the materials will pave the way to memristor-based devices robust enough for enabling the new electronic systems envisaged. This approach is based on the development of both new materials and production methods that could fulfill the market requirements.

The sol-gel process is recognized as a versatile route in modifying chemical composition that allows easy and inexpensive film processing on a variety of substrates and appears promising in the fabrication of non-volatile memories and memristive devices.

In this work, ZnO thin films were prepared by the sol-gel route for memristive applications. The research work here presented contributed to the particular work package (WP1) of the ''MaDEleNA'' project aimed at developing novel organic and inorganic materials whose properties are suitable to produce memristive devices.

A brief outline of the whole thesis is presented in the following. The thesis starts with a short chapter **(Chapter I**) introducing a fundamental description of the memristor element with a brief background. The section addresses theoretical concepts of memristor and different memristive switching mechanisms and presents the literature reports on metal oxide based memristive devices including ZnO layers.

In **Chapter II**, the fabrication techniques employed to prepare thin films, with special focus on sol-gel method are described. Some of the literature reports regarding ZnO-based memristors are presented in **Chapter III**.

Chapter IV describes the sol-gel syntheses of undoped and doped ZnO xerogel powders and thin films. The chapter presents a variety of experimental conditions for sol synthesis, substrates cleaning and modification, sol deposition of both single layer and multi-layers on different substrates, and the investigation on different curing and

annealing conditions to obtain ZnO films with suitable features toward the final application.

An overview of the characterization techniques employed to determine the effect of different synthesis and processing conditions on the final materials is presented in **Chapter V**.

Chapter VI, which is the core part of this thesis work, is mainly devoted to the characterization study of ZnO-based building blocks. The emphasis is given to the fabrication of dense, uniform and defect-free ZnO layers for the memristive application by changing the curing conditions and the top metal electrode in the final memristive building block. According to the same objective, the introduction of dopants to modify the functional oxide layer is presented in **chapter VII**. The thesis is completed with a short chapter presenting the main conclusions of this PhD work.

Chapter I

Introduction

1.1 Background: Introduction to Memristor

Memristors are the fourth class of electrical circuit element, added to the three fundamental elements; resistor, capacitor, and inductor [1]. These electrical circuit elements are defined in terms of the relation between two of the four fundamental circuit variables, namely, current (i), voltage (v), charge (q) and flux (φ). The current is defined as the time derivative of the charge. According to Faraday‘s law, the voltage is defined as the time derivative of the flux, whereas the resistor is defined by the relationship between voltage and current.

Theoretically, the memristor, i.e. “memory resistor”, is a type of hypothetical non-linear passive circuit element that maintains a relationship between the time integrals of current and voltage across a two-terminal element. It was first envisioned by a circuit theorist Professor Leon Chua in 1971 [1]. Chua extrapolated a conceptual symmetry between the resistor (voltage vs. current), the capacitor (voltage vs. charge) and the inductor (magnetic flux linkage vs. current). The existence of the memristor as another fundamental non-linear circuit element linking magnetic flux and charge was then inferred (Figure 1). Unlike a resistor, the memristor presents a dynamic relationship between current and voltage that includes a memory of the past applied voltages or currents. Accordingly, the memristors’ electrical resistance is not constant but depends on the history of the current that had previously flowed through the device. The present resistance depends on how much electric charge has flowed through it in that direction in the past and the device remembers its history showing non-volatility property [2]. When the electric power supply is turned off, the memristor remembers its most recent resistance until it is turned on again [3]-[4]. Hence, the resistance of the memristor depends on the integral of the input applied to the terminals rather than on the instantaneous values of the input. Thus, the memristor's resistance varies according to a device’s memristance function [3]. In fact, a peculiar feature of a memristor is its memory function, which originates from a resistance state that the device remembers after being subjected to a potential difference over a certain period of time.

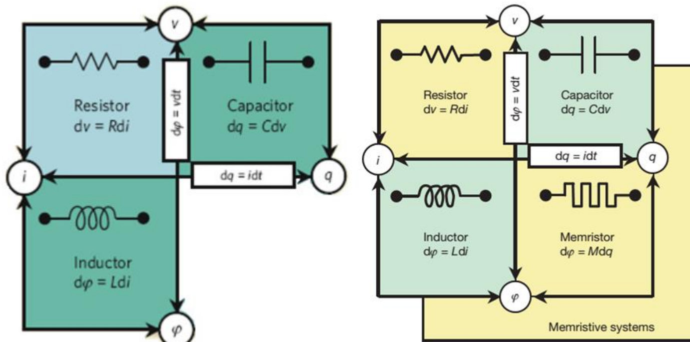

Figure I-1. The basic two-terminal circuit elements: resistor, capacitor and inductor; and *memristor* (the fourth fundamental two-terminal added to these basic circuit elements by Chua) (The image was reprinted from Nature with permission from [3])

Although memristive switching was theoretically introduced in 1971, the connection between Chua's theoretical explanation and the practical demonstration of a memristor device was achieved by Hewlett-Packard Labs only in 2008. Based on the study of TiO_2 thin films [3], a group at HP laboratories claimed to have found the Chua's missing memristor. The HP group was the first to demonstrate that a solid-state device could have the characteristics of a memristor based on the behavior of nanoscale thin films. The device neither uses magnetic flux as the theoretical memristor suggested, nor do stores charge as a capacitor does. Instead, it has achieved a resistance dependent on the history of the current. L. Chua has then argued in 2011 that the memristor definition could be generalized to cover all forms of two-terminal non-volatile memory devices. These devices are based on resistance switching effects regardless of the device material and physical operating mechanism [2].

1.2 Description of the memristive switching phenomena

Non-volatile resistance switching is a phenomenon exhibited by metal oxides with semiconductor properties sandwiched between two metal electrodes. They are fabricated from thin films structure with metal-metal oxide-metal (M-MeOx-M) building blocks. The switching mechanism is qualitatively straightforward. Upon applying a sufficient voltage across the metal electrodes, the resistance of the oxide films changes by several orders

of magnitude. The resistance of the system can be reversed back by applying a reverse bias across the electrodes.

The resistive switching behavior basically shows two different resistance states, i.e. high resistance state (HRS) and low resistance state (LRS), which can be switched from one to the other by an appropriate electric stimulus. When a resistance state decreases, it represents a 'set' or 'On' state switching operation; an increase of resistance state is known as a 'reset'/'Off' switching operation. In some cases, the 'On' and 'Off' switching can be observed by applying the same voltage polarity, while in other cases, the 'On' and 'Off' switching requires opposite polarities. The switching operation is said to be unipolar when the switching procedure is not dependent on the polarity of the voltage and current signals. On the other hand, the behavior is called bipolar when the set to 'ON' state occurs at one voltage polarity and the reset to the 'OFF' state on reversed voltage polarity. Figure (2) shows a schematic sketch of the I-V characteristics for the two switching modes.

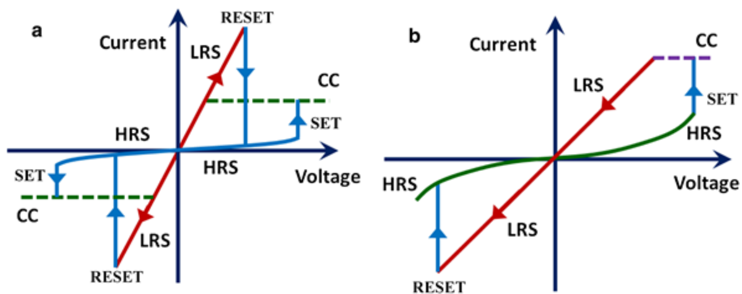

Figure I-2. Schematic of metal-oxide memory's I-V curves, showing the two modes of operation: (a) unipolar (set to LRS (red) /reset to HRS (blue) can occur at the same polarity) and (b) bipolar (the switching direction depends on the polarity of the applied voltage: set to LRS (red) can only occur at one polarity and reset to HRS (green) can only occur at the reverse polarity). Dashed lines indicate that the real voltage at the system will differ from the control voltage because of the compliance current (CC) in action. (The image was reprinted with permission from [5])

For most of the memristive materials, an electroforming step is required to initiate switching from a high resistive state to a less resistive one by applying a voltage that must be higher than both of the subsequent ON or OFF switching voltages. Electroforming is a non-destructive process, which drives the device into the conducting state and is necessary for many binary oxides to activate defects in stoichiometric films. Thus, the forming process activates the device, which as a consequence starts to display resistive switching effects.

1.3 Memristive switching mechanisms

Many studies show that the memristive switching behavior exhibited by oxide thin films has attracted extensive attention after the first report in 2008 [3]. The active layer in the memristive building block can be composed of one or more metal oxides with semiconducting properties. Different factors play a key role in defining the instantaneous resistive state of the device. The applied electric field and the compliance current can be externally manipulated during the electrical measurement and characterization of the device. Current compliance is normally applied to prevent hard breakdown during the set.

Memristive switching can occur due to a large range of physical mechanisms. Hence, some theoretical models have been proposed for explaining the resistive switching behavior.

The filamentary type memristive system is the most studied model for resistive switching in metal oxide memristors. It is the mechanism through which the formation and rupture of conductive filaments consisting of oxygen vacancies or metallic ions inside the active oxide layer are considered to be responsible for the resistance switching. Formation and rupture of the filaments cause the device to switch from the “Off” state to the “On” state and vice versa. The existence of one or more filaments between the two metal electrode terminals creates a low resistance state (LRS), while the absence of these filaments generates a high resistance state (HRS). Two types of models, which are briefly described in the following, have been proposed accounting for the origins of the filamentary conductive bridge by R. Waser [6]-[7].

1.3.1 Cation migration/Electrochemical metallization memory (ECM)

One of the models is based on cation migration, where the mobile cations coming from an electrochemically active and reactive electrode drift and discharge at the counter electrode under the applied voltage [8]. When a positive voltage is applied, oxidation occurs and mobile metallic cations are generated. The mobile cations migrate towards the bottom electrode (BE) through the oxide layer and are reduced to metal atoms by the electrons flowing from the cathode. These processes of successive precipitation of the metal atoms at the cathode lead to the growth of the metal protrusion. The process reaches the top electrode (TE) to form conductive filaments and finally the cell is turned to the 'ON' state. Upon changing the polarity of the bias voltage, the electrochemical dissolution of the conductive bridges takes place. The metal atoms dissolve at the edge of the conductive filaments which eventually annihilate the filament and changing the cell into the 'OFF' state.

In Figure (3), the case of Ag/ZnO: Mg/Pt device structure is illustrated showing the oxidation of Ag, resulting in the generation of Ag^+ when a positive voltage is applied to the Ag top electrode (Figure 3 a). The mobile Ag^+ cations migrate to the bottom electrode through the oxide layer leading to the successive precipitation of Ag metal atoms at the cathode; this leads to switch the system to the ON state (Figure 3 b-c). Reversing the voltage polarity leads to the electrochemical dissolution across the conducting bridge and resets the system to the OFF state (Figure 3 d).

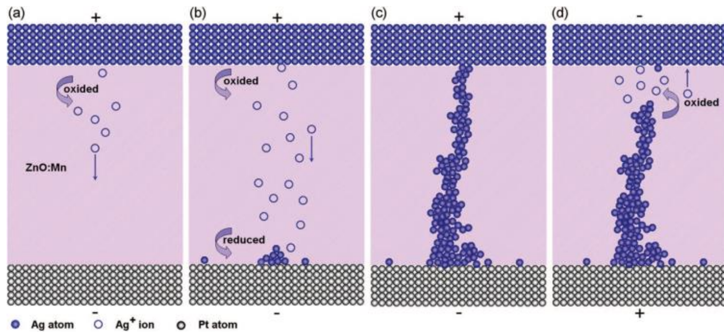

Figure I-3. A schematic diagram of the mechanism of resistive switching effects in Ag/ZnO:Mn/Pt devices. (a) The oxidation of Ag at TE, (b) The migration of the Ag^{+} ions toward the cathode , (c) The precipitation of Ag metal atoms at the Pt BE (d) by reversing the voltage polarity, the electrochemical dissolution of the conducting bridge is obtained (The image was reprinted with permission from Ref. [8]).

1.3.2 Anion migration/Valence change memory (VCM)

The other model is based on anion migration, also known as valence change memory (VCM) [6]. Under an applied voltage, the conductive filament normally extended from anode to cathode because of the generation and movement of oxygen vacancies under a high electric field. By applying a positive voltage to the top electrode (TE), the oxygen ions migrate to the top electrode and oxygen vacancies are created close to the interface between the oxide layer and the top electrode. The abundant oxygen vacancies on the surface of the oxide grains would be driven towards the bottom electrode (BE) and assemble a conducting channel along the grain boundaries of the device when a sufficiently positive bias voltage is applied [9]. When the conducting channel connects both electrodes due to the simultaneous transport of the injected electrons from TE to BE, the device switches from the ‘OFF’ state to the ‘ON’ state (Figure 4). By applying a negative bias, oxygen ions adsorbed by the top electrode would be released back to the active oxide layer from the electrode-oxide layer interfaces and recombines with the oxygen vacancies. As a result, the conducting filaments would break near the interface and the conducting filaments would finally rupture as more oxygen vacancies are

neutralized. This resulted in the resistance of the memristive cell to be switched back to the ‘OFF’ state.

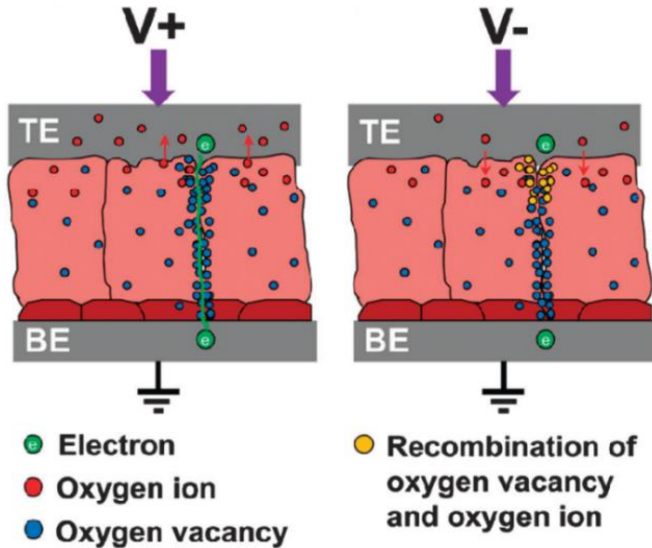

Figure I-4. Schematic representation of oxygen vacancies driven conduction in memristive devices showing that positive voltage drives the SET condition (left) and negative voltage drives the RESET condition (right). The image was reproduced from Ref. [9] with permission from the PCCP Owner Societies

In the interface type resistive switching, the current flow through the oxide film is determined by the barrier at the interface between the metal oxide semiconductor layer and the electrode. The resistive switching might result from the resistance change at the metal/metal oxide interface, in addition to the switching that results in the matrix. The interface barrier can be modified by electrical stimuli, leading to the formation of the two resistance states. Hence, several interface property including interface reaction and the inter-diffusion have an influence on the resistive switching behavior. In addition, the direct work function, electronegativity and oxygen affinity property of the metal electrode are also factors affecting the resistive switching.

1.4 Characteristics of memristive switching responses

A memristor has some typical characteristic and important features [10]-[11]. Any two-terminal circuit element is a memristor [1], only if it exhibits a pinched hysteresis loop [11] for the periodic input current signals or respective input voltage signals. This results in a periodic voltage or respective current response of the same frequency in the voltage-current (I-V) plane. The hysteresis loops are very valuable when memristive systems are to be identified, and the loops normally run through the origin in the i-v plot (Figure 5). This fact further underlines that the memristor is not an energy storage device. The hysteresis loops are formed since the current through the memristor does not vary linearly with the applied voltage, unlike a resistor that follows Ohm's law. Hence, the responses with the pinched hysteresis loop are the fingerprints of memristors [11].

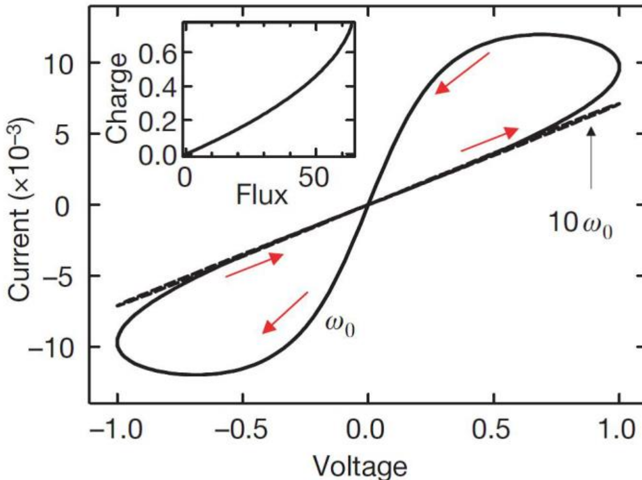

Figure I-5. Typical behavior of memristors. The nonlinear behavior of the current with the applied voltage, resulting in hysteresis loops rather than straight lines. The inset figure shows that memristors require nonlinear q-φ plots. (The image was reprinted from Nature with permission from Ref. [3])

Another typical feature is the frequency dependence of memristors and memristive systems. The memristance of the system depends on the frequency (ω) of the applied signal. If the signal frequency (ω) is high, the memory resistance of the memristor has a very short time to respond to the charge that passes through, resulting in the decrease in loop width of the hysteresis loops. Hence, the hysteresis loops seem to collapse to a straight line and the extent increases with frequency [12]. Consequently, the memristor seems to act as an ordinary resistor. The frequency value responsible for such a collapse of the hysteresis curves depends on the internal states of each system and will therefore generally not be the same for different types of memristors.

1.5 Metal oxide-based memristive devices

Metal oxides have attracted significant attention as active layers in metal/semiconductor/metal cell structures for resistive random access memories (RRAMs) devices because of their wide range of electrical properties [13]. The challenges arise from the performance of the actual device in terms of power consumption, switching speed, and other technological limitations. Among the emerging memory technologies, resistive memory devices are one of the most promising given its high speed, good cycling endurance [14], ease of fabrication, the simplicity of its structure and scalability.

Plenty of binary metal oxides and mostly transition metal oxides have been found to exhibit resistive switching behavior. Resistive switching characteristics with different switching behaviors, including bipolar and unipolar, have been investigated in various metal oxides. Several metal oxides have been studied with the aim to explore the physical origins of resistive switching [15]-[16] and the interest for practical memory applications. Apart from TiO_2 and other metal oxides, recently zinc oxide has become a popular material in memristive devices and several works on ZnO-based memristive switching has been reported in the literature [17]-[19]. Table (1) presents list of different oxide materials used in memristive devices fabrication, with variety of top and bottom electrodes used for each active layer and the corresponding switching mode.

Table I-1. Various metal oxides used in memristive devices compiled from Ref. [5] and [16]

Metal oxides	Bottom electrode	Top electrode	Switching mode
NiO	Pt	Pt	Unipolar/Bipolar
	Pt	W	Unipolar
	Ni	Ni, TiN	Unipolar
TiO_x	Al	Al	Bipolar
	TiN	Pt	Unipolar
	Pt	Pt	Unipolar/Bipolar
HfO_2	Ta	TiN	Bipolar
	Pt	Pt	Unipolar
ZrO_2	Ti	Pt	Bipolar
	Pt	Pt	Unipolar
	Pt	Ti	Unipolar/Bipolar
WO_x	TiN	W	Unipolar
	Pt	W	Bipolar
Al_2O_3	Ti	Pt	Bipolar
	Pt	Ti	Unipolar
	Pt	TiN	Bipolar
ZnO	Pt	Pt	Bipolar/Unipolar
	Au	Au	Bipolar
	ITO	ITO	Unipolar
	TiN	Pt	Bipolar
TaO_x	Pt	Pt	Bipolar/Unipolar
	Ta	Pt	Bipolar
CoO	Pt, Ta	Pt, Ta	Bipolar
Cu_2O	Cu	Ni, Co	Unipolar
	Cu	Al, Pt, Ti	Bipolar
TiO_2	Pt	Pt	Unipolar/Bipolar
	Ru	Pt, Al	Bipolar
SiO_x	TiW	TiW	Unipolar
	n-Si	p-Si	Bipolar
MnO_2	Pt	Ti	Bipolar

1.5.1 General properties of ZnO

Metal oxide materials having wide band gap including MgO, tin oxide (SnO_2), titanium oxide (TiO_2) and zinc oxide (ZnO) have been studied for different applications. The wide band gap materials are promising materials due to their inherent properties such as high breakdown voltage, and high electron mobility, which are suitable for the fabrication of high power, high temperature and short-wavelength electronic devices for different applications.

ZnO is a well-studied semiconductor material [20]-[21] with high electron mobility, high thermal conductivity, large piezoelectric constants, large exciton binding energy (60 meV), and it offers numerous advantages over other metal oxides. ZnO thin films display good transparency [22] and have found the application in lasers [23]-[26], piezoelectric devices [27], light emitting diodes [28], surface acoustic wave devices [29], as electron transport layer in solar cells [30], thin film transistors [31] and sensors [32]-[33].

Furthermore, zinc oxide is characterized by direct band-gap energy of approximately 3.2-3.4 eV at room temperature [34]. It has a melting point of 1975 ^{o}C that implies strong bond, suggesting that ZnO is a thermally and chemically resistant material [35]. Although under certain growth conditions, ZnO has been reported to present p-type conductivity [36], generally it behaves as n-type semiconductor material [37]. The n-type conductivity is ascribed to intrinsic defects such as zinc interstitials, oxygen vacancies and anti-sites [38]. ZnO n-type conductivity can be enhanced by introducing dopant elements such as boron, aluminum, gallium, indium and others.

ZnO can be found in wurtzite, zinc blende and rocksalt type crystal structures. These crystal structures shared by ZnO are shown in Figure (6).

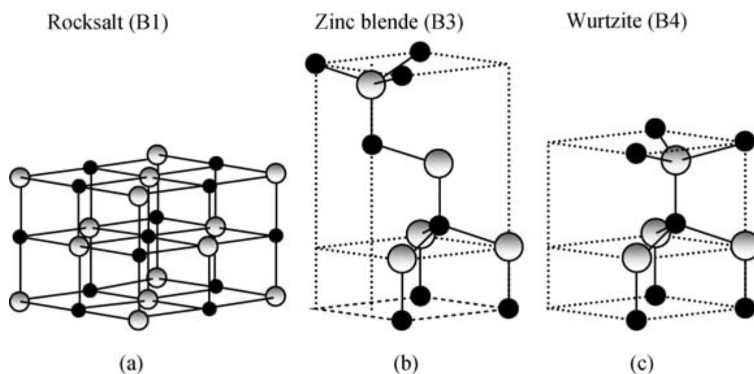

Figure I-6. Schematic representation of ZnO crystal structures [39]: (a) cubic rock-salt (B1), (b) cubic zinc blende (B3), and (c) hexagonal wurtzite (B4). Shaded gray and black spheres denote Zn and O atoms, respectively

The cubic zinc blende ZnO structure can be stabilized only by growth on cubic substrates or closely lattice-matched substrates [40]. The rock-salt structure can be obtained at relatively high pressure. The Wurtzite type structure is the phase thermodynamically stable under ambient conditions. The lattice parameters are a = 0.3249 nm and c = 0.5207 nm (c/a ratio of 1.602) at 300 K indicating that ZnO structure is close to an ideal hexagonal close-packed structure (c/a ratio 1.633). Hexagonal wurtzite structure ZnO consists of zinc atoms, which are tetrahedrally coordinated to four oxygen atoms. The tetrahedral coordination gives rise to polar symmetry along the hexagonal axis. The features of ZnO are responsible for its properties including piezoelectricity and spontaneous polarization, and are also a key factor in crystal growth orientation and defect generation.

1.5.2 ZnO-based memristive switching

A wide range of materials has been studied for potential application as a resistive switching layer [15], [38] ever since TiO_2-based memristor was fabricated in HP lab as a physical model of the two terminal devices [3]. This breakthrough opened perspectives for the observation of resistive switching phenomena in other inorganic thin films oxides. Aside from titanium oxide, zinc oxide has also been widely investigated and showed promising results in view of fabricating resistive switching devices. Resistive phenomena occurring in ZnO thin films are still not well understood and efforts have been devoted to understanding the development of the generalized physical model.

As in the case of other metal oxides, a number of switching mechanisms for ZnO-based devices have been proposed. One of the widely accepted and diffused switching mechanisms in memristive ZnO thin films is the filamentary conducting model [41]-[44]. This is generally characterized by the presence of several electrically active defects like oxygen vacancies and Zn interstitial, which are often present in ZnO thin films and expected to be responsible for the formation and rupture of conducting filaments.

By applying different compliance currents and RESET voltages, controllable LRS and HRS states, under homogeneous resistive switching were demonstrated in ZnO thin films [45]. The control of the input signals appears crucial for improving the device performance, but the main challenge is the control of conducting filament formation and rupture. This is due to the fact that filaments have random orientations, different sizes

and various locations, which can lead to non-uniformity of resistance state, a variation of operating voltage, and low reproducibility [46]-[47]. The random characteristics make the conducting filament difficult to form along the same path in repetitive switching cycles and lead the devices to show a large variation of switching voltages. Various methods including embedding metal nanoparticles [48], interface engineering and doping of ZnO films with different impurities have been proposed to overcome these drawbacks and improve the resistive switching performance of the ZnO-based devices.

One of the important methods for controlling the concentration and profile of mobile ions is interface engineering, which mainly includes selecting a proper electrode, and/or inserting a buffer layer between electrode and oxide film. It has been experimentally proved that the electrode plays an important role in resistive switching, and hence a careful selection of the appropriate material is required. Both the top and bottom electrodes are generally specified as either reactive or inert. In addition to optimizing the interfacial properties, selecting proper electrode is crucial for pointing out the mechanism of resistive switching.

For interface and filamentary type memristive switching mechanism, different electrodes will cause different behaviors of the interface and different device performance. For instance, ZnO-based memristors with Pt, Cr and Au electrodes having a ZnO thickness of 400 nm are presented in the literature [49]. The observed memristive behavior with Pt electrode shows a better hysteretic bipolar switching with reproducible switching response compared to Cr and Au metal electrodes. The TiN top electrode used in TiN/ZnO/Pt device structure reported in [50] was found to provide the formation of the filamentary conductive path with the TiN layer serving as an oxygen reservoir. The reverse bias could cause the oxygen vacancies to be neutralized by the existing oxygen ions, eventually resulting in the annihilation of the existing filaments. The report showed the asymmetrical bipolar resistive switching behavior that can be attributed to the effect of TiN on the reset process. The Au top electrode used in Au/ZnO/ Fluorine doped Tin Oxide (FTO) memory cell also showed that the endurance measurements ensured controllable, reversible and reproducible switching between ON and OFF states [51].

Introducing a thin seed layer between the electrode and the functional layer is another effective way to modify the interface barrier height and optimize the interface property. For instance, the incorporation of thin ZnO seed layer in ZnO-based memristive

switching device (Figure 7) was reported for tuning the morphology of the electrodeposited ZnO films and optimizing the oxygen vacancy concentration of the layers [9].

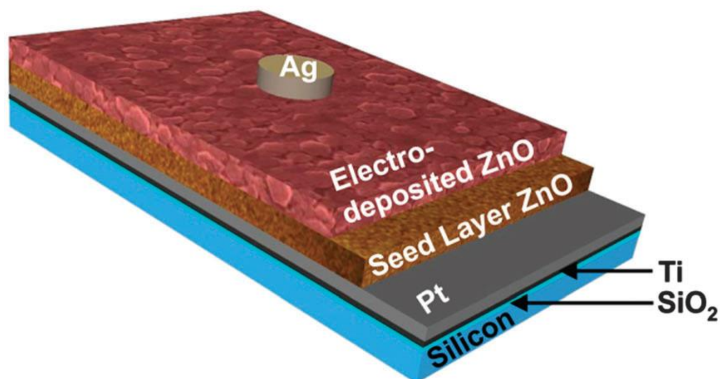

Figure I-7. The schematic of the Ag/ZnO/Pt-based structure with incorporated sputtered ZnO seed layer. The image was reproduced from Ref. [9] with permission from the PCCP Owner Societies

For anion migration type switching mechanism, the material of the buffer layer is usually an oxidizable metal or a metal oxide, such as few nanometers thick Ti or TiO_2. By using a thin Ti layer as the reactive buffer layer between the anode and HfO_2, excellent memory performances have been demonstrated [52]. The reason for using such a buffer layer is that for this type of resistive switching memory, the filament formation and rupture are associated with the distribution of mobile oxygen ions and oxygen vacancies in the oxide films. Hence, such an oxidizable buffer layer can be considered as the oxygen reservoir and help to stabilize the local oxygen migration for the filament formation and rupture. The resistive switching characteristics are expected to be more stable and reliable if the regions where the formation and rupture of the filaments occur can be controlled. The buffer layer can effectively control the concentration and profile of the mobile oxygen ions, thus leading to a great improvement in the uniform performance of the device.

Doping on the other hand has been used to improve the electrical, morphological and structural properties of ZnO films for different applications [53]-[57]. Many factors,

including the type and concentration of dopant, strongly influence both the morphological and electrical properties of ZnO thin films. ZnO doping is commonly achieved by replacing Zn^{2+} ions with cations of same or higher oxidation states. Typical dopant elements such as Mg, Al, In and Ga has been used to improve the electrical and optical properties of sol-gel derived ZnO films for different applications [53]-[54], [58]. However, properties of the final materials can be affected by the dopant concentration. For instance, Al doping beyond 1 at % was found to negatively change the electrical resistivity and further increase cause Al segregation at the grain boundary [54]; and a similar trend was observed in the case of In and Ga [53] doping. Hence, as reported in the literature [53], a doping level up to 1 at % is suggested to be the suitable dopant level to avoid changes in the structural properties that could lead to deterioration of the film properties.

The band gap of ZnO can be tailored by doping ZnO with group II elements. The ionic radius of the Mg^{2+} ion (72 pm) closely matches with the ionic radius of Zn^{2+} ion (74 pm) and makes the incorporation of Mg^{2+} ion into ZnO lattice feasible. However, Mg substitution results in elongation of the 'a' parameter and contraction of the 'c' parameter of the unit cell; c-axis compression in the hexagonal lattice is more pronounced as the Mg dopant concentration increases [59]. The Mg-doping of ZnO increases the carrier concentration; the increase in the donor concentration results in the occupancy of the states in the conduction band. In addition, Mg^{2+} incorporation widens the ZnO gap by raising the conduction-band potential and lowering the valence-band potential at certain ratios.

The substitution of Zn^{2+} ions with Al^{3+} (54 pm) in ZnO lattice alters the electrical conductivity through the increase of electronic charge carriers. Moreover, the addition of Al^{3+} ions to Zn^{2+} sol solution also increases the number of nucleation sites resulting in the formation of smaller grains with dense and uniform morphology [54], and higher grain boundary density. The increase in grain boundary density by introducing a seed layer in electrodeposited ZnO films for the memristive device was reported to improve the memristive switching performances [9]. As a matter of fact, the grain boundaries are assumed to assist and improve the memristive switching process as they are likely a site of defect aggregation and conductive path formation. The investigation on monoclinic HfO_2 pointed out that the segregation and movement of the defects such as oxygen vacancies were enhanced along the grain boundary [60]. Good results in terms of

memory application, compared to other non-stoichiometric oxides, were reported in [61] for Al-doped ZnO thin films-based devices grown by reactive sputtering on both sapphire and silicon substrate.

Inspired by the first TiO_2-based memristor by HP, ZnO thin films have been addressed as promising candidates for the fabrication of resistive switching cells, as an alternative to the conventional memory devices. However, a great effort is required to develop ZnO-based memristive devices to a stage where optimization of the overall device structure (building blocks) will pave the way for the development of materials and synthesis approach that could fulfill the requirements. These aspects promote the assembly of high-density memory devices, with low cost and dimensions, good endurance, fast operation, and reduced power consumption. In accordance with these requirements, the thesis investigates the state of the art concerning the suitable features required for ZnO-based thin films having a well-defined resistive switching behavior.

Chapter II

Fabrication Techniques of Thin Films

The fabrication techniques of thin films significantly influence the device performance and play a crucial role in making the device efficient and cost-effective. A variety of deposition techniques used in the fabrication of thin films can be broadly categorized as either ''top-down'' or ''bottom-up'' approaches.

In the case of ''top-down'' approach, the thin films are derived from a bulk and obtained by the progressive removal of material, until the desired layer properties are obtained. This approach typically utilizes standard lithography and etching techniques to create thin films.

In the ''bottom-up'' method, the material is obtained starting from atomic or molecular precursors by gradually growing it until the final structure is formed. It is a synthetic route in which the composition, size, and morphology of the desired structure are well controlled during the fabrication process [62]. Bottom-up approaches are particularly attractive for nano-scale applications, whereas the top-down processes could face the fundamental scaling limits. In both methods, control of the synthesis parameters and environmental conditions are the two fundamental requisites.

Different fabrication techniques including molecular beam epitaxy (MBE), sputter deposition, pulsed laser deposition (PLD), atomic layer deposition (ALD), spray pyrolysis and sol-gel method has been used to prepare thin films and will be highlighted in this section with special emphasis on sol-gel processing.

2.1 Molecular Beam Epitaxy

The molecular beam epitaxy (MBE) technique is essentially a sophisticated evaporation method in which molecular beams interact on a heated crystalline substrate under ultra-high vacuum (UHV) conditions to produce thin films. MBE is presently used in the most semiconductor industry, where the performance of the device depends on precise control of dopants and in the production of extremely thin crystal layers. MBE is used for the fabrication of numerous important devices such as light-emitting diodes, laser diodes, field effect transistors, and other electronic application.

2.2 Sputter Deposition

Sputter deposition is a widely used technique to deposit thin films on substrates based on ion bombardment of a source material (the target). Ion bombardment results in a vapor created by a purely physical process, i.e. the sputtering of the target material. The most common approach for growing thin films by sputter deposition is the use of a magnetron source in which positive ions present in the plasma of a magnetically enhanced glow discharge bombard the target.

The microstructure of thin films is conditioned by the mobility of the atoms during growth. The energy supply to the atoms is provided by different mechanisms including thermal effect, ionic bombarding and chemical reactions at the substrate. Reactive sputtering is a commonly used process to fabricate thin film coatings on a wide variety of substrates. In contrast to the various evaporation techniques, sputtering does not require melting of the base material.

2.3 Pulsed Laser Deposition

Pulsed laser deposition (PLD) is a growth technique where a high-power pulsed laser beam is focused inside a vacuum chamber to strike a target of the material to be deposited (figure 1) [69]-[70]. Apart from its several advantages, there are also some drawbacks to perform PLD for thin film growth. For instance, light elements like oxygen or lithium have different expansion velocities and angular distributions in a plume as compared to heavier elements. Therefore, an addition source to supplement these elements is required to obtain the desired film composition.

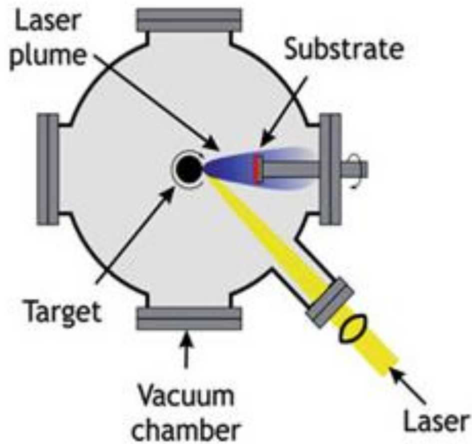

Figure II-1. Schematic of pulsed laser deposition (PLD) [69]. The incoming laser beam is focused onto a target, thereby vaporizing the material of the surface region. The ejected material is partially ionized and forms the ablation plume that is directed towards the substrate.

2.4 Atomic Layer Deposition

Atomic layer deposition (ALD) is a class of chemical vapor deposition devoted to a surface controlled thin film deposition based on the sequential use of the gas phase chemical process. The growth of oxide thin films with the technique is promising in particular for a broad range of materials with particular electrical properties, extending from insulating, semiconducting and metallic to superconducting [76]. Atomic layer deposition has found application in the fabrication of several memory devices due to the promise over the control of thickness, uniformity, quality and material properties. Moreover, ALD has found most exciting applications in field effect transistors, thin film solar cells, and fuel cells [77]. Schematic of a general ALD process is illustrated in Figure (2). Plasma-Enhanced ALD (PEALD) methods utilize reactive plasma species as precursors for ALD surface reactions. The main advantages of PEALD include lower

temperature process capability as well as new pathways for chemical reactions that would be inaccessible by purely thermal methods.

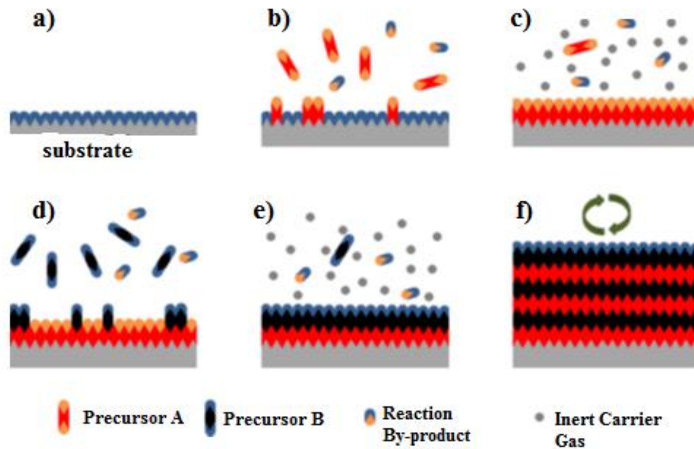

Figure II-2. Schematic representation and steps in ALD process. (a) Substrate surface, (b) Precursor A is pulsed and reacts with the surface, (c) Excess precursor and reaction by-products are purged with an inert carrier gas, (d) Precursor B is pulsed and reacts with surface. (e) Excess precursor and reaction by-products are purged with an inert carrier gas. (f) Steps b-e is repeated until the desired material thickness is achieved [The image was adapted from Ref. [77] with permission]

2.5 Spray pyrolysis

Spray pyrolysis is a relatively simple and cost-effective processing method used to prepare thin and thick films, ceramic coatings, and powders. The typical spray pyrolysis equipment consists of an atomizer for the precursor solution, a substrate heater, and a temperature controller. The schematic representation of spray pyrolysis is shown in Figure (3). Thin film deposition, using the spray pyrolysis technique, involves the impact of the droplets created by atomization of the precursor solution onto the heated substrate surface followed by spread over and thermal treatment [81].

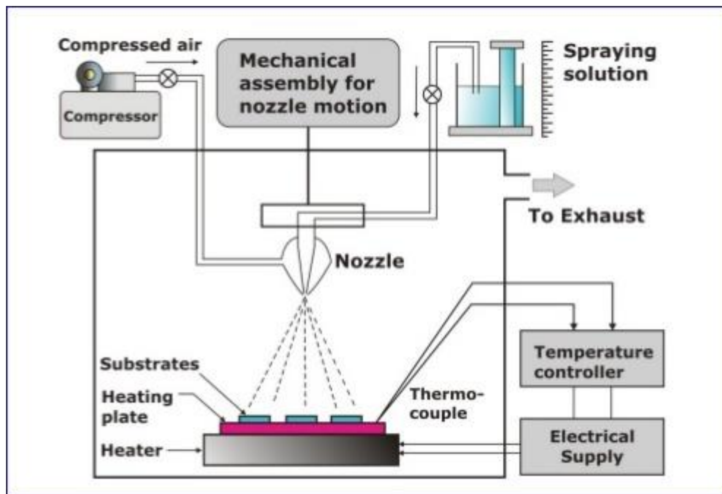

Figure II-3. Schematic diagram of spray pyrolysis equipment

2.6 Sol-gel deposition

The sol-gel method is a well-known chemical route for the preparation of glass and ceramic materials [84]. From the beginning, the most important applications of the sol-gel route were found in the preparation of metal oxide thin films [85]. Basically, the sol-gel process is a wet chemistry method in which molecular precursors transform into an oxide network through hydrolysis-condensation reactions. The process involves the evolution of oxide networks through the formation of a colloidal suspension (sol) and gelation of the sol to form a network in a continuous liquid phase (gel). The technique enables the processing of powders, ceramics, and thin films directly from mixture solution. Figure (4) shows the schematic representation of various routes in the sol-gel process providing different types of materials.

From the gel phase, xerogels are obtained by evaporation of the liquid phase and aerogels are produced by solvent extraction under supercritical conditions. The films are prepared by coating of the precursor solution over the substrates by means of spraying, dipping or spinning. The solvent is removed during the deposition and subsequent drying process, resulting in densification of the films. A thermal treatment is necessary to achieve the target oxide composition and structural features.

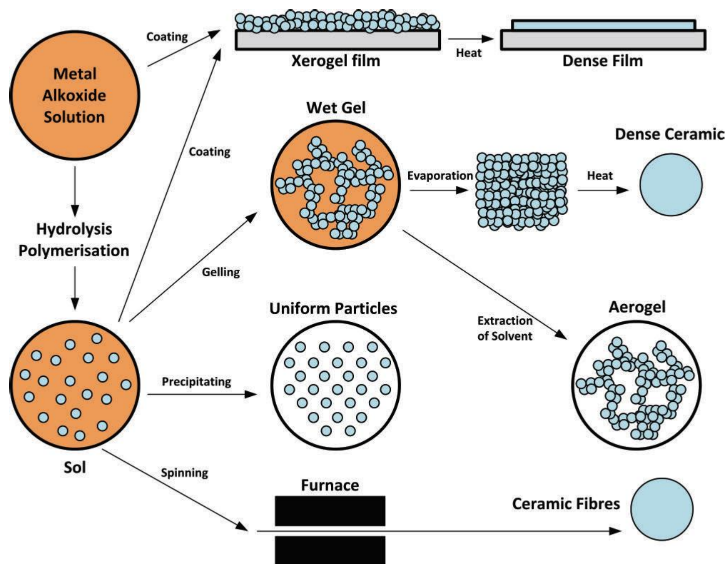

Figure II-4. Schematic of various routes in the sol-gel process [84]. A metal oxide film can be produced by spin-coating a precursor solution or sol to form a dried gel (xerogel), and then using a thermal treatment to densify the film

The main requirement in the solution state is the achievement of good homogeneity in the precursor mixture, which has considerable advantages for generating a pure-phase product and can also result in lower synthesis temperatures [87]. The main steps of thin films preparation by the sol-gel process include the preparation of the precursor solution, deposition of the prepared sol on the substrate by the chosen technique, and the thermal treatments of the deposited films. In general, many parameters affect the preparation of thin films like the nature and concentration of the precursor, the choice of solvent and additives, the coating and deposition parameters, the nature of the substrate, and the selection of the pre- and post-heat treatment conditions.

Sol-gel fabrication has been widely applied to the preparation of ZnO thin films; and is obtained starting from either aqueous solutions of inorganic salts or organic salts or alkoxides, dissolved in alcoholic media [88]. The following sub-sections summarize the main protocols used in the sol-gel synthesis of ZnO thin films and highlight the processing parameters influencing their properties.

2.6.1 Sol-gel preparation of ZnO

2.6.1.1 Selection of Zn precursor

Several zinc precursors including nitrate, chloride, perchlorate, acetylacetonate, and alkoxides such as ethoxide and propoxide have been used to prepare ZnO thin films. Despite offering chemical advantages, metal alkoxides are not very popular due to sensitivity to moisture, high reactivity and high cost. On the other hand, metal salts are preferable because of their low cost and commercial availability that appear to be more appropriate for large scale applications.

Nitrates [89], chlorides [90], perchlorates and acetates [91]-[92] were used as sol-gel precursors for ZnO, providing thin films with different morphological features and crystallization [89]. Films prepared from zinc nitrate show a rapid and random crystallization compared to the ZnO films prepared from zinc acetate precursor, which displayed also a smoother surface. Using zinc perchlorate resulted in coagulation of particles and yielded a turbid suspension. It was reported that the preparation from zinc chloride or zinc nitrate under similar reaction conditions initially formed clear colloidal suspensions that however coagulated faster than in the case of zinc perchlorates [93]. Not reproducible results were obtained from sols prepared using zinc nitrate, whereas the sols prepared from zinc acetate dihydrate led to reproducible system under a variety of experimental conditions [94].

Zinc nitrate and chloride present high solubility in water or organic solvents, but one main drawback is related to the difficult removal of the anionic species that are retained in the final material. Therefore, zinc acetate dihydrate [88], [91]-[92] found wide application in the preparation of ZnO thin films. In addition to practical advantages such as low cost and ease of handling, the acetate groups decompose during curing and annealing processes [95] leaving the films as volatile by-products.

2.6.2 Over-view of the ZnO based sol-gel mechanism

From a chemical point of view, the formation of metal oxide is the result of a complex sequence of interconnected reactions. The basis of the synthesis are the two fundamental steps regulating the entire sol-gel process, namely hydrolysis of the metal precursor and condensation to form the oxide network [84].

As reported above, in the case of ZnO the syntheses usually employ metal salts as precursors. The precursors are hydrolyzed and condensed in aqueous or organic solvents to form inorganic polymers composed of M-O-M bonds [84], [96]. According to Brinker et al., hydrolysis of inorganic salts proceeds by the removal of proton from an aquo-complex $[MO_NH_{2N}]^{z+}$ to form hydroxo (M-OH) or oxo (M=O) ligands:

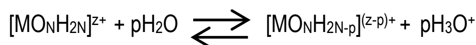

$$[MO_NH_{2N}]^{z+} + pH_2O \rightleftharpoons [MO_NH_{2N-p}]^{(z-p)+} + pH_3O^+$$

where N is coordination number of water molecule around M and p is defined as the hydrolysis molar ratio. Condensation reactions involving hydroxo ligands result in the formation of bridging hydroxyl (M-OH-M) or bridging oxygen (M-O-M) bonds depending on the coordination number of M and the acidity of the bridging hydroxyl.

As reported above, zinc acetate dihydrate (ZAD) is usually employed as ZnO precursor because of the easy removal of the acetate anions during the thermal treatment. The next section describes the reactions occurring in ZAD solutions with the addition of amino-based additives.

Hydrated zinc acetate is soluble in solvents like ethanol or 2-methoxyethanol in the presence of different amino additives, which acts as a base and at the same time as a complexing agent. The additives, commonly known as stabilizers, have various roles such as reacting with precursor and facilitating the formation of complexes. Moreover, they are believed to play the role of chelating ligands, which avoid the rapid precipitation and allow stable solutions to be formed. The most frequently used stabilizers in the sol-gel derived ZnO systems are monoethanolamine (MEA) and diethanolamine (DEA). Comparative studies of the effects of different amino-additives including monoethanolamine (MEA), diethanolamine (DEA) and triethanolamine (TEA) on the sol behavior and the properties of ZnO thin films has been reported in [97]. The most stable, transparent and homogeneous sols were prepared using MEA and DEA, which present lower boiling temperatures (170 °C and 270 °C, respectively) than TEA (335 °C). As a consequence, the reported study pointed out that the use of additives with low boiling temperature (in particular MEA) assists in the more effective removal of organics during thermal treatments of the films.

The hydrolysis and condensation reactions of the ZAD precursor are relatively slow as MEA can act as a complexing agent, thus improving the stability of ZnO sols. Zinc acetate dihydrate Zn $(C_2H_3O_2)\cdot 2H_2O$ in solution produces mono-acetate $(C_2H_3O_2)$ Zn^+ species [98]. The reaction between $(C_2H_3O_2)$ Zn^+ and MEA would result in the formation of a chelated species with the release of acetic acid.

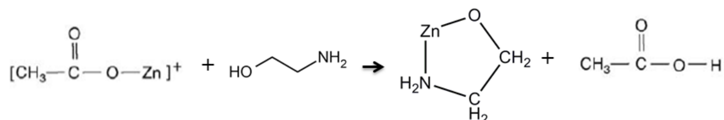

The acetate group plays a relevant role by complexing Zn^{2+} in competition with the MEA [99]. The general schematic representations of the complex chemical relationships of the main species are indicated in Figure (5). The three nucleophilic species (MEA, OH^- and CH_3COO^-) compete for the Zn^{2+} sites. The attack of the hydroxy group leads to the formation of zinc-oxo-acetate oligomers, which are expected to appear at the initial stage from gradually forced hydrolysis of Zn-MEA or Zn-$OCOCH_3$ soluble complexes. The progressive condensation of the hydrolyzed moieties gives rise to colloids [99].

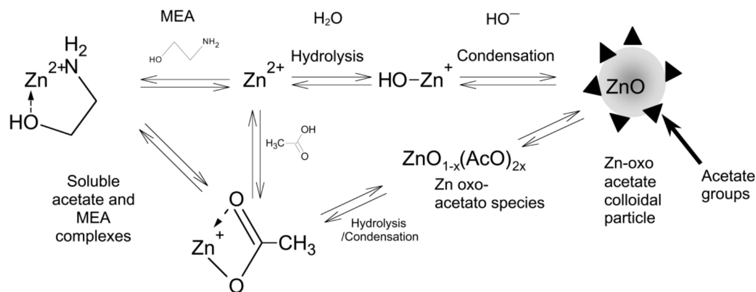

Figure II-5. Schematic representation of hydrolysis and condensation reactions involved in the sol-gel process from zinc acetate as a metal precursor; to form colloidal moieties which can be deposited as a film precursor resulting in solid ZnO films [The image was reproduced from Ref. [99] with permission].

2.6.3 Film deposition by spin coating

Sol-gel derived ZnO films are commonly deposited by either dip-coating [101] or spin coating techniques. Spin-coating is widely employed for the reproducible fabrication of thin film coatings over large areas with high structural uniformity [102]. It is one of the most common techniques for applying thin films to substrates and is used in a wide variety application. The advantage of spin coating is mainly its ability to quickly and easily produce uniform films from a few nanometers. Moreover, the technique is preferable for the relatively easy setup.

Spin coating generally involves the application of a thin film evenly across the surface of a substrate by coating a sol of the desired material while the substrate is rotating (Figure 6).

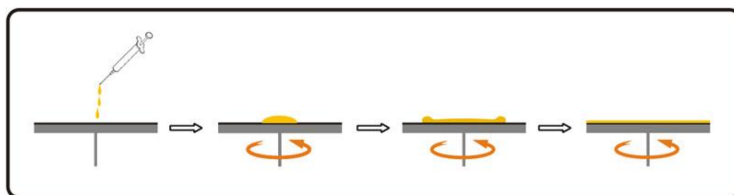

Figure II-6. Schematic representation of typical spin-coating process: First the solution is applied to the substrate; then the substrate is rotated with the desirable rotational speed; the solution spread over the substrates and finally uniform thin film will be obtained

During spin coating, the liquid film thins by centrifugal draining and evaporation. Basically, the process can be divided into different stages including deposition, spin-up and spin-off as shown in Figure (7). During deposition stage, an excess of liquid is dispensed on the surface. The deposition can be done using a nozzle that pours the coating solution or by dropping using a syringe, provided that the solution wets the substrate completely during the first stage. The liquid flows radially outward (spin-up stage) driven by centrifugal force; followed by flowing of excess liquid to the perimeter and leaving as a droplet (spin-off stage). The spin-off stage is normally characterized by gradual fluid thinning. The evaporation stage simultaneously happens and overlaps the other stages for sol-gel coating [96]. The rotation of the substrate at high speed and the action of spinning cause the solution to spread out and leave a very uniform layer on the

surface of the substrate. During this time, the solvent evaporates leaving the desired material on the substrate.

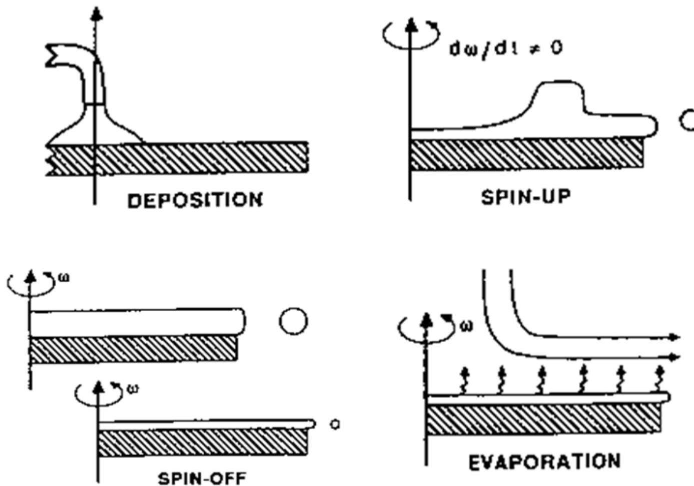

Figure II-7. The stages of the batch spin-coating process (adapted from C.J Brinker et al. [Ref. [96])

There are several inter-related processing and spinning parameters that affect the features and properties of the final films. Moreover, the final films thickness and other properties will depend on the nature of the solution. For instance, the final films get thicker with an increase in the viscosity and concentration of the solution; and the reverse holds for the dependency of the film thickness on angular velocity and spinning time. The spinning rate is one of the parameters that affect the degree of radial (centrifugal) force applied to the solution as well as the velocity and characteristic turbulence of air immediately above it. Furthermore, the surface tension of the solution and the wettability of the substrates play a crucial role to obtain the films with the desired features and properties.

In this section, different thin film deposition techniques including sputtering, MBE, ALD and PLD were highlighted. Even though the deposition techniques mentioned above have been successfully applied for ZnO preparation, there are also drawbacks in their use for the fabrication of devices; like the requirement of high deposition

temperature and vacuum conditions that imply high fabrication costs. The sol-gel fabrication is a cost-efficient method and can fulfill most of the above mentioned requirements. It is a readily controlled method to produce well-defined morphological features in the resulting solid material and has emerged as one of the most suitable processing routes in producing thin metal oxide thin films on various substrates. Indeed, depending on the synthesis conditions, the method provides control over variety of properties including stoichiometry, porosity, morphology and crystallinity of the films.

Chapter III
ZnO based Memristors

ZnO thin films have been prepared using different fabrication techniques described in chapter II for variety of applications. It is reported in the literatures that different fabrication techniques led to ZnO films with different features and properties. For instance, laser-MBE has been used for the formation of epitaxial ZnO thin films [63]. ZnO thin films with better structural and optical properties have also been grown on (111) ZnS substrates by plasma-assisted MBE [64]. However, it was found that films with better quality were obtained under high-temperature growth condition. Molecular beam epitaxy was used to fabricate the memory devices under a high vacuum (2 x 10^{-7} Pa) on ZnO thin films deposited on Au (5 nm)/Si and conductive-AFM tip as one electrode to probe the memristive characteristics of a ZnO/Au device [65]. The reported resistive switching was stable with a resistance ratio of two orders of magnitude.

ZnO nanowires were produced using a sputter deposition technique on various types of substrates to give either crystalline or single crystal, depending on the growth condition [66]. ZnO films have been deposited by different sputtering deposition techniques with large crystallite sizes and minimal surface roughness [67]. The magnetron sputtering method has become popular due to its high deposition rate, and suitable adhesion of the films on the substrate. However, the control of sputtering parameters makes the whole process difficult and complex. With this connection, a change in the conditions of sputter deposited ZnO films can cause a change in the stoichiometry of ZnO, influencing its crystalline structure and morphological properties [68].

Most oxide materials including ZnO thin films were grown by pulsed laser deposition on different substrates [71]. High-quality ZnO thin films demanded relatively higher deposition temperature [72]. The formation of highly crystalline ZnO film at low temperature could be possible by altering the oxygen partial pressure in the deposition chamber. ZnO films showing reliable switching characteristics at low voltages and good retention were grown by D.C discharge assisted PLD [73]. Al/ZnO/FTO resistive switching device structure, exhibiting on/off ratios of about one order of magnitude and switching mechanism ascribable to the formation and breaking of conductive filaments

due to movement of oxygen vacancies at the interface of ZnO with the metal electrode were also reported [74]. Moreover, integration of epitaxial ZnO deposited by PLD on TiN buffer layers and grown on Si (001) substrates was presented in the literature [75]. The epitaxial Pt/ZnO/TiN structure exhibited bipolar resistive switching characteristics with low set and reset voltages and switching repeatability up to 20 cycles. However, the on/off ratio was found to be relatively low.

ZnO thin layers deposited by ALD were recently investigated for resistive switching devices due to the fact that the film thickness is expected to be strictly controlled. As a matter of fact, ALD has found application in the deposition of ZnO layers with a controlled thickness to the atomic level and uniformity over large areas also for producing thin layers on flexible substrates at relatively low temperatures [78]. Bipolar resistive switching was observed in ZnO thin films on Pt/Ti/SiO_2/Si substrate and using Al as a top electrode [79]. The films were deposited at a temperature of 150 °C by plasma-enhanced ALD. The resistance ratio more than 10^3 was obtained with endurance-tested up to 50 cycles. Al-doped ZnO films were also prepared by ALD due to the possible control of the electronic properties through the variation of the amount of incorporated Al as reported in [80]. The control of Al incorporation into ZnO was easily achieved by ALD process; this is one of the important parameters to vary on/off ratio between HRS and LRS, retention and endurance properties of Al-doped ZnO devices. The resistive switching memory device with very large Al amount (20 at. %) exhibited the maximum resistance ratio. However, the endurance against cyclic program operations and memory retention property were unstable and inferior respect to low Al loadings.

The influence of the solution nature and properties on the characteristics of the films was studied on ZnO thin films deposited by spray pyrolysis technique [82], indicating the surface tension and dissociation enthalpy of the precursor play an important role in control over the film microstructure. The literature [83] reports on the memristive response obtained with the Ag/WO_3/ITO memristive cell structure, depositing WO_3 by spray pyrolysis technique. Nevertheless, the morphological study of the films revealed that the layer present an interconnected porous microstructure.

In general, the deposition techniques mentioned above have been successfully applied to ZnO preparation. However, there are also drawbacks in their use

for the fabrication of the memristive building blocks. MBE technique provides ZnO films with stable resistive switching with a resistance ratio of two orders of magnitude but the operation requires high vacuum conditions [65]. ALD is also investigated to deposit ZnO layers with atomic thickness control. Nevertheless, the resulting ZnO thin films show unstable and poor resistive switching characteristics due to their low initial resistivity [80]. Sputtered ZnO thin films show promising resistive switching properties, such as high on/off ratio (up to 10^4) and low operating voltages [86]. The deposition method is suitable for its high deposition rate and allows getting good adhesion of the films on the substrate. PLD has been found as a promising synthetic pathway as well, resulting in ZnO thin films showing reliable switching characteristics at low voltages and with good retention [73]. An additional advantage in using PLD is the possibility to growth epitaxial ZnO layers with improved switching behavior with respect to textured/polycrystalline ZnO thin films. However, the obtained layers display low on/off ratio [75].

3.1 Sol-gel based ZnO memristors

Sol-gel route has advantages in terms of cost-effectiveness and in the ease of realizing large area devices. Most importantly, the wet chemical method provides a control over a variety of properties, including stoichiometry, porosity, crystallinity, and morphology that are important features required for memristive device application. For compositions like TiO_2 [108], it has been found to be promising in order to obtain reproducible current-voltage switching cycles with the absence of short-circuits, provided that the obtained layers should be dense, free of holes and cracks and have a constant thickness through the films. The influence of film thickness on memristive behavior was studied on sol-gel derived TiO_2/ZnO stack layers spin coated on indium tin oxide (ITO) substrates at different spinning speed. The sample deposited with higher spinning rate resulted in films with thinner thickness, which provided better memristive behavior with high resistance ratio (R_{off}/R_{on}) compared to samples deposited at lower spinning speed [109].

Sol-gel derived ZnO thin films have been prepared by spin coating technique for different applications [103]-[106]. The correlations established between the processing parameters of ZnO thin films structure and optical characteristics of the respective films suggested that the film properties can be controlled by spinning parameters to obtain

uniform and smooth layers with good adhesion to the substrates [106]. At particular values of deposition time and cycle number, with increasing the spinning rate it was observed that the thickness of the deposited ZnO films decreased slowly and finally approached a constant value. The two-stage spin coating procedure aimed to evenly distribute the solution at low speed, and then to remove excess solution and enhance coating uniformity by increasing the speed [107]. The XRD analysis revealed the increase in preferred c-axis orientation of ZnO films as the number of spin coating cycles increased.

At present, there are only a few reports regarding sol-gel derived ZnO thin films with a memristive response [110]-[113]. The memristive behavior of zinc oxide-based device with Pt/ZnO/ITO structure prepared by sol-gel spin coating technique was reported as a function of annealing process [110]. The deposited thin films were annealed at low temperature (350 °C) for different annealing time, but low resistance ratio was measured for all the samples. ZnO films were prepared by sol-gel spin coating on ITO substrate by varying the spin coating rate (1000 rpm, 3000 rpm and 5000 rpm) to study its effect on the memristive behavior [111]. The resistance ratio obtained from the reported study at the selected optimum spin coating speed (3000 rpm) was found to be 1.346. Zinc oxide spin-coated onto fluorine-doped tin oxide (FTO) coated glass slides and in a sandwich configuration with sputtered Au top electrode showed high on/off ratio that was dependent on the voltage scan rate [113]. The report presented resistance ratios at low reading voltage (0.1 V) are 1.34×10^4, 2.2×10^4 and 3.4×10^3 for 500 mV/s, 100 mV/s and 10 mV/s, respectively, with good stability and reproducibility. On the other hand, sol-gel ZnO films of thickness about 40 nm sandwiched between Al electrodes (100 nm) and annealed at 300 °C for 1 h displayed a resistance ratio (R_{off}/R_{on}) comparable to the films prepared by other conventional vacuum deposition [112]. The reported acceptable switching performances level was achieved at an annealing temperature that is low enough to be compatible with the plastic substrates; thus it is promising for application in low-cost flexible memory devices. However, no information were provided on the complete removal of the organic compounds by thermal decomposition at the indicated annealing conditions.

Despite these reports discussing the responses in sol-gel based ZnO, questions remain about the influence of material features and device structure on the

memristive response; such as crystallinity, surface quality, defects, structure of the memristive building blocks and nature of the electrode. The production of stable phases with controlled composition, structure and morphology in ZnO films is also another desired feature of the selected processing technique.

In general, the influence of the processing conditions on sol-gel derived ZnO layers for memristive switching application did not receive attention yet. In particular, the dependence of ZnO films features from the chemical composition of the sol and nature of substrates has to be studied in detail. The study of synthesis conditions and processing parameters for ZnO thin films preparation, based on the characterization of both xerogel powders and coatings is the main theme of this thesis. The following chapters describe the experimental work aimed to the preparation of undoped and doped ZnO coatings to be applied as active layers for memristive building blocks.

Chapter IV
Chemical Synthesis and Processing

In this section, the sol-gel syntheses of undoped, Mg-doped and Al-doped ZnO xerogel powders and thin films will be presented. The experimental conditions for the sol synthesis, the deposition of both single layer and multi-layers on different substrates, and the film curing and annealing have been varied to improve the overall processing of sol-gel derived ZnO thin films toward the final application.

4.1 Preparation of ZnO sol

Zinc oxide (ZnO) sol was prepared from zinc acetate dihydrate (ZAD) precursor. Monoethanolamine (MEA) and ethanol were used as a stabilizer and solvent, respectively. Zinc acetate dihydrate ($Zn(CH_3COO)_2 .2H_2O$, Riedel-De-Haen, ≥99.5 %) was dissolved in ethanol (C_6H_6O, Sigma-Aldrich, ≥99.8 %) to prepare ZnO sol with different precursor concentration. Monoethanolamine ($H_2NCH_2CH_2OH$, 99 %) acts simultaneously as a chemical reaction control agent and a base.

Zinc oxide sol synthesis was performed in an oven dried two-necked 50 mL round bottom flask by dissolving zinc acetate dehydrate in ethanol. Monoethanolamine was then added drop-by-drop to the alcoholic solution while stirring. The mixture was continuously stirred and refluxed at 80 ^oC for 2 h, under N_2. The resulting solution was then cooled down to room temperature under nitrogen flow, and finally a clear and colorless sol was obtained. Figure (1) shows the flow diagram representing the preparation of ZnO sol.

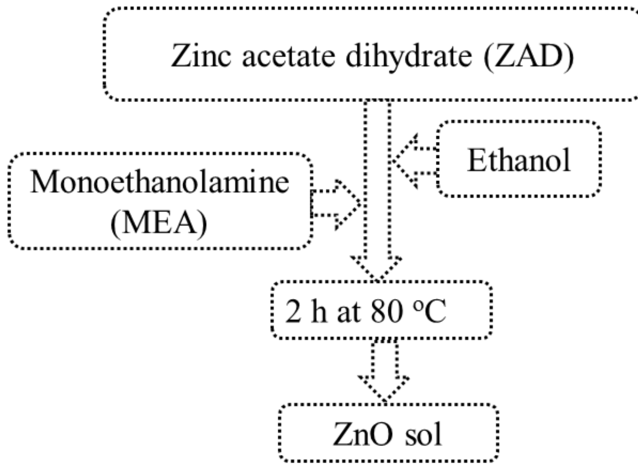

Figure IV-1. Flow diagram of ZnO sol preparation

Different ZnO sols were prepared by varying the concentration of zinc acetate dihydrate (0.07 M, 0.1 M and 0.3 M) and the precursor to MEA (ZAD: MEA) molar ratio. Table (1) summarizes the synthesis parameters used in the synthesis protocol.

Table IV-1. Molar concentration and molar ratios of ZnO sol

ZnO	
[ZAD] (M)	**ZAD:MEA (molar ratio)**
0.1	1:1.34
0.1	1:2
0.3	1:1.34
0.07	1.34
0.1	1:0.5

4.1.1 Xerogel powders preparation

The prepared ZnO sols were transferred to cleaned and dried Petri dishes. The Petri dishes were semi-sealed with aluminum foil and kept for drying in an air atmosphere at room temperature for few days. The xerogel powders were obtained after gelling and drying the sol. The room temperature dried ZnO powders were pre-heated in air at 150 °C or 250 °C for 1 h. After curing, the xerogel powders were annealed in an air atmosphere at 400 ^{o}C for 4 h with the heating rate of 1 ^{o}C/min and cooled down to room temperature.

4.1.2 Preparation of ZnO thin films

4.1.2.1 Substrate cleaning and chemical treatment

In order to achieve uniform and defect-free film, the substrates must be free of dust particles; the elimination of contaminants assists in modifying the surface wettability and improves the adhesion between the sol and the substrate, allowing the deposition of pinhole-free films. Soda-lime glass, silica glass, silicon wafer and engineered platinum (Pt (50 nm) / Ti (5 nm)/SiO_2) substrates have been used for the deposition of ZnO sol. Soda-lime glass and silica glass substrates were sliced into approximately 1 cm x 1 cm using diamond tipped glass cutter. Piranha solution (prepared with sulfuric acid and hydrogen peroxide in 3:1, volume ratio) was used to clean soda-lime glass, silica glass and silicon wafer substrates. The substrates were treated with the piranha solution for about 30 min and subsequently washed several times with distilled water. After that, all the substrates were placed in distilled water for 1 h, rinsed with ethanol and dried at 80 ^{o}C for 1 h in the oven.

On the other hand, different cleaning and treatment procedures were used for the platinum (Pt/Ti/SiO_2) substrates, which were prepared by electron beam evaporation at FBK-BioMEMS (Trento, Italy) for the fabrication of the memristive building blocks described in the following chapter. The Pt (50 nm) /Ti (5 nm) /SiO_2 substrates of 2 cm x 2 cm sized were used as a bottom electrode throughout the electrical measurements. The Pt substrates were first brushed, rinsed with acetone, and then with 2-propanol. A final rinsing with deionized water was then performed. The platinum substrates used for

electrical measurements on memristive building blocks were dried under nitrogen atmosphere and then oxygen plasma etched to increase the adhesion between the layer and $Pt/Ti/SiO_2$ substrate. Drying and oxygen plasma etching were performed in a clean room (FBK-MTLab, Trento). The substrates used for the other characterizations were dried in an air atmosphere in the general laboratory. All the substrates were used for the deposition of sol immediately after the cleaning and modification procedure.

4.1.2.2 Thin films production and spin coating

The solutions were dropped onto the substrate using a glass pipette and the substrates were then rotated at high speed in order to spread the sol over the substrate by centrifugal force. The preparation of ZnO coatings was achieved using the Model P6700 series spin coater. After testing several protocols, the spin coating conditions were set as following: 1300 rpm for 2 s (0→1300: 2 s), 2000 rpm for 2 s (1300→2000: 2 s), and finally 3000 rpm for 50 s (2000→3000: 1 s). Figure (2) shows the flow diagram of the preparation of multi-layered ZnO thin films using the spin coating technique.

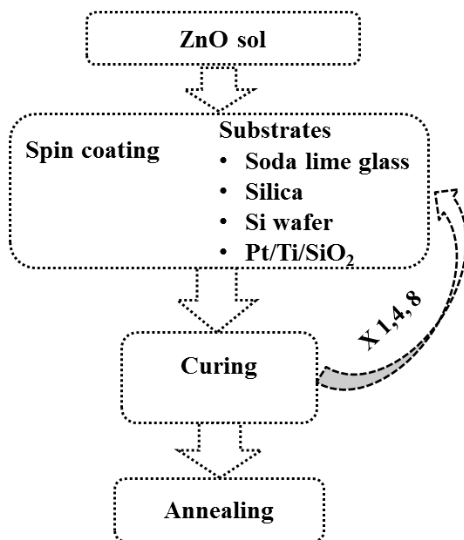

Figure IV-2. Flow diagram of ZnO thin films preparation

For the electrical measurements, the ZnO films were deposited with spin coating condition reported above in a clean room environment at FBK-MTLab, Trento. Prior to spin coating, fresh ZnO sol was transferred into a glass syringe and filtered to remove dust particles through Millipore Millex-FG Hydrophobic PTFE (Teflon) filters of 0.2 μm. The filtered ZnO sol was then deposited on oxygen plasma treated platinum substrates. Upon completion of the spin coating, all the prepared films were kept in air for 20 min at room temperature for evaporating the solvent and consolidating the coatings.

4.1.2.3 Curing and annealing conditions

Among the factors affecting the properties of sol-gel derived multilayered thin films the thermal curing treatment after each layer deposition and the final annealing strongly influence the resulting layers. Table (2) summarizes the curing and annealing steps employed in the series of the syntheses. The samples were cooled to room temperature each time after curing prior to the deposition of the successive layer.

Table IV-2. Thermal treatment conditions

Curing		**Annealing**	
Temp. (^{o}C)	Time	Temp. (^{o}C)	Time
150	10 min, 1 h	400	1 h
250	1 h		4 h
300	10 min		

The final annealing temperature of 400 °C was selected taking into consideration the thermal stability requirements of the engineered Pt (50 nm)/Ti (5 nm)/SiO_2) substrate and was applied to the films deposited on all substrates. All the thermal treatments were performed in an air atmosphere. The annealing procedures were performed with 1 ^{o}C/min heating and cooling rates.

4.2 Preparation of doped ZnO samples

Figure (3) shows the general flow diagram representing the preparation of Mg and Al-doped ZnO thin films using the sol-gel technique.

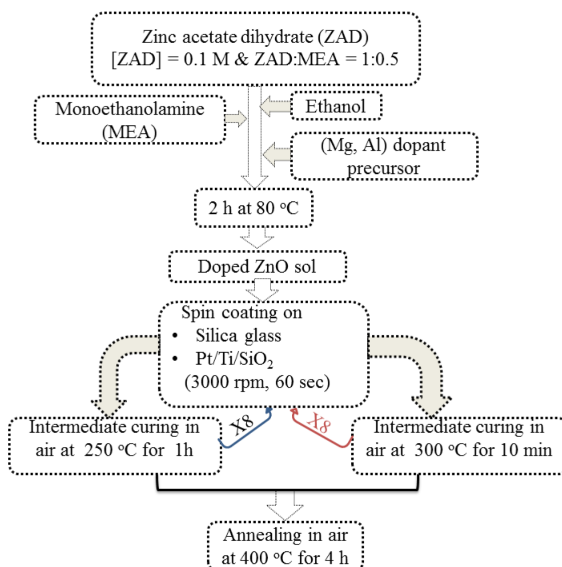

Figure IV-3. Flow diagram of Mg and Al-doped ZnO thin films preparation

4.2.1 Mg-doped ZnO

Zinc acetate dihydrate (ZAD), ethanol and monoethanolamine (MEA) were used as starting material, solvent and stabilizer, respectively. First, 0.878 g of zinc acetate dihydrate was dissolved in 39.4 ml ethanol and then MEA (0.12 ml) was slowly added under magnetic stirring to prepare a solution of ZAD (0.1M). Zinc acetate dihydrate (ZAD) to MEA molar ratio was maintained at 1:0.5. Magnesium doping of ZnO (Mg-doped ZnO) was performed by using magnesium acetate tetra-hydrate $(CH_3COO)_2Mg.4H_2O$, Sigma-Aldrich, ≥ 99 %). 4.6 x 10^{-3} g and 8.7 x 10^{-3} g of magnesium acetate tetra-hydrate were respectively added to the above solution for preparing 0.5 at % and

1.0 at % Mg-doped ZnO sols. The resulting mixture was stirred for 2 h at 80 °C, and then cooled down to room temperature to yield a clear and homogeneous solution.

Mg-doped ZnO films were prepared by spin-coating onto the cleaned $Pt/Ti/SiO_2$ and silica glass substrates with spin coating condition reported above in ambient condition. Afterward, the films were treated at different intermediate curing conditions (300 °C for 10 min, and 250 °C for 1 h) in air to evaporate the volatile material and organic residues. Finally, the Mg-doped ZnO films were annealed in air at 400 °C for 4 h. Mg-doped ZnO xerogel powders were also prepared from the sols by drying in an air atmosphere at room temperature. The xerogel powders were thermally treated at a final annealing temperature of 400 °C for 4 h with the heating and cooling rate of 1 °C/min.

4.2.2 Al-doped ZnO

Aluminum acetate basic ($(CH_3CO_2)_2$ AlOH, Aldrich) was found to be scarcely soluble in ethanol and therefore it could not be used in the film preparation. Two aluminum precursors have been selected for the preparation of Al-doped ZnO sol:

1. **Aluminum nitrate:** aluminum nitrate nonahydrate ($(Al(NO_3)_3.9H_2O$, Fluka, ≥98%)
2. **Aluminum isopropoxide** ($[(CH_3)CHO]_3Al$, Sigma-Aldrich, ≥99.99%)

For the preparation of the Al-doped ZnO sol, zinc acetate dihydrate (ZAD) was dissolved in ethanol followed by drop-by-drop addition of MEA (ZAD concentration: 0.1 M; ZAD to MEA molar ratio: 1:0.5). The appropriate amount of the aluminum precursor for obtaining the sol with Al content of either 0.5 at % or 1 at % was added to the solution while stirring. Thus, 0.12 g and 0.23 g of aluminum nitrate nano-hydrate were added to the solution, whereas 4.1×10^{-3} g and 8.3×10^{-3} g of aluminum isopropoxide were used for preparing 0.5 at % and 1.0 at % Al-doped ZnO sols, respectively. The resulting solution was magnetically stirred at 80 °C for 2 h under reflux and cooled down to room temperature. Xerogel powders were prepared from Al-doped ZnO sols as reported above for Mg-doped sols.

The Al-doped ZnO sols were then deposited at room temperature on cleaned platinum (Pt (50 nm)/Ti (5 nm)/SiO_2) and silica glass substrates by spin coating technique. The films were cured at two different temperatures (250 °C for 1 h and 300 °C for 10 min) in the oven to evaporate the solvent and remove organic residuals. The spin coating to the preheating procedure was repeated eight times to obtain multilayers; and the films then were finally annealed at 400 °C for 4 h.

For the sake of clarity, Table (3) summarizes all the prepared samples, according to the sol synthesis conditions, thin films deposition of single and multi-layers on different substrates with different intermediate curing and annealing conditions for undoped, Mg and Al- doped ZnO samples.

Table IV-3. ZnO sol concentration and different ZAD: MEA molar ratio used in preparation of both undoped and doped ZnO thin films, number of layers deposited on soda lime glass, silica glass, silicon wafer and platinum substrates, different intermediate curing and annealing conditions applied for all the samples

Undoped ZnO										
Sol conditions		**Thin films processing**								
[ZAD] (M)	ZAD:MEA (molar ratio)	Substrates				**Number of layers**	**Intermediate curing conditions**		**Annealing conditions**	
		glass	silicon	silica	Pt/Ti/SiO_2		T (°C)	time	T (°C)	time (h)
0.07	1:1.34	✓				1, 4, 8	150	10 min	400	4
0.3	1:1.34	✓				1, 4, 8	150	10 min		4
0.1	1:2	✓				1, 4, 8	150	10 min		4
0.1	1:1.34	✓				1, 4, 8	150	10 min		1
0.1	1:1.34	✓				1, 4, 8	150	10 min		4
0.1	1:1.34	✓		✓	✓	8	250	1 h		1
0.1	1:1.34	✓	✓	✓	✓	8	250	1 h		4
0.1	1:1.34			✓	✓	8	300	10 min		4
0.1	1:0.5	✓	✓	✓	✓	4, 8	250	1 h		4
						8	300	10 min		4
Al and Mg-doped ZnO										
0.1	1:0.5			✓	✓	8	250	1 h	400	4
							300	10 min		

Chapter V
Characterization Techniques and Instruments

A comprehensive characterization is necessary to determine the effect of different synthesis and processing conditions on the final device properties and performance. This chapter provides an overview of all the characterization techniques applied in this work emphasizing on surface and compositional analysis, structural investigation, thermal behavior and electrical measurements.

5.1 Surface and compositional analysis

5.1.1 Scanning Electron Microscopy (SEM) and Field Emission-SEM (FE-SEM)

Scanning electron microscopy (SEM) has been used to provide the information on the surface morphological features of the ZnO sample, which were observed by using a JSM-5500 (JEOL technics Ltd) scanning electron microscope with an accelerating voltage of 10 kV. At the early stage of this study, the low magnification SEM images have been used to optimize the single and multilayered sol-gel derived ZnO films. SEM analysis has been mainly applied to analyze the quality, and uniformity of the layers.

Furthermore, field emission scanning electron microscopy (FE-SEM) was used to acquire high-resolution images and get comprehensive information of the films' surface. By means of FE-SEM, surfaces images can be recorded with a resolution in the nano-metric scale and a high depth of focus. Moreover, the thickness of the ZnO layers can be estimated from the FE-SEM cross-sectional images. The FE-SEM analyses of undoped ZnO films and Mg-doped films were run by using a Zeiss supra 40 scanning electron microscope operating at 5 kV (BIOtech -University of Trento, Italy).

For the Al-doped ZnO samples, a Jeol JSM-7401F Field Emission scanning electron microscope (FBK-MINALaB, Trento) operating at 15 kV was used. The analyses were performed in a high vacuum (vacuum pressure of the source at 2.2×10^{-8} Pa and a vacuum pressure of the sample at 9.63×10^{-5} Pa).

The images of all samples were recorded after depositing thin conductive gold metal layers on the films using the SC7620 Mini Sputter Coater (VG Microtech).

5.1.2 Atomic Force Microscopy (AFM)

Atomic force microscopy (AFM) falls under the Scanning Probe Microscopy (SPM) family of techniques. It uses a fine tip to measure surface properties through an interaction between the tip and surface. It has been recognized as a tool for the imaging of sample surfaces down to atomic scale providing information on surface topography with atomic resolution. AFM can also provide quantitative measurements of the grain size and surface roughness of the films.

Atomic force microscopy data were acquired using an Asylum Research Cypher equipped with the Environmental Scanner module, at a sample temperature of 25 °C. Measurements were performed in AC mode in air, using AC-240TS probes (Olympus, nominal spring constant 2 N/m, nominal resonant frequency 70 kHz). The surface quality and roughness of the undoped, Mg and Al-doped ZnO thin films were investigated. The analysis was performed in Fondazione Bruno Kessler (FBK-LaBSSAH), Trento.

5.1.3 X-ray photoelectron (XPS) and UV-photoelectron spectroscopy (UPS) analysis

X-ray photoelectron spectroscopy (XPS) and UV-photoelectron spectroscopy (UPS) are techniques devoted to studying surface characteristics of materials, providing the elemental composition and electronic properties of the materials. XPS uses high-energy X-ray photons to excite core electrons in the near surface region and can be applied to a broad range of materials. It provides quantitative and structural information including elemental composition, and oxidation state of the elements from the top surface layers (about 10 nm) of the investigated material. UPS uses lower energy photons in the UV region as a source to excite valence electrons and the photoelectrons emitted from the valence band region of the materials of interest are probed.

The composition and electronic surface properties of the undoped, Mg and Al-doped ZnO films deposited on the platinum substrate were investigated both by X-ray photoelectron spectroscopy and ultraviolet photoelectron spectroscopy. The analyses were performed in an ultrahigh vacuum chamber of a base pressure of 10^{-10} mbar equipped with $CLAM_2$ Electron Hemispherical Analyzer (Figure 1). Monochromatic MgKα excitation with the energy of 1253.6 eV was used as X-ray source for XPS, and a helium discharge lamp at 21.22 eV was used for UPS analysis. The electron energy analyzer of hemispherical type (VS WHA100) with a sphere's radius of 100 mm was used. The analyzer acts as a narrow energy pass filter, letting pass only the electrons that have a specific kinetic energy. It has three main components: the lenses system to focalize and adjust initial electron energy, the analyzer, composed by two hemispherical and concentrical lenses, and five Channel Electron Multipliers (Channeltrons) to collect and reveal the electrons.

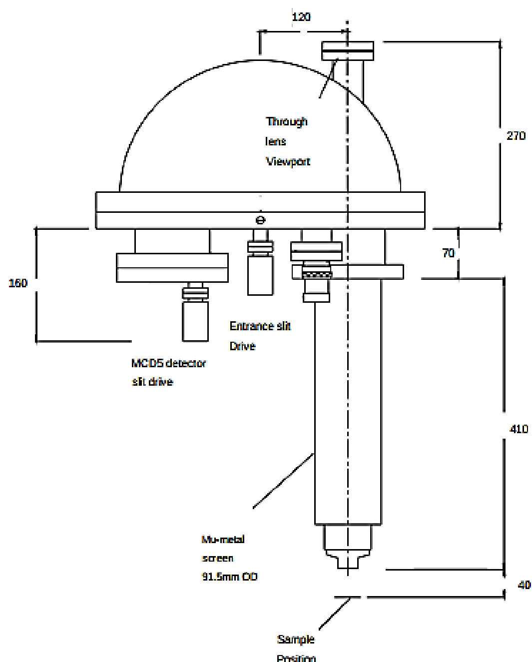

Figure V-1. Scheme of the CLAM2 electron energy analyzer

The maximum energy resolution for XPS and UPS techniques is 0.5 and 0.1 eV, respectively. The collection geometry was aligned so that the sample surface is typically normal to the analyzer in XPS and UPS spectroscopies while excitation sources are positioned at different angles with respect to the sample's surface. Figure (2) shows the scheme of the collection/excitation geometry.

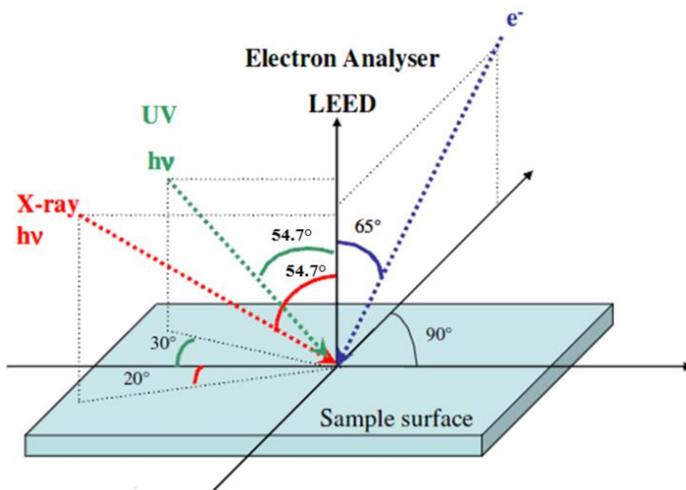

Figure V-2. Excitation and collection geometry with respect to sample's surface

The analyzer is interfaced with a PSP RESOLVE power supply unit which receives signals from the analyzer and gives a digital output signal in terms of counts. Then, the acquisition software (PSP Collect) plots the output as a function of electrons kinetic energy (for UPS analysis) or binding energy (for XPS analysis). The analyses were performed in IMEM-CNR, Trento (Italy).

5.2 Structural Analysis

5.2.1 X-Ray Diffraction Analysis

The X-ray diffraction technique is employed here to analyze the structural characteristics of the multi-layered undoped, Mg and Al-doped ZnO thin films as well as of xerogel powder samples.

The crystalline structure of the undoped ZnO thin films deposited on soda-lime glass, silica glass, silicon wafer and platinum substrates were studied by Rigaku D-Max III X-ray powder diffractometer. The measurements of the ZnO thin films were performed in a glancing incidence mode to make the measurement more sensitive to the near surface of the sample. Accordingly, asymmetric scan geometry was adopted to enhance the signal to noise ratio and the scan was collected with grazing incidence angle (θ) of 0.5^{o}. On the other hand, the annealed ZnO xerogel powders were analyzed using the conventional θ - 2θ scanning configuration.

In general, the XRD traces for the ZnO films and xerogel powders were recorded in the 2θ range of $30\text{-}40^{o}$ to avoid the strong signal coming from the platinum substrate. The instrument operated in a step scan mode with 0.15^{o} increments and the acquisition time was adjusted to 120 sec at each step. The analysis was conducted at 40 kV and 30 mA with a CuKα radiation (λ=0.154 nm) and a graphite monochromator. All the diffractograms recorded were fitted to evaluate peak position and crystallite sizes using MDI (Material Data, Livermore, CA, USA) Jade 8® software. The evaluation of crystalline size was done by the Scherer formula [114] using the full width at half maximum (FWHM) of the individual peaks.

The XRD analyses performed on the Mg and Al-doped ZnO films deposited on platinum substrates have been performed using a diffractometer having set up different from the one discussed above and shown in Figure (3). XRD data were acquired on an Italstructures IPD3000 instrument equipped with a Cu anode source operating at 40 kV and 30 mA, a multilayer monochromator to suppress Kβ radiation and 100 μm slits.

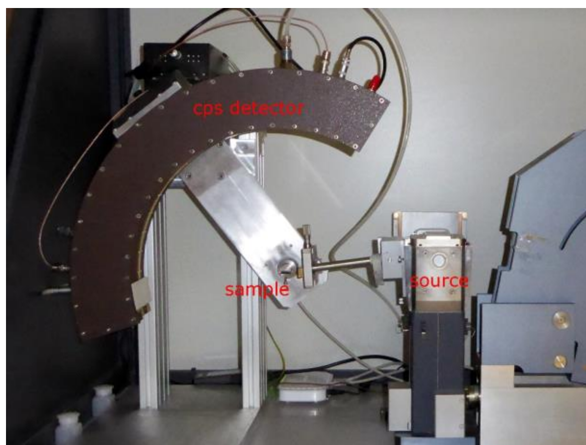

Figure V-3. Experimental setup of the diffractometer (Italstructures IPD3000/CPS120)

The sample was positioned in reflection geometry with a fixed omega angle with respect to the incident beam, and patterns were collected by means of an Inel CPS120 detector. The measurements were performed in glancing incidence mode to make the measurement more sensitive to the surface of the films; different incidence angles were tested to maximize the signal coming from the deposition layers. Finally, an omega angle of 3° was selected with an acquisition time of 900 sec for all the samples.

5.2.2 Fourier-Transform Infrared Spectroscopy

Fourier-Transform Infrared Spectroscopy (FTIR) is a versatile technique used to identify chemical bonds and functional groups in molecules. The structural information on the undoped, Mg and Al-doped ZnO xerogel powders samples of different composition and with different thermal treatment were investigated by Fourier-Transform Infrared Spectroscopy (FTIR) with a Thermo Optics Avatar 330 FTIR instrument. The spectra were recorded in transmission mode on KBr pellets in the range of 4000 - 400 cm^{-1} collecting 64 scans with a resolution of 4 cm^{-1}.

Moreover, Diffuse Reflectance Infrared Fourier Transform spectroscopy (DRIFTS) was used in an attempt to acquire information on ZnO thin films deposited on

platinum and silicon wafer substrates. Cleaned bare platinum and silicon wafer substrates were used to adjust the signal and to collect the background spectra. The DRIFTS spectra were then recorded in the frequency range of 4000 - 400 cm^{-1} using (256 scans, resolution of 4 cm^{-1}).

On the other hand, Attenuated Total reflection-ATR was used to collect structural information on the ZnO films deposited on a soda-lime glass substrate. A single crystal of ZnSe (refractive index, n = 2.41) with the incident beam coming at an angle of 45° has been used. The spectra were recorded in the frequency range of 4000 - 650 cm^{-1} using 128 scans and resolution of 4 cm^{-1}.

5.2.3 Micro-Raman spectroscopy

The general setup for Raman scattering experiments is shown in Figure (4) and consists of a monochromatic light source for excitation, optical equipment to bring the laser beam on the sample and collect the scattered light, a spectrometer to analyze the scattered light and a detector to collect the signal. Monochromatic laser light is focused on a sample; the scattered light is collected, and analyzed by a spectrometer and a CCD detector. The analysis was performed at the micro-Raman laboratory, CNR-IFN, Trento.

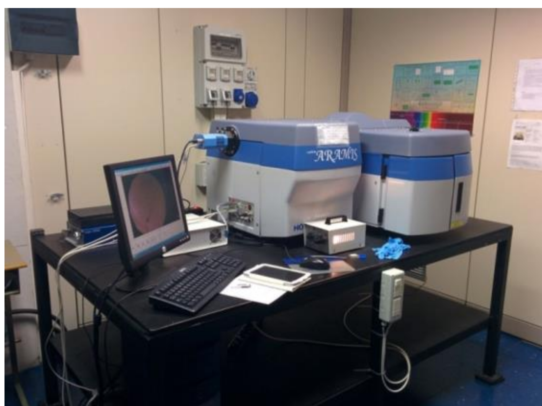

Figure V-4. Experimental setup for Raman scattering experiments

The Micro-Raman spectra were recorded on undoped and Al-doped multi-layer ZnO thin films deposited on platinum (Pt/Ti/SiO_2) and silicon wafer substrates. Moreover, the spectra were acquired on the bare substrates as a reference. The measurements were performed at room temperature on a Labram Aramis (Horiba Jobin-Yvon) instrument equipped with an optical microscope of 100 X objectives. He-Ne laser operating at 632.8 nm was used for excitation of the Raman signal with appropriate holographic notch filters for eliminating the laser line after excitation. The slit width of the spectrometer was typically set at 100 µm. A holographic grating having 1800 grooves/ mm and a charge-coupled device (CCD) detector were used for the collection of all Raman spectra. The resolution was ±1 cm^{-1}. Spectral analysis and curve fitting were performed with LabSpec Spectroscopy software.

5.2.4 Optical Transmittance Measurements

Transmission measurements were performed on undoped and Al-doped ZnO thin films deposited on silica glass substrates. A double beam Cary Varian-5000 spectrophotometer was used in the range between 200 and 800 nm. The sample holder allowed considering a circular area on the samples with 1 cm diameter. The optical parameters of the films were obtained at 632.8 nm by Point-wise Unconstrained Optimization Approach (PUMA) [115] software. The software was used to estimate the refractive index and the thickness of the multilayered thin films. The overall porosity of the thin films was then determined from the refractive index of the samples obtained using simulation and the reference refractive index of ZnO thin films at 632.8 nm.

5.3 Thermal Analysis

5.3.1 Thermogravimetric/differential thermal analysis (TG/DTA)

The thermal behavior of the undoped and Al-doped ZnO xerogel powders prepared from different sol composition has been studied by differential thermal analysis (DTA) and thermogravimetric analysis (TGA). Mg-doped xerogel powders were analyzed in differential scanning calorimetry (DSC) mode. A thermobalance STA 409 NETZSCH apparatus (Netzsch-Geratebau GmbH, Germany) was used. Alumina powders were used

as a reference. The heat treatment was carried out in a static air atmosphere at a heating rate of 10 °C /min from 20 °C to 500 °C.

5.4 Memristive building blocks fabrication and Electrical Measurements

The Electrical measurements are performed to detect the change in resistance state of the material and are the key step in the characterization of the active layers for a memristive application. The electrical behavior of ZnO layers was studied on the films deposited on the 2 cm x 2 cm Pt (50 nm) /Ti (5 nm) /SiO_2 substrates (prepared by electron beam evaporation at FBK-BioMEMS), which were used as a bottom electrode throughout the electrical measurements.

Top electrodes with different forms and types were deposited on the ZnO layers to run the electrical measurements. In the first set of experiments, the electrical measurements were performed on 4-layered ZnO films sandwiched between platinum (Pt/Ti/SiO_2) substrate as a bottom electrode and a silver wire that was used as a top electrode. Figure (5) shows the simplified scheme of ZnO cell structure.

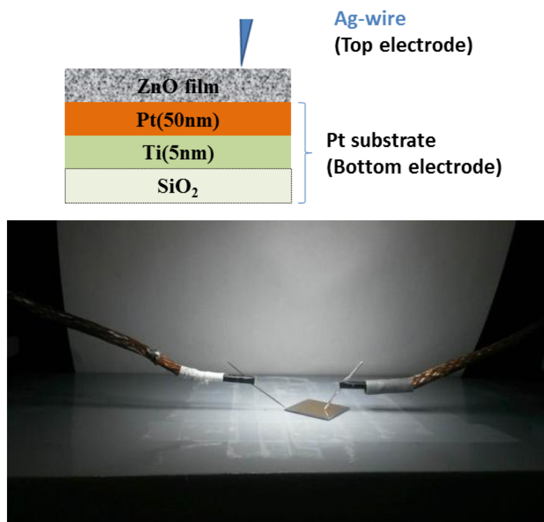

Figure V-5. Set up for the electrical measurement of ZnO films deposited on Pt/Ti/SiO_2 bottom electrode with Ag wire as the top electrode

Keithley 2410 broad purpose Source-Meter unit was used to measure the current-voltage (I-V) characteristics of ZnO thin films. The measurement was performed at room temperature in an air atmosphere. The unit was connected to a PC through a GPIB card and controlled by a software user interface Labview, National Instruments. During the measurement, the bias voltage was applied to the top electrode while the bottom electrode was put to the ground.

The second sets of measurements were performed on the ZnO layers sandwiched between Pt/Ti/SiO_2 substrate as a bottom electrode and Ag-dishes as a top electrode (Figure 6). The silver top electrode was deposited on ZnO thin films by electron beam evaporation at FBK-BioMEMS.

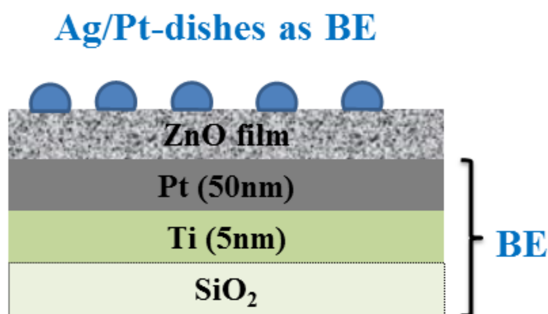

Figure V-6. The schematic device structure of ZnO films with Ag/Pt-dishes as a top electrode (TE) and Pt/Ti/SiO_2 substrate as a bottom electrode (BE)

The circular shaped Ag-dishes with a diameter of 295 ± 10 μm and 60 ± 1 nm thick was deposited on 2 cm x 2 cm ZnO layers patterned by using shadow mask with dish-shaped patterns. For this purpose, a silver rod source (99.99 % purity, supplied by Umicore) in a vacuum chamber using an electron beam evaporator EBX-16C (Ulvac) was used. The pressure in a vacuum chamber was maintained at 1.9 x 10^{-7} torr and the evaporation rate was adjusted to 0.1 nm sec^{-1}. The I-V curves were then acquired with a setup composed of a Faraday cage, a stereoscopic microscope SKU:H800, a camera coupled to microscope (AmScope), micromanipulators with Tungsten probes, a 2410 High Voltage SourceMeter (Keithley) connected to a PC through a GPIB card and controlled by a

software user interface (Labview, National Instruments). The measurements were performed in an ambient atmosphere at room temperature.

Additionally, Pt-dishes (260 ± 10 μm in diameter, 40 ± 2 nm thick) patterned by shadow mask were deposited on another set of samples by electron beam evaporation (FBK-BioMEMS) under vacuum conditions (vacuum chamber at $2.5x10^{-7}$ torr). The electrical measurements were then performed on both undoped and Al-doped ZnO thin films after deposition of Pt-dishes as a top electrode (Figure 6). The current-voltage (I-V) characteristics were acquired by a custom setup composed of micromanipulators with tungsten probes wired to NI PXIe-1073 chassis connected to a PC through a PCI-express card and controlled by a software user interface developed within the Labview environment. The chassis was equipped with NI-PXIe-4139 source measure unit capable of current or voltage controlled source and measure. The current-voltage (I-V) characteristics were carried in voltage sweeping mode at a different frequency. All of the operation voltages were applied to the top electrode, with which the $Pt/Ti/SiO_2$ bottom electrode was grounded. Parts of the measurements were acquired in the presence of LED illuminator light (Figure 7) to study the effect of light on the memristive response. The I-V curves were recorded in an ambient atmosphere at room temperature.

Figure V-7. Electrical measurement setup (LED light illuminator)

Chapter VI

Results and Discussions (I): Undoped ZnO Samples

6.1 Preliminary Experiments

ZnO thin films were prepared from ZnO sols according to the different conditions reported in chapter IV. A preliminary test of the sol stability as a function of aging was made on a ZnO sol prepared from ZAD solution 0.1 M and ZAD to MEA molar ratio of 1:1.34, by observing the sol under a UV laser beam. Figure (1) shows the images of the as-prepared ZnO sols and of the solution after aging at room temperature for 1, 3 and 6 days, respectively. The ZnO sol appeared to be sufficiently stable even after 6 days aging, without particles segregation or extensive formation of gelatinous aggregates.

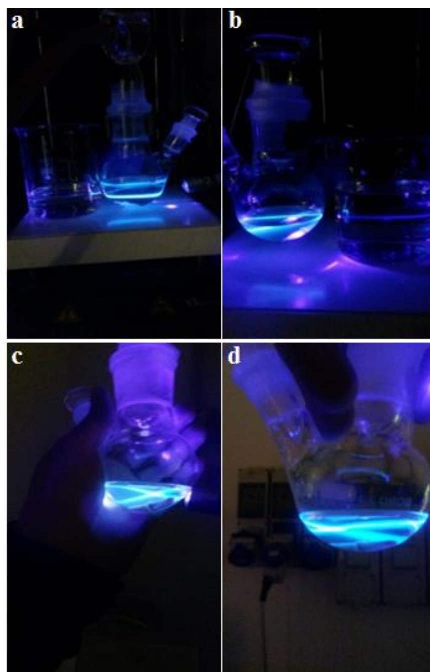

Figure VI-1. Photographic images of ZnO sol under blue UV laser beam a)Fresh sol b)after 1 day c) after 3 days d) after 6 days

The prepared thin films were characterized by means of multiple characterization techniques. Low magnification scanning electron microscopy was used to give a quick survey regarding films' morphology. The ZnO xerogel powders were studied in order to better investigate the effect of different curing and annealing conditions for the films and to select the appropriate composition in ZnO sol.

The low magnification SEM (X3000) images of ZnO thin films deposited on soda lime glass substrates with zinc acetate dihydrate concentration of 0.1 M and ZAD to MEA molar ratio of 1:1.34 are shown in Figure (2). The effect of a number of layers on the features of the films was studied on a single layer, 4 and 8 layered ZnO thin films, cured at 150 ^{o}C for 10 min between each deposition/layer, and finally annealed at 400 ^{o}C for 1 h. The single layered film showed scattered and discontinuous grains. Increasing the number of layers assists in avoiding the formation of voids and pores, by covering the whole area and this appears to affect also the grain distribution. In addition, it was observed from the SEM images that the grains become relatively uniform and dense with repeating the film deposition. The quality of the films appeared to be affected by the number of deposited layers and therefore multiple layers were deposited on the substrates to ensure more uniform films.

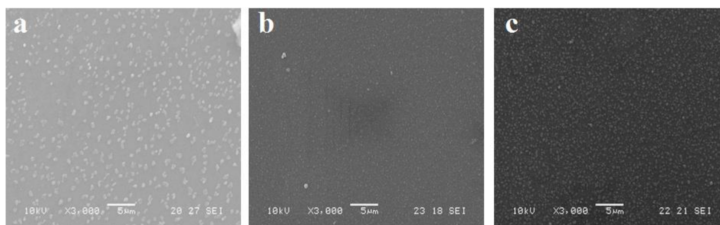

Figure VI-2. SEM images of ZnO films a) 1 layer, b) 4 layers), c) 8 layers

In addition to uniformity and homogeneity of the layers that are critical features for memristive switching application, it is also important to adjust the final annealing time and temperature to ensure complete removal of organics. The final annealing temperature of the films is limited to 400 ^{o}C, according to the thermal stability of the engineered Pt substrate. However, an increase of annealing time to 4 h will be expected to increase the possibility to remove the organic residuals completely and enhance the

crystallization of ZnO. On the basis of the thermal analyses (described later in the text) run on the xerogel powders to assess both the removal of organic by-products and the ZnO crystallization, the final annealing step for the films was run at 400 °C with the duration of 4 h.

The influence of precursor concentration on the morphological features and surface qualities of the films was also studied. Figure (3) shows the SEM images recorded on 8 layered ZnO thin films deposited on soda lime glass substrate with zinc acetate dihydrate (ZAD) concentration of 0.07, 0.1 and 0.3 M (ZAD to MEA molar ratio of 1:1.34).

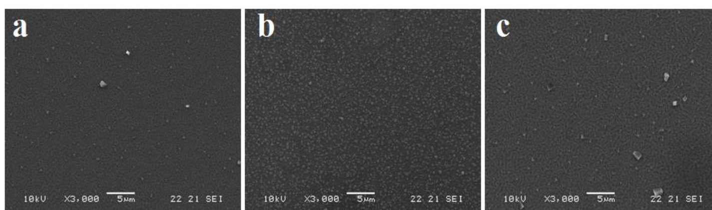

Figure VI-3. SEM images of 8 layered ZnO films deposited on glass substrate with [ZAD] of a) 0.07 M b) 0.1 M c) 0.3 M

The grain size and distribution presented some dependence on the precursor concentration (Figure 3). The surface morphology of the films prepared from 0.07 M Zn solution showed uneven and relatively small grains and revealed uncoated regions. Based on the preliminary SEM survey, the 0.1 M Zn solution was preferred to 0.3 M solution and applied to all the following syntheses since it appears promising to give a more uniform grain distribution in the films.

The low magnification SEM analyses were then recorded on ZnO films coated on soda lime glass with 0.1 M ZAD sols prepared with changing the ZAD to MEA molar ratio. However, no clear indication of the effect of MEA content on films deposited onto glass was obtained from the images recorded on 8-layered ZnO films with ZAD to MEA molar ratio of 1:0.5, 1:1.34 and 1:2, cured at 150 °C for 10 min and annealed at 400 °C for 4 h (Figure 4 a-c).

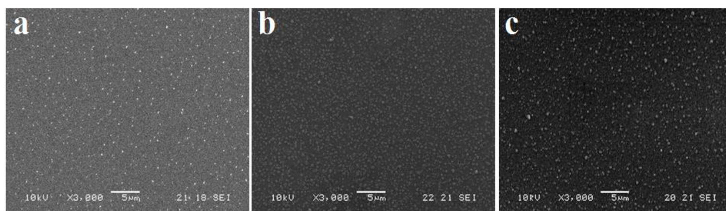

Figure VI-4. SEM images of 8 layered ZnO films deposited on glass substrate with ZAD: MEA of a) 1:0.5 b) 1:1.34 c) 1:2

Therefore, a second experiment was made by changing the substrate. ZnO sol with ZAD to MEA molar ratio of 1:0.5 and 1: 1.34 were deposited on Platinum (Pt/Ti/SiO_2) and silicon wafer substrates. Figure (5 a-b and c-d) displayed 8-layered ZnO films of different ZAD to MEA molar ratio coated on platinum and silicon wafer substrates, respectively.

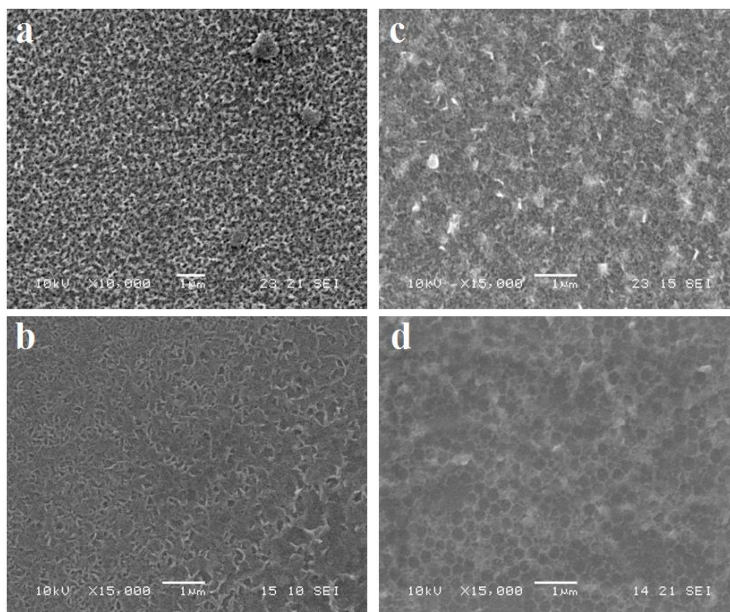

Figure VI-5. ZnO films deposited on a) Pt with 1:0.5 b) Pt with 1:1.34 c) Si with 1:0.5 d) Si with 1:1.34 ZAD to MEA molar ratio

From Figure (5 b and d), the negative effect of the high MEA content on film quality can be observed on both platinum and silicon wafer substrates. The films present a porous like surface morphology for higher MEA content that could be attributed to the organics released during film thermal treatment.

The study reported above suggested also the influence of the substrate on the morphology of ZnO films. This evidence was confirmed by the comparison of the SEM images of ZnO films deposited on different substrates, with ZAD: MEA molar ratio of 1:0.5 cured at 150 ^{o}C and annealed at 400 ^{o}C for 4 h (Figure 6 a-c)).

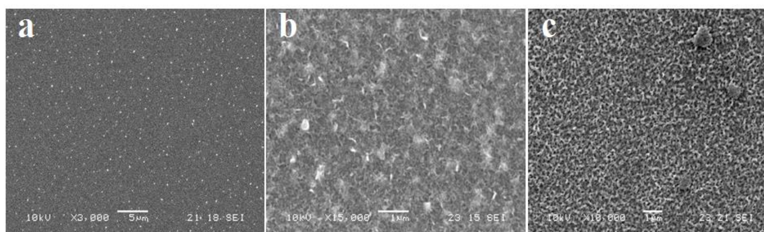

Figure VI-6 SEM images of ZnO films deposited on a) soda lime glass b) silicon c) platinum substrates

The low magnification SEM results discussed above suggest that the surface quality of the films depends on substrate and number of layers. The influence of ZAD to MEA ratio in the sol is also highlighted but further analyses are required to select the appropriate MEA content.

6.2 Characterization of ZnO powders

The effect of composition and concentration of ZnO sol on morphological and structural features has to be addressed more in details. The organics retention in the films leads to uncontrolled impurity content in the layers that affects the crystallization extent of the films and can inhibit the successful deposition of the top electrodes for the memristive application using fabrication techniques that operate under high vacuum conditions. Thus, an improvement of curing and annealing steps is a critical requirement.

To this aim, structural and thermal studies have been performed on ZnO xerogel powders. Taking into consideration the curing steps in film preparation, the thermal behavior has been investigated on ZnO xerogel powders preheated at different

temperatures by differential thermal analysis (DTA) and thermogravimetric analysis (TGA).

The analysis was performed on the powders prepared from ZnO sol with ZAD to MEA molar ratio of 1:0.5 and 1:1.34. Figure (7) shows the TGA traces of powders preheated at 150 °C for 1 h, which are characterized by three weight loss steps. Beside the different intensity for the two samples prepared with different MEA content, the analysis lead to similar total weight loss in the temperature range 20-400 °C (60 and 65 %, respectively). The first weight loss observed up to 150 °C in TGA plot was attributed to the release of absorbed water. The other steps that extend up to about 400 °C can be ascribed to the decomposition and release of the organic residuals, namely acetate and amine groups, and the condensation of OH groups chemisorbed on the oxide surface. It is worth of noting that the TGA curves in Figure (7) suggest that the thermal evolution is not completed at 400 °C.

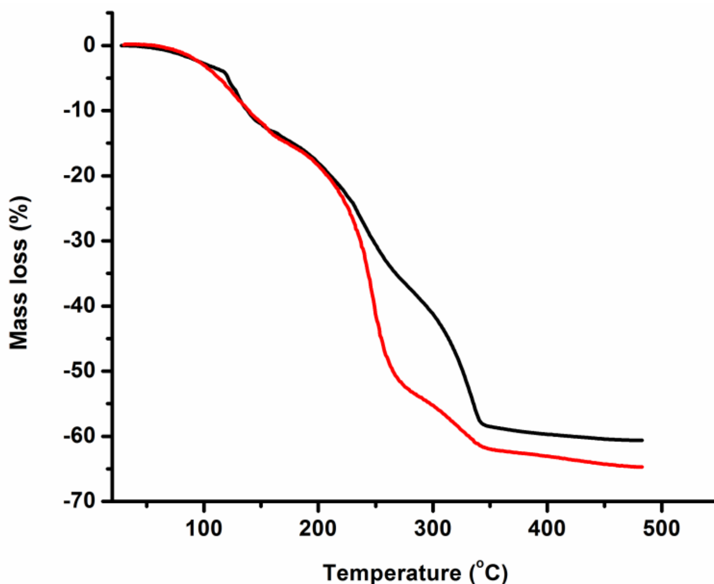

Figure VI-7. TG plot of ZnO powders prepared from ZAD to MEA molar ratio of 1:0.5 (black) and 1:1.34 (red), and preheated at 150 °C

Figure (8) shows the TGA analyses on ZnO xerogel powders pretreated at 250 °C for 1 h, presenting a total weight loss up to 400 °C of about 3 % and 10 % for the samples prepared with low and high MEA content, respectively. The increase in curing temperature from 150 to 250 °C leads to the decrease in the total weight loss particularly for the sample prepared with a low MEA content, which appears thermally stable up to 300 °C.

However, the weight loss continues above 400 °C also for the powders cured at 250 °C. As reported above, the final annealing temperature of films cannot be higher than 400 °C for the stability issues of the engineered Pt/Ti/SiO_2 substrate. Even if the thermal behavior of films and powders could be different, the TGA results suggest that a longer duration of the final annealing step could better ensure the complete organics removal from the ZnO layers and assist the ZnO crystallization.

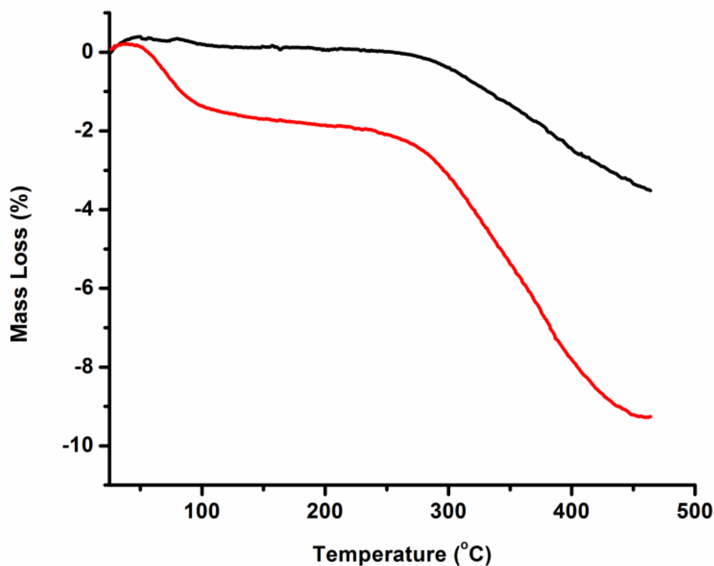

Figure VI-8. TG plot of ZnO powders prepared from ZAD to MEA molar ratio of 1:0.5 (black) and 1:1.34 (red), preheated at 250 °C

The combined TG/DTA plot of ZnO powders prepared from ZAD to MEA molar ratio of 1:0.5 and 1:1.34 and cured at 250 °C for 1 h is shown in Figure (9). The broad

exothermic peak in the DTA curve corresponding to the second weight loss step is associated with the decomposition of residual organics. In addition, the sharp component of the exothermic peak that is overlapped to the broad peak was assigned to the ZnO crystallization [116]. The crystallization peak is observed at 370 °C for the sample prepared from the molar ratio of 1:0.5 whereas the peak shifts to 392 °C for the sample with higher MEA content. In general, the thermal analyses on ZnO powders suggest that the curing temperature of 250 °C and the use of low MEA concentration in the ZnO sol are favorable conditions for improving organics removal and ZnO crystallization.

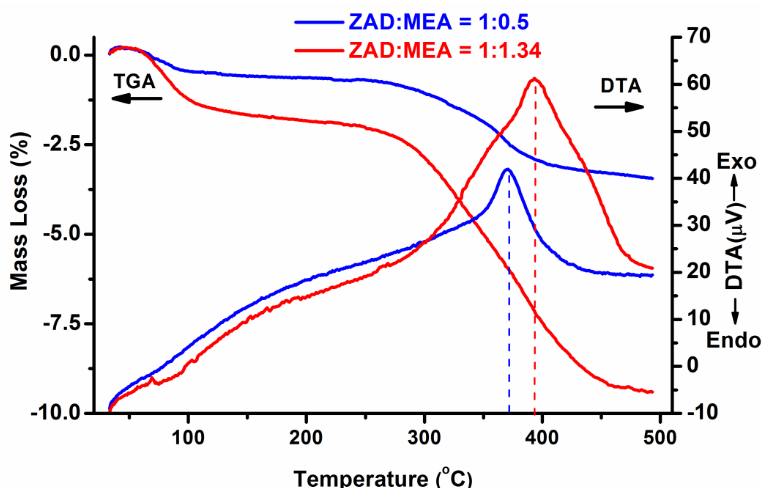

Figure VI-9. TG/DTA plot of ZnO powders preheated at 250 °C

The FTIR analysis was performed on ZnO xerogel powders prepared from high and low MEA content in ZnO sol in order to have more information on the effect of the thermal treatment of the samples. Figure (10) shows the FTIR spectra recorded on ZnO xerogel powders with ZAD to MEA molar ratio of 1:0.5 and heat-treated at 150, 250 and 400 °C. The signal position and the corresponding modes of vibration are summarized in Table (1). The broad absorption band at 3390 cm^{-1} is the result of the overlapping of the O-H stretching vibrations from absorbed water and N-H stretching vibration contributed from MEA. In the spectra of all samples, the intensity of this absorption band decreases as the temperature increases from 150 °C to 250 °C and the

signal vanishes for the xerogel powders treated at 400 ^{o}C. The peaks located at 1580 cm^{-1} and 1405 cm^{-1} represent the asymmetric and symmetric stretching vibrations of C=O bond of the acetate group, respectively. The signals at 1040-1080 cm^{-1} arise from both MEA and acetate groups. The new peak at 435 cm^{-1}, corresponding to the stretching vibration of ZnO [117], appears in the spectrum of ZnO xerogel powders treated at 250 ^{o}C and can be clearly observed for the powder annealed at 400 ^{o}C for 4 h. The signals corresponding to organic residuals are not detectable for the sample treated at 400 ^{o}C.

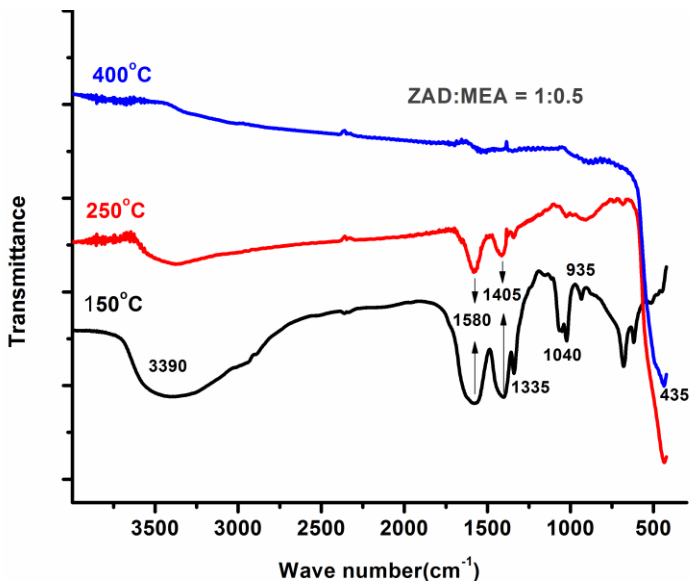

Figure VI-10. FTIR spectra of ZnO xerogel powders with ZAD: EA molar ratio of 1:0.5 heat treated at 150 ^{o}C (black) and 250 ^{o}C (red); and annealed at 400 ^{o}C (blue)

Table VI-1. FTIR signals detected in ZnO powders with assignments [118]

Peak position (cm^{-1})	Assignment
3390	$\nu_{(O-H)}$ (H_2O), $\nu_{(N-H)}$ (MEA)
1634	$\delta_{(HOH)}$ (H_2O)
1580	$\nu_{as\ (COO-)}$ (ZAD), $\delta_{ip\ (N-H)}$ (MEA)
1405, 1335	$\nu s_{(COO-)}$ (ZAD)
1080	$\nu_{(C-O)}$ (MEA), acetate (ZAD)
1040	$\nu_{(C-N)}$ (MEA), acetate (ZAD)
927	$\delta_{oop\ (N-H)}$ (MEA)
674	Skeletal (ZAD)
612	Skeletal (ZAD)
435	Zn-O stretching vibration

The FTIR spectra of ZnO xerogel powders with ZAD to MEA molar ratio of 1:1.34 and heat treated at 150, 250 and 400 °C shown in Figure (11), do not present substantial differences with those recorded on a sample prepared from low MEA content (Figure 10).

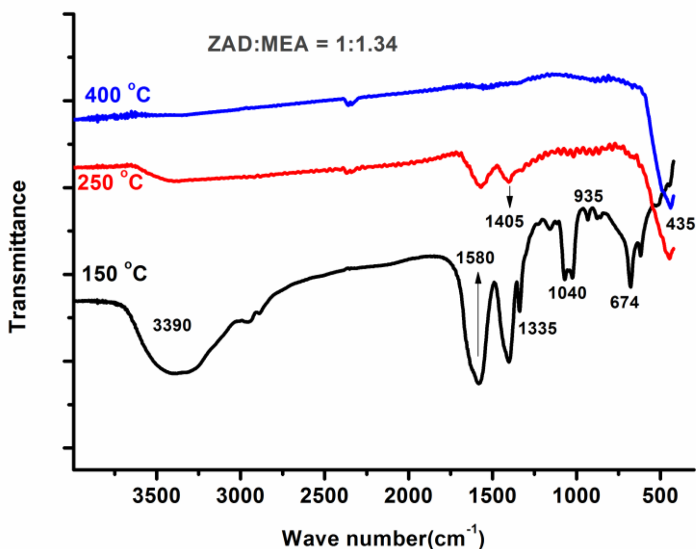

Figure VI-11. FTIR spectra of ZnO xerogel powders with ZAD: EA molar ratio of 1:1.34 heat treated at 150 °C (black) and 250 °C (red); and annealed at 400 °C (blue)

The spectra of both sets of samples are characterized by the signals coming from ZAD and MEA precursors with different relative intensities of acetate- and amine- related vibrations.

In agreement with the results obtained from the thermal analysis performed on xerogel powders, the FTIR analyses suggested that curing at 250 °C and annealing at 400 °C are suitable conditions for the preparation of organic-free ZnO thin films. In addition, from the thermal analyses, the use of low MEA in sol appeared to be a favorable condition for ZnO crystallization. XRD analyses were run on ZnO xerogel powders prepared from high and low MEA content annealed at 400 °C for 4 h. Figure (12) shows the diffractograms (in the 2θ range = 30-40°) collected on xerogel powder samples prepared from ZAD to MEA ratio of 1:0.5 and 1:1.34. The selected 2θ range was adopted for comparing the XRD results of the powders with those acquired on the films deposited onto the Pt/Ti/SiO_2 substrate (in order to eliminate the Pt signal, according to the experimental description in Chapter V).

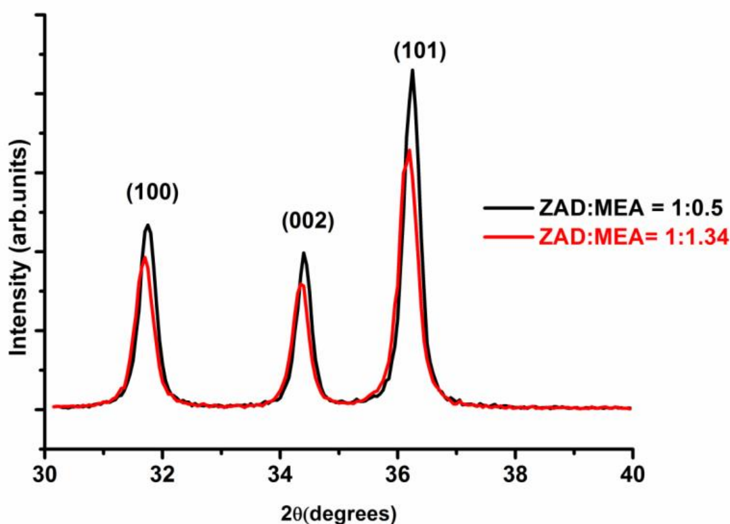

Figure VI-12. XRD traces of ZnO powders annealed at 400 °C for 4 h

The XRD traces recorded on powder samples show the presence of the crystalline ZnO structure with hexagonal wurtzite type phase according to the standard reference data (JCPDS card 36-1451). The XRD patters of both samples present the main peaks corresponding to ZnO, where the reflections are assigned to (100), (002) and (101) planes with the respective 2θ positions reported in Table (2). The slight increase in relative peak intensity in the ZnO sol with low MEA content was observed as compared to the sample with high MEA content. The experimental peak positions with respect to the theoretical ones (2θ theoretical) and the relative intensities (I/I_o) of the ZnO powders were reported in Table (2). No preferred orientation is present for the two treated powders, in comparison with reference data. The mean crystallite sizes, D (nm) of both samples were estimated from XRD patterns using the full width at half maximum (FWHM) of the diffraction peak according to Scherrer's formula:

$$D = K\lambda / (FWHM) \cos\theta$$

where K=0.94 is the shape factor, λ is the X-ray wavelength (1.54 Aº for Cu) and θ is the Bragg angle of the diffraction peak. According to the values reported in Table (2), the reductions of crystallite size with the increase in the amount of MEA content in ZnO sample is observed.

Table VI-2. Crystallite size, the peak positions of reference ZnO (2θ theoretical) and the sample (2θ experimental), and the relative intensities of ZnO xerogel powders annealed at 400 ^{o}C for 4 h

	ZAD:MEA=1:0.5				**ZAD:MEA=1:1.34**		
hkl	2θ(th)	2θ(exp.)	I/I_o	D (nm)	2θ(exp.)	I/I_o	D (nm)
100	31.76	31.72	0.548	33.5±0.7	31.67	0.541	18.5±0.5
002	34.42	34.34	0.408	38.4±0.9	34.37	0.411	18.6±0.6
101	36.25	36.25	1.00	34.0±0.6	36.19	1.00	16.6±0.4

6.3 Characterization of multilayer ZnO films

To further investigate the effect of substrates and MEA content on the film properties, high magnification FE-SEM images of ZnO films were acquired on films deposited on soda-lime glass, silica glass, silicon wafer and platinum substrates. The FE-SEM study provided the detailed information about the morphology of coatings at a nanometric level in relation with the MEA content. The FE-SEM images of 8-layer ZnO films with ZAD: MEA = 1:0.5 deposited on soda-lime glass, silica, silicon wafer and platinum substrates are shown in Figure (13 a-d). All the FE-SEM images displayed spherical-shaped grains regardless of the nature of substrates. However, the quality of the layers depends on the nature of the substrates. Films deposited on soda-lime glass, silica and platinum show relatively uneven and less regular grain distributions (Figure 13 a-c). On the other hand, the films deposited on silicon wafer (Figure 13 d) reveal uniform and dense grain packing.

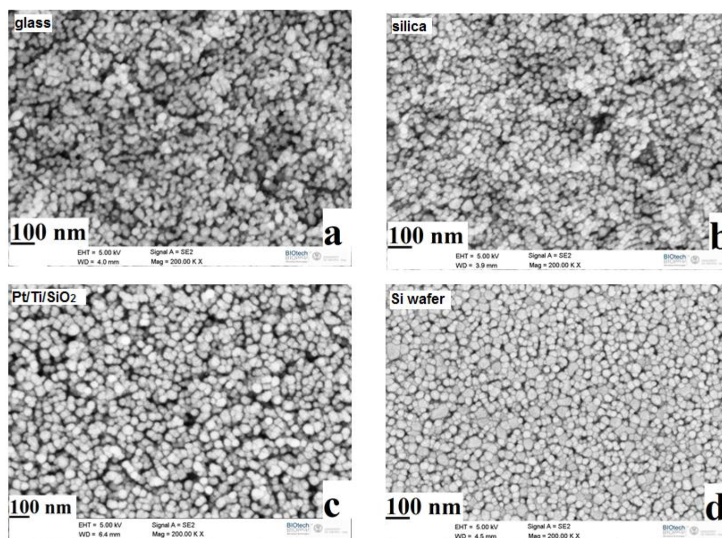

Figure VI-13. FE-SEM images of ZnO films prepared from ZAD: MEA ratio of 1:0.5 deposited on: a) soda-lime glass b) silica c) Pt/Ti/SiO_2 d) Si wafer substrate

Figure (14 a-d) shows FE-SEM images of ZnO films with ZAD to MEA ratio of 1:1.34 deposited on soda-lime glass, silica glass, platinum and silicon wafer substrates. The ZnO films coated on silica, platinum and silicon wafer show uniform grains. The film deposited on glass substrate (Figure 14 a) exhibits agglomeration of small grains. In the case of films deposited on silicon substrate with high MEA content (Figure 14 d), the particles are less densely packed compared to the films prepared from low MEA content (Figure 13 d). The coatings prepared on platinum substrates displayed round-shape particles with sizes of about 30-50 nm for both MEA contents, with a small increase in grain sizes with decreasing the MEA concentration in agreement with the trend pointed out by XRD for the crystallite sizes in the powders (Table 2).

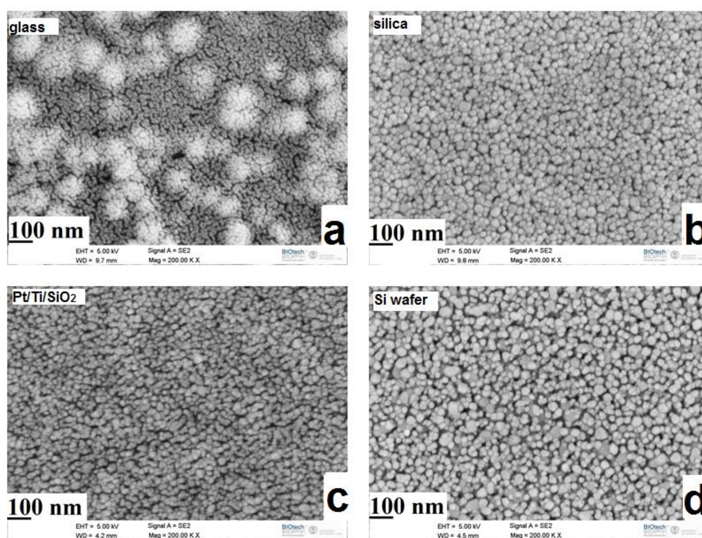

Figure VI-14. FE-SEM images of ZnO films prepared from ZAD: MEA ratio of 1:1.34 deposited on: a) soda-lime glass b) silica c) Pt/Ti/SiO_2 d) silicon wafer substrate

The thickness of the films was estimated by looking at the cross-sectional FE-SEM image. The thickness of 8-layered films coated on the glass substrate was found to be 140 nm from cross-sectional FE-SEM images as shown in Figure (15). Unfortunately,

it was not possible to acquire the cross-sectional image and consequently measure the thickness of the films deposited on the platinum substrate.

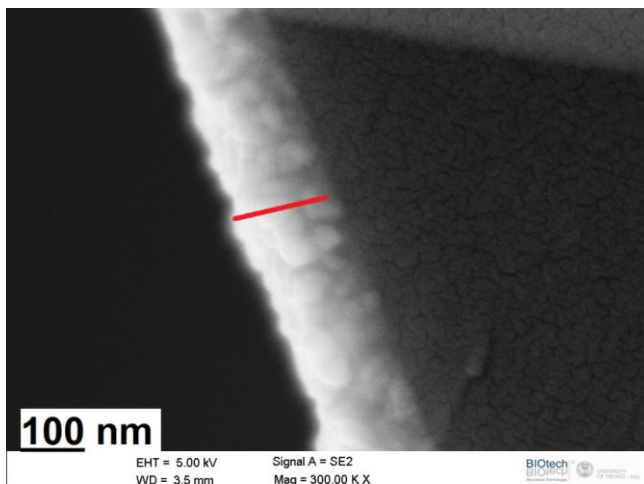

Figure VI-15. Cross-sectional FE-SEM image of ZnO films prepared from ZAD: MEA ratio of 1:1.34 deposited on soda-lime glass

Transmission measurements were recorded on 8-layered ZnO deposited on silica glass substrates in order to get more insight in the structural properties of ZnO films. The optical transmission spectra, acquired in the wavelength range from 200 nm to 1500 nm on bare silica glass substrate, and ZnO films deposited on silica glass substrate with ZAD to MEA molar ratio of 1:0.5 and 1:1.34, are presented in Figure (16). The transmittance is about 80 % in the visible region. The slight increase in transmittance observed for the films prepared with higher MEA content is probably due to the different thickness.

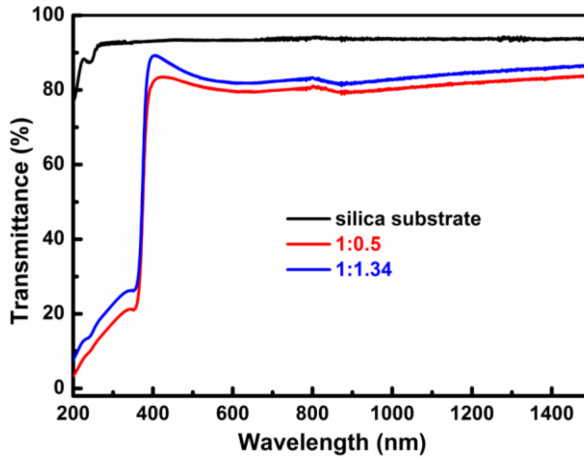

Figure VI-16. Transmission spectrum of bare substrate (black line) and ZnO sample with 1:0.5 (red) and 1:1.34 (blue) deposited on silica glass substrate

To estimate refractive index, porosity and thickness of the ZnO films from the optical spectra, “Point-wise Unconstrained Minimization Approach” (PUMA) software was used. Unfortunately, the PUMA analysis cannot be applied for analyzing the films deposited on silicon wafer and platinum substrates. Hence, the analysis was performed only on the ZnO films deposited on silica glass substrates. For the PUMA analysis, only the spectral region between 350 and 750 nm of the spectra was considered in order to estimate the thickness and the refractive index of the films. Figure (17) presents the experimental and the simulated transmission spectra of 8-layered ZnO samples prepared from ZAD to MEA of 1:0.5 and 1:1.34.

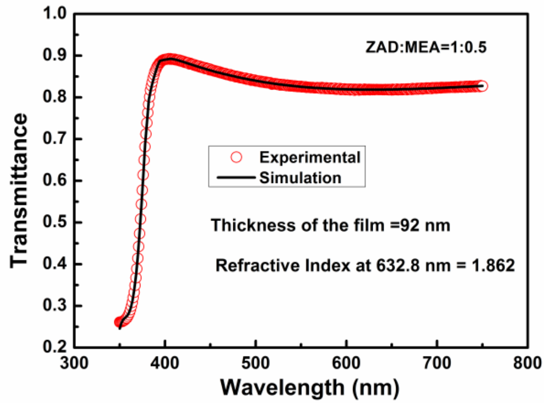

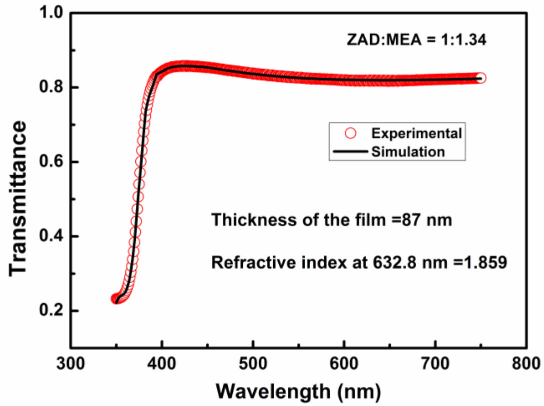

Figure VI-17. Transmittance spectrum of the samples (red line) and simulated transmission spectrum (black line) for the samples

The measured refractive index of the film, '*n measured'* is defined according to the following equation.

$$n\ measured = \frac{n\ reference * V\ reference + n\ air * V\ void}{V\ total} \qquad (6.1)$$

where *n reference* is the refractive index of the densified films taken as a reference, i.e 1.989 at 632.8 nm for ZnO. *V reference* is the volume of the densified film, *n air* is the refractive index of the air that is assumed to be equal to 1, *V voids* is the volume of the voids, and *V total* is the film total volume.

Porosity can be defined as

$$P = \frac{V\ voids}{V\ total} \qquad (6.2)$$

From equation (1),

$$P = \frac{n\ reference - n\ measured}{n\ reference - 1} \qquad (6.3)$$

The values of refractive index, porosity and thickness of both samples are reported in Table (3) and the results reveal that small differences derive from varying the MEA content in ZnO sol. The porosity of the films was slightly higher for the ZnO film prepared from high MEA. The estimated thickness of the 8-layered ZnO films was 87 and 92 nm for high and low MEA contents, respectively.

Table VI-3. Refractive index (n) and porosity and thickness of ZnO films of different composition deposited on silica glass substrate

ZAD:MEA	n	Porosity, P	Thickness (nm)
1:1.34	1.859	0.131	87
1:0.5	1.862	0.128	92

Figure (18) shows the micro-Raman spectra recorded on 8-layered ZnO films prepared with low (1:0.5) and high (1:1.34) MEA content and deposited on $Pt/Ti/SiO_2$ substrate. The peaks related to the ZnO phase appeared at 327 cm^{-1} and 435 cm^{-1} for both samples. The E_2 $^{(high)}$ mode at 435 cm^{-1} corresponds to the band characteristic of the wurtzite-like phase. The signal at 327 cm^{-1} is assigned to second order scattering E_2 $^{(high)}$ - E_2 $^{(low)}$ mode. The E_1 (LO) band at about 578 cm^{-1}, related to the presence of defects such as oxygen vacancy and zinc interstitial, suggesting relatively a very low defect density in the films. The peak intensity in the Raman spectrum of the sample prepared from lower MEA content (1:0.5) is relatively higher compared to the samples having higher MEA content (1:1.34). The intensity and shape of signals in the spectrum of ZnO films with lower MEA is the consequence of the improved crystallization, in agreement with the indications from other techniques.

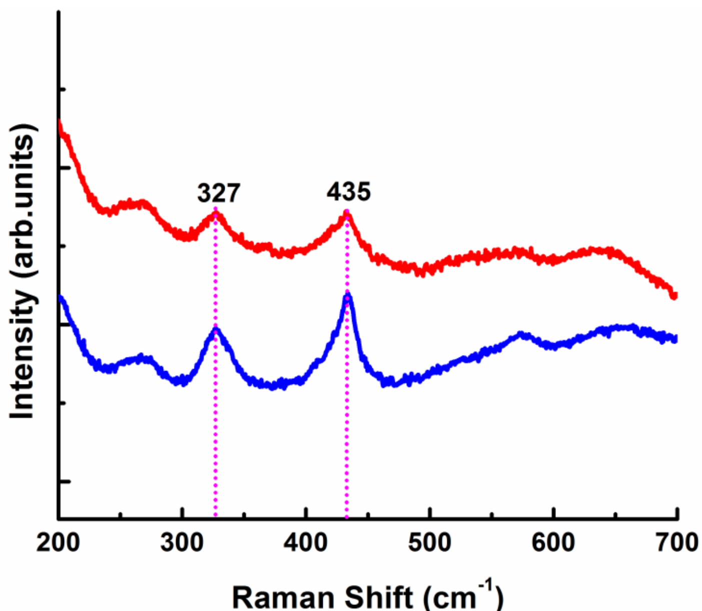

Figure VI-18. Raman spectra of 8-layered ZnO films on Platinum substrate, and prepared from ZAD to MEA molar ratio of 1:1.34 (red) and 1:0.5 (blue)

XRD analysis was first performed on 8 layers ZnO film deposited on soda lime glass substrate. Figure (19) shows XRD patterns recorded on ZnO samples prepared with ZAD to MEA of 1:1.34, preheated at 250 ^{o}C for 1 h and annealed at 400 ^{o}C either for 1 h or 4 h. The reason for running the annealing step at 400 °C for long time (4 h) was discussed in the previous section with the need to effectively remove organics residual and assist ZnO crystallization. For the films annealed for 1 h, the (002) signal of the XRD patterns is found at 34.24^{o}. On the other hand, the same peak in the films annealed for 4 h appears at 34.40^{o}, in good agreement with the theoretical peak position of ZnO (2θ = 34.42^{o} as reported also in Table (2)). In both samples, preferential growth is observed along (002) plane indicating that the films are oriented along c-axis perpendicular to the substrate.

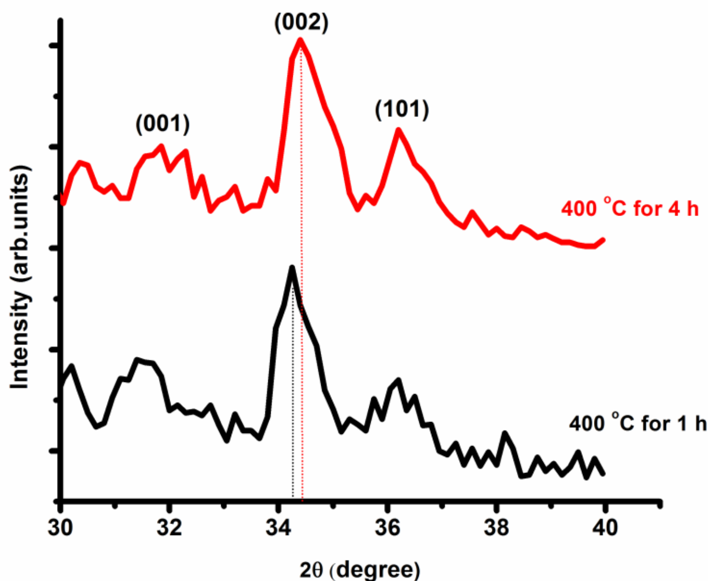

Figure VI-19. XRD patterns of 8-layered ZnO films deposited on soda lime glass substrate, and prepared from ZAD to MEA molar ratio of 1:1.34 annealed at 400 °C for 1 h and 4 h

Afterwards, the XRD traces were recorded on ZnO films prepared from different ZAD to MEA molar ratio and deposited on different substrates. All the samples used in this analysis were cured at 250 °C for 1 h and annealed at 400 °C for 4 h. Figure (20 a-d) shows the XRD patterns recorded on ZnO films prepared with ZAD to MEA molar ratio of 1:0.5, deposited on silica glass, soda-lime glass, Pt/Ti/SiO_2 and silicon wafer substrates. According to the (100), (002) and (101) diffraction peaks, the XRD traces showed in all cases the presence of crystalline ZnO in the wurtzite phase. The XRD patterns also showed the enhanced intensity of the (002) diffraction peak indicating preferential growth along the c-axis orientation (perpendicular to the substrate). The degree of preferential orientation was higher for the ZnO films deposited on Pt/Ti/SiO_2 substrate and particularly evident on silicon wafer substrates compared to films deposited on glass and silica substrates.

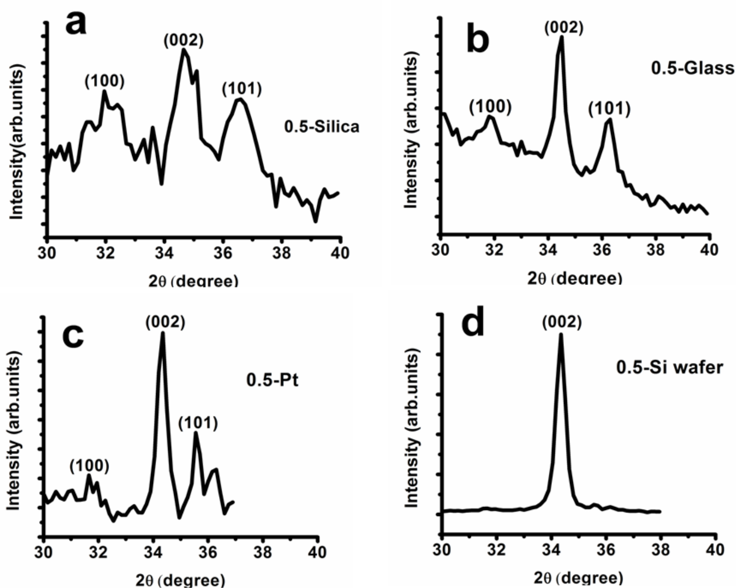

Figure VI-20. XRD patterns of 8-layered ZnO films prepared from ZAD to MEA molar ratio of 1:0.5 and deposited on a) silica b) soda lime glass c) Pt/Ti/SiO_2 d) silicon wafer substrate

The XRD traces recorded on ZnO films with high MEA content (ZAD to MEA ratio of 1:1.34) deposited on silica, soda-lime glass, silicon wafer and platinum substrates are shown in Figure (21). Similar results were obtained in terms of crystalline phase (wurtzite) relative intensities of (100), (002) and (101) diffraction peaks, pointing out again the preferential growth of the crystallites along the c-axis perpendicular to the substrate.

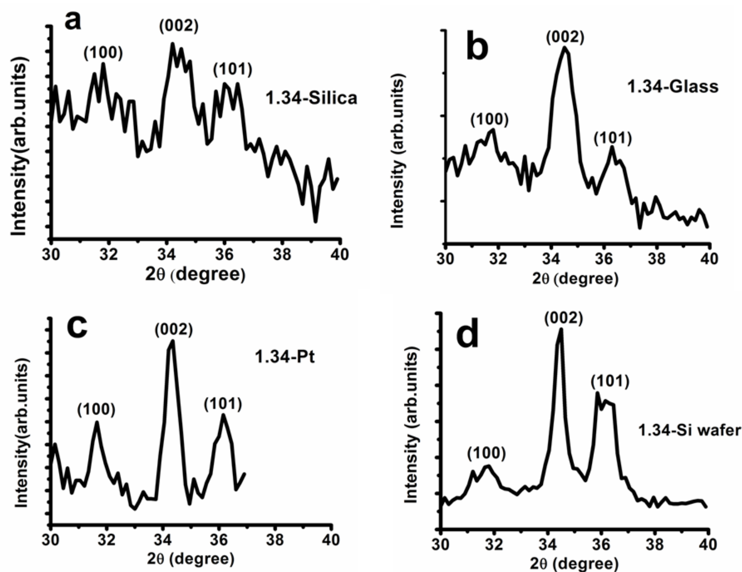

Figure VI-21. XRD patterns of 8-layered ZnO films prepared from ZAD to MEA molar ratio of 1:1.34 and deposited on a) silica glass b) soda lime glass c) Pt/Ti/SiO_2 d) silicon wafer substrate

Comparing the films prepared from low and high MEA content (Figure 20 and 21), relatively higher degree of preferential orientation on all substrates was observed in the case of lower MEA content in ZnO sol. In particular, XRD patterns of ZnO thin films with low MEA content deposited on silicon wafer (Figure 20 d) showed only the (002) diffraction peak.

As for powders, the mean crystallite size, D (nm) was estimated from XRD patterns according to Scherrer's equation. Due to the low signal to noise ratio of the XRD spectra acquired from the samples deposited on soda-lime glass and silica, the mean crystallite sizes (D, nm) can be calculated only for the films deposited on Pt/Ti/SiO_2 and silicon wafer substrates. The results are reported in Table (4).

Table VI-4. Crystallite size, D (nm) ZnO films with both high and low MEA content and deposited on a silicon wafer and platinum substrates.

	D(nm), (002)	
Substrate	**ZAD:MEA = 1:0.5**	**ZADMEA = 1:1.34**
Silicon wafer	25.1 ± 0.8	18.1 ± 1
$Pt/Ti/SiO_2$	23 ± 2	17 ± 2

With decreasing the ZAD to MEA ratio to 1:0.5, the crystallite dimensions increase for films both on $Pt/Ti/SiO_2$ and Si wafer substrates, in agreement with the trend observed for ZnO xerogel powders previously reported in Table (2).

The curing and annealing steps, optimized on the basis of the thermal and structural characterization of the ZnO samples, allow to produce multilayer films that were proved to be stable under the vacuum conditions required for the preparation of the memristor building block by deposition of dish-type top electrodes (as described in chapter V). However, new experiments were done in order to verify the possibility of using less time-consuming curing conditions and consequently improving the overall fabrication procedure. The next section presents the results obtained on the multi-layer ZnO films produced by changing the intermediate curing of each layer keeping synthesis conditions, number of layers and final annealing conditions constant. The new samples obtained with curing steps of 10 min at 300 ^{o}C are compared to the ZnO films cured at 250 ^{o}C for 1 h.

By observing the FE-SEM images presented in Figure (22), no substantial difference can be appreciated for the 8-layered ZnO films cured both at 250 ^{o}C for 1 h and 300 ^{o}C for 10 min after each layer deposition and finally annealed at 400°C for 4 h.

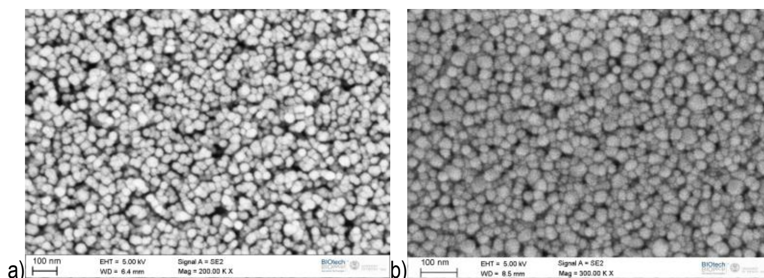

Figure VI-22. FE-SEM images of ZnO films cured at a) 250 °C for 1 h b) 300 °C for 10 min and finally annealed at 400°C for 4 h

A thorough investigation of surface morphology by AFM was also performed on the ZnO films treated with the two different curing steps (Figure 23).

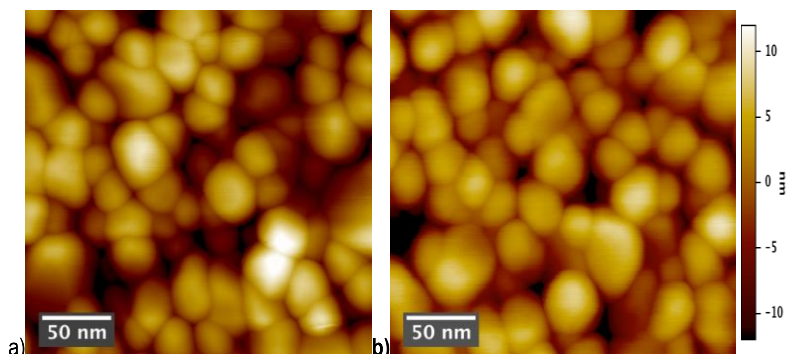

Figure VI-23. AFM images of ZnO films cured at a) 250 °C for 1 h b) 300 °C for 10 min

The average grain sizes of the films were 42.4 ± 4.7 and 30 ± 0.9 nm for the films cured at 250 °C and 300 °C, respectively. The surface roughness was also determined by the AFM analysis and the values are 4.9 ± 0.2 and 4.5 ± 0.2 nm for the films cured at 250 °C and 300 °C, respectively, showing no remarkable effects of curing on the surface roughness of the ZnO films.

The optical transmission measurements were also recorded on samples treated in both preheating conditions to determine the optical constants using "Point-wise Unconstrained Minimization Approach" (PUMA) software. Figure (24) presents the

simulated and transmission spectra of 8-layered ZnO samples deposited on silica substrates; cured at 250 °C for 1 h and 300 °C for 10 min.

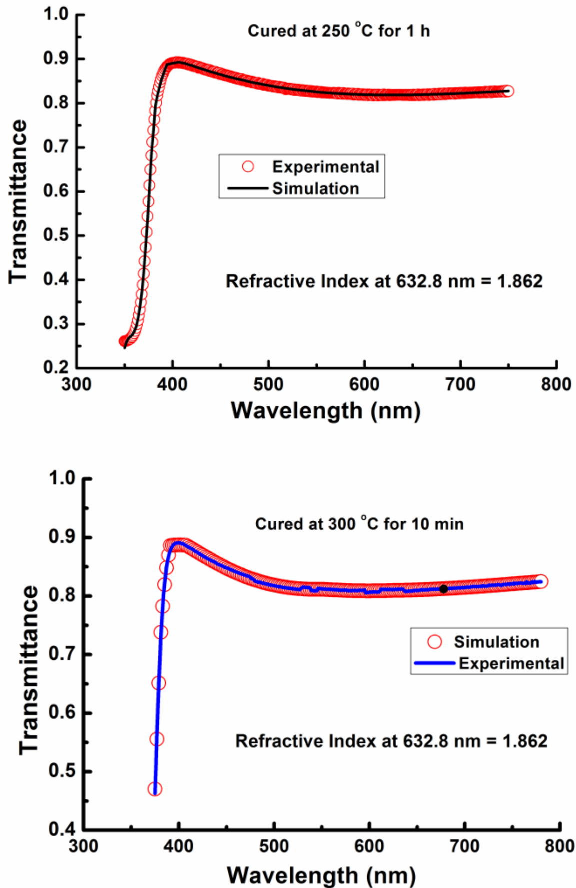

Figure VI-24. Transmittance spectra of the simulated and that of the ZnO samples cured at 250 °C for 1 h and 300 °C for 10 min

The values of refractive index, overall porosity and thickness of the samples are reported in Table (5). The refractive index and porosity of the ZnO films were determined using equation 6.1 and equation 6.3, respectively. The thickness of the 8-layered ZnO films was reduced by curing each layer at 300 °C. In general, the results reported in Table (5)

point out that less porous films were obtained for the ZnO films cured at 300 °C for 10 min compared to the sample treated at 250 °C for 1 h.

Table VI-5. Refractive index (n), porosity and thickness of ZnO films cured in different condition

Curing T (°C)	n	Porosity	Thickness (nm)
250	1.85	0.14	96
300	1.88	0.11	85

Micro-Raman measurements were performed on ZnO films cured at 250 °C for 1 h and 300 °C for 10 min. The spectra shown in Figure (25) present peaks related to the ZnO thin films at 326 cm^{-1}, 434 cm^{-1} and 578 cm^{-1}. Besides the already discussed $E_2^{(high)}$ mode at 434 cm^{-1} and $E_2^{(high)}$ - $E_2^{(low)}$ mode at 326 cm^{-1}, the peak at 578 cm^{-1} assigned to the longitudinal optical (LO) modes and attributed to defects such as oxygen vacancy and Zn interstitial increases in intensity.

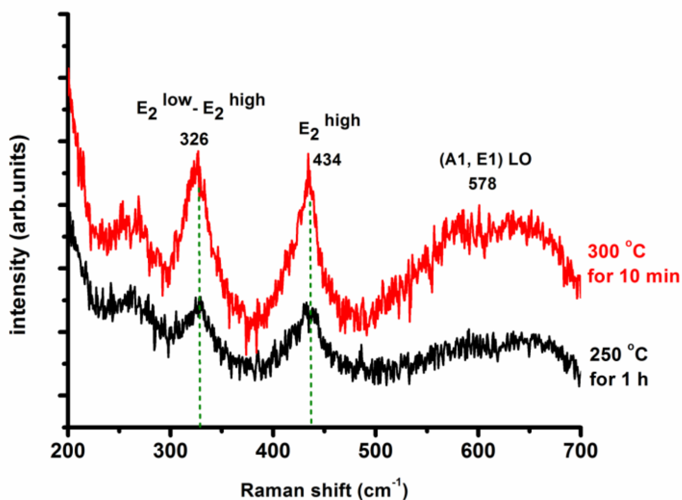

Figure VI-25. Raman spectra of ZnO films cured at 250 °C and 300 °C

For highlighting any possible change in structure, the XRD patterns were also recorded on a wide 2θ range on the films deposited on $Pt/Ti/SiO_2$ substrate and cured both at 300 °C for 10 min and 250 °C for 1 h (Figure 26). The patterns were analyzed using the Maud software, adopting a full-pattern quantitative modeling approach based on the Rietveld method. Both films were crystalline displaying the ZnO hexagonal wurtzite type structure. The broad signal in the diffraction angle range of about 20-30° corresponding to the amorphous silica glass (SiO_2) and the strong peaks attributed to platinum are a contribution from the $Pt/Ti/SiO_2$ substrate. The average crystalline domains dimension was determined by assuming an isotropic shape and a Lorentzian broadening model and implemented in the Maud software. The crystallite sizes were 18 nm and 15 nm for the samples cured at 250 °C and at 300 °C, respectively.

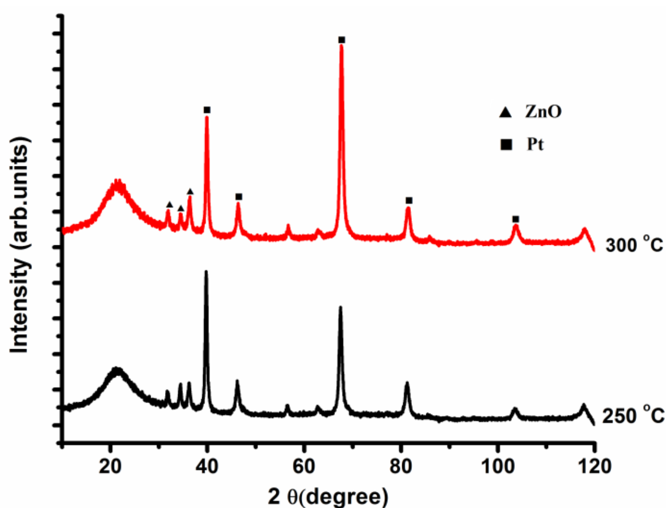

Figure VI-26. XRD patterns of ZnO thin films cured at 250 °C and 300 °C

In conclusion, the analyses performed on the ZnO films prepared with intermediate layer treatment at 300°C for 10 min assure that the less time-consuming curing steps do not substantially modify the morphological and structural features of the metal oxide layers and may be adopted in order to carry out a scaling-up of the ZnO film fabrication by sol-gel route.

6.4 Electrical characterization of the ZnO-based memristive building blocks

The electrical measurements were performed on ZnO films with a different number of layers deposited on Pt/Ti/SiO_2 substrate as a bottom electrode and different types of top electrodes.

Although both studied MEA contents in sol (ZAD to MEA molar ratio of 1:1.34 and 1:0.5) lead to the formation of valuable features in the structure of semiconductor film for memristive application, the lower concentration was chosen to fabricate the building block considering that both porosity and carbon-based contamination could be detrimental for the memristive response.

Initially, the measurements were performed on the films prepared from ZAD to MEA molar ratio of 1:0.5, cured at 250 ^{o}C for 1 h and annealed at 400 ^{o}C for 4 h. The fabrication of the memristor building blocks required that all the steps from film deposition to layer curing and to final film annealing have to be performed in a clean room. The availability of the clean room for long experimental procedures is a critical issue and therefore the experiments were run with ZnO films with a lower number of layers. Figure (27) shows I-V curves of a 4-layered ZnO sample deposited on Pt/Ti/SiO_2 as the bottom electrode and using the Ag-wire as the top electrode.

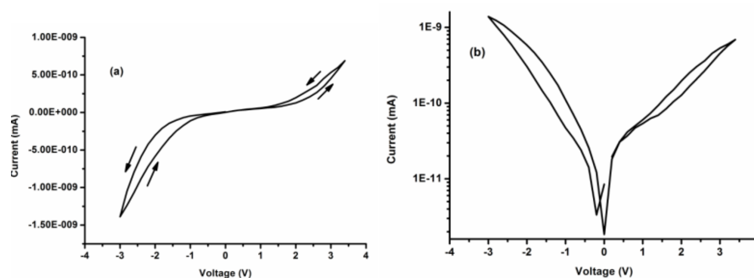

Figure VI-27. a) I-V characteristics of the 4 layered ZnO layers b) Log plots of I-V characteristics

The measurements were performed in voltage-controlled steps where the operation voltages were applied to the top Ag-wire electrode with the Pt/Ti/SiO_2 bottom electrode being grounded. The fabricated cell shows memristive switching behavior; the I-V plot indicates that the characteristic switching loop of a memristor is obtained with sweep

voltage between -3 V and 3.4 V. The I-V curves exhibit a pinched hysteresis loop centered at the origin, which is a fingerprint of the memristive switching behavior [119].

The memristive behavior of ZnO thin films with top electrodes of different nature was investigated more in detail. Since it was proved that the deposition of four layers with the optimized curing and annealing conditions led to the sufficient elimination of the defects, the 4-layer ZnO films on the Pt/Ti/SiO_2 substrate was again chosen for the fabrication of the memristive cell. Thus, the electrical measurements were performed on ZnO films prepared from ZAD to MEA ratio of 1:0.5 sandwiched between Pt/Ti/SiO_2 substrate as the bottom electrode and silver dishes deposited by electron beam evaporation as a top electrode (Figure 28).

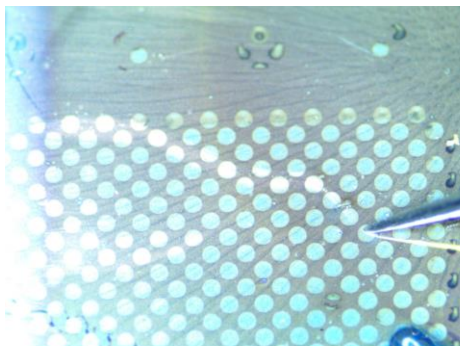

Figure VI-28. Optical microscopy image of the array of Ag dish electrodes deposited by electron beam evaporation

Figure (29) shows the I-V curves obtained from the ZnO-based memristive cell. Initially, a sweep 0V→-3V→0V→+3V→0V in a DC mode with a compliance current of 1 mA and 100 mVs^{-1} rate was performed. However, it showed the absence of any current flow through the ZnO layer. Therefore, the voltage window was increased and a sweep of 0V→-5V→0V→+5V→0V was carried out with 1 mA compliance and 167 mVs^{-1} rates (Figure 29 a). Initially, the semiconductor layer existed in the high resistive state (HRS, region 1). The SET was observed at around -0.8 V (region 2), reaching the compliance current and low resistant state (LRS, region 3), and finally, getting back to HRS (RESET, region 4). After that, the SET (region 6) was observed at around 2.5 V forming LRS

(region 7). The absence of RESET in the 1st sweep led to the conductive behavior of the cell during the 2nd and 3rd sweeps. More likely the formation of oxygen vacancies and Ag^+ filaments is responsible for the SET at the negative and positive voltages, correspondingly, by analogy with previously reported systems [120]-[121]. After that, the compliance current was adjusted to 20 mA with 167 mVs^{-1} scan rate, leading to the switching behavior displayed in Figure (29 b-d). Initially, the device displayed SET around -3.5 V (4th cycle, region 2) and the LRS was formed that experienced a RESET (region 5) during the 5th cycle. The following cycle number 6th was similar to the 5th one with a drift of SET and RESET positions. Since both SET and RESET voltage in a cycle are of the same polarity, the observed memristor behavior was attributed to the unipolar resistive switch [122] with a characteristic higher observed magnitude of RESET voltage compare to SET voltage.

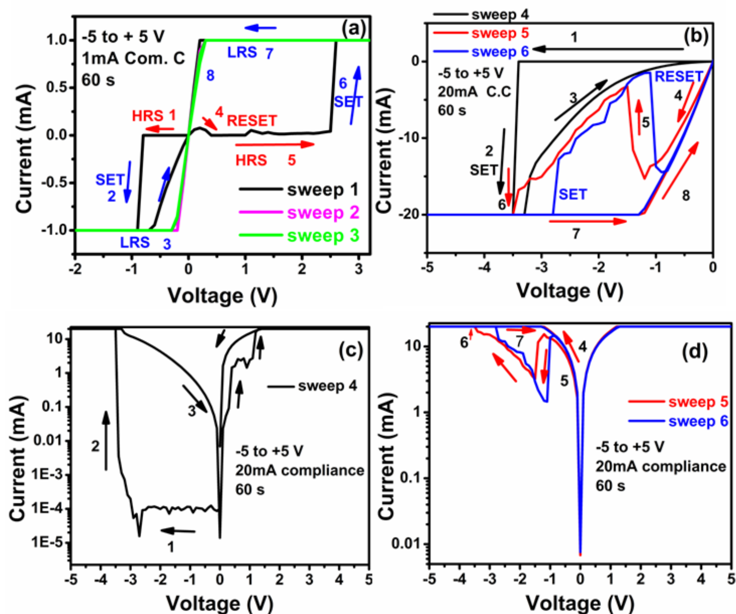

Figure VI-29. (a) I-V curves from 4 layers ZnO-based memristive cell with 1 mA compliance; (b) I-V curves from the memristive cell with 20 mA compliance; (c) logarithmic plot of the 4th sweep, (d) logarithmic plot of the 5th and 6th sweeps

Although the fabricated device displayed the memristive response, it lacks durability and reproducibility. Hence, some improvement approaches have been made here to improve the resistive switching responses of the ZnO thin layers. An improvement could be achieved by substituting the electrochemically active electrode (Ag-dish top electrode) by Pt-dishes that will open an opportunity to simplify the switching mechanism, leading to the more predictable charge carriers competition-free device. Moreover, the intermediate curing between each layer was changed to 300 °C for 10 min by keeping the final annealing temperature to 400 °C for 4 h. In the final building blocks that have been analyzed in this work, the number of layers was also increased from four to eight. Hence, the electrical measurements were performed on 8-layered ZnO films sandwiched between Pt-dishes as a top electrode and Pt/Ti/SiO_2 substrate as a bottom electrode. The current-voltage (I-V) characteristics of a Pt/ZnO/Pt/Ti/SiO_2 memristive cell were acquired in the presence of LED light in order to observe any possible change in the memristive cell. A current compliance (CC) of 15 mA was selected to avoid permanent breakdown of the memristive cell and no damage to the top electrode was observed during the measurement. Figure (30 a) shows I-V curve of the Pt/ZnO/Pt/Ti/SiO_2 memristive cell smoothly swept between -2V and 3 V for 10 cycles.

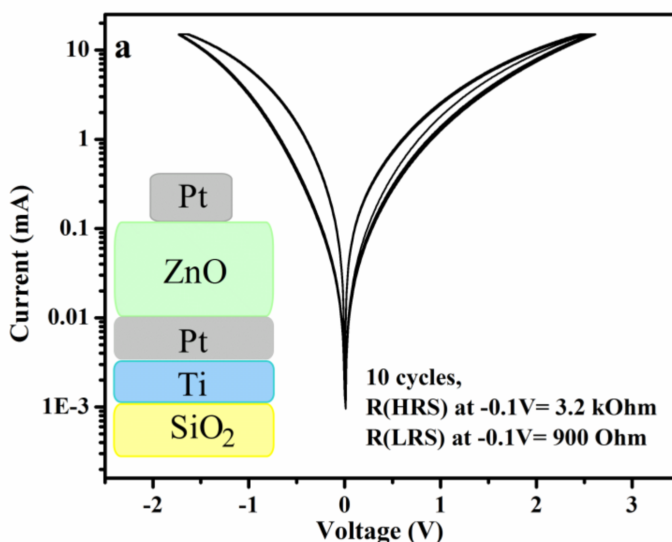

a)

b)

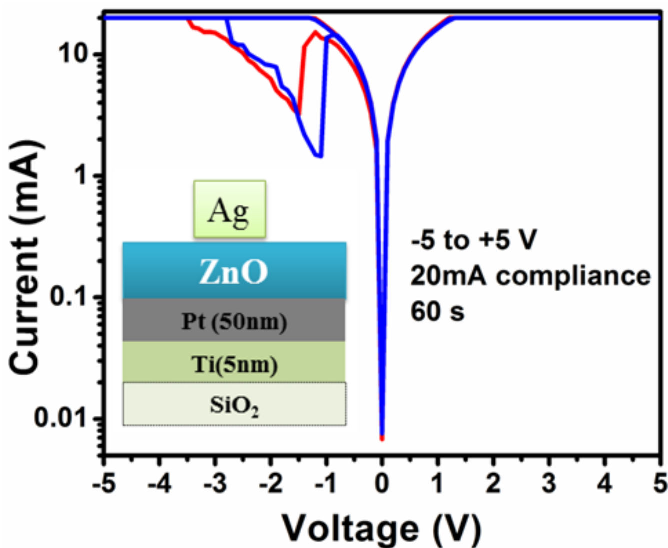

Figure VI-30. (a) I-V curves of 8-layers ZnO thin films cured at 300 °C for 10 min and annealed at 400°C for 4 h (Pt/ZnO/Pt/Ti/SiO_2 structure), (b) schematic device structure (inset) of 4-layers ZnO films with Ag-dishes as top electrode (Ag/ZnO/Pt/Ti/SiO_2 structure) cured at 250 °C for 1 h and its I-V characteristic curve

The I-V curves exhibit a pinched hysteresis loop centered at the origin [119], displaying unipolar switching. High resistance state (HRS) and low resistance state (LRS) were set at -0.1V; and the resistance values are 3.2 kΩ and 900 Ω, respectively. No electroforming process was required for the Pt/ZnO/Pt memristive cell; and according to the literature, this behavior could be attributed to pre-existing electronic charge carriers such as oxygen vacancies in the ZnO layers [123]. Indeed, the observed intensity of the band at 578 cm^{-1} in the Raman spectrum of the ZnO film prepared with intermediate curing at 300°C (Figure 25) supports this hypothesis.

Moreover, the observed asymmetric switching response observed in Ag/ZnO/Pt structure (Figure 30 b) suggests the device is a non-ideal memristor [2]. This behavior may be attributed to the asymmetrical nature of the device structure resulting from the different nature of electrodes and uneven distribution of the possible charge

carriers within the oxide layer. Changing the memristive cell structure by replacing Ag top electrode with Pt-dishes showed stable and uniform switching cycles. This could possibly be due to the uniform formation and rupture of the conducting filaments when inert top electrode is used; resulting from the absence of the competing charge carriers coming from the reactive Ag-dishes. It is reported in a literature [19] that stable response with narrow dispersion of the resistance states and switching voltages was acquired from ZnO films prepared by RF magnetron sputtering with symmetric Pt/ZnO/Pt stack structure. A forming process was however required to initiate the switching property of the memristive cell.

Compared to the Ag/ZnO/Pt structure (Figure 30 b), the acquired stable response and uniformity of the switching cycles in Pt/ZnO/Pt memristive cell structure shown in Figure (30 b) exhibited promising resistive switching characteristics. In general, by changing number of layers, intermediate curing and top electrode, a more stable response with lower compliance current (15 mA) was obtained compared to the one obtained with 20 mA and previously discussed for the 4-layers Ag/ZnO/Pt (Figure 30 b) memristive cell.

Chapter VII

Results and Discussions (II): Doping of ZnO

In order to obtain reproducible current-voltage switching cycles with the absence of short circuits, the obtained layers should be dense, free of holes and cracks and have a constant thickness through the films. Accordingly, emphasis should be given in the production of dense and defect-free ZnO layers for memristive applications by optimizing both synthesis and processing conditions. In addition to changing the curing conditions and the top metal electrode, the possibility to modify the functional oxide layer should also be considered.

In this chapter, doping of ZnO, which is expected to affect the morphological and structural properties of the ZnO layer, will be presented as one of the several modification approaches proposed to modify the resistive switching performance of ZnO thin films.

In the following two sub-sections, the sol-gel preparation of Mg and Al-doped ZnO xerogel powders and thin films and the effect of doping and curing conditions on morphological, structural and electronic properties will be discussed, in relation to the possible impact on the memristive switching performance of ZnO layers. The introduction of Mg can contribute in tailoring the band gap of ZnO. The ionic radius of Mg^{2+} is close to that of Zn^{2+}, and replacement of Zn by Mg consequently is expected to cause no significant change in the final structure. The electrical properties of ZnO layers depend on the concentrations of the possible charge carriers including the contributions from the Al^{3+} on substitutional sites of Zn^{2+} ions, Zn and Al interstitial atoms and oxygen vacancies. Moreover, an addition of Al^{3+} ions to Zn^{2+} sol solution is expected to increase the number of nucleation sites, resulting in higher grain boundary density and the formation of smaller grains [54]. Grain boundaries are anticipated to improve memristive switching process [9] by providing sites with defect aggregation and a conductive path formation, as previously highlighted in the introduction section. The two dopant elements have been then chosen mainly taking into account the ionic radius (that is similar to that of zinc in the case of Mg and smaller in the case of Al) and the electronic properties, besides the suitability and the availability of precursors for sol-gel syntheses.

7.1 Mg-doped ZnO samples

To investigate the thermal behavior of undoped and Mg-doped ZnO xerogel powder samples, thermal analysis were performed on xerogel powders samples. The combined TGA/DSC patterns of 0.5 and 1 % Mg-doped ZnO samples, cured at 300 °C, are presented in Figure (1). The weight loss step up to 100 °C corresponds to the removal of adsorbed water, while the major weight loss is due to the decomposition of residual organics. The total weight loss calculated for 0.5 % and 1 % Mg-doped ZnO samples were 10 and 17 %, respectively. At this moment, it was not possible to give a clear explanation of the different weight loss observed. The DSC plots present endothermic peaks below 200 °C mainly attributable to water evaporation, whose intensity is higher for the 1 % Mg-doped sample. As discussed in the previous section, the broad exothermic effects observed in the DSC traces at about 400 °C and resulting from organics removal, appear overlapped to the sharp peaks attributed to the crystallization of ZnO. These peaks are found at 386 °C for both 0.5 and 1 % Mg-doped samples. The thermal behavior of the doped samples cured at 250 °C (not shown here) is similar besides the slight difference in weight losses.

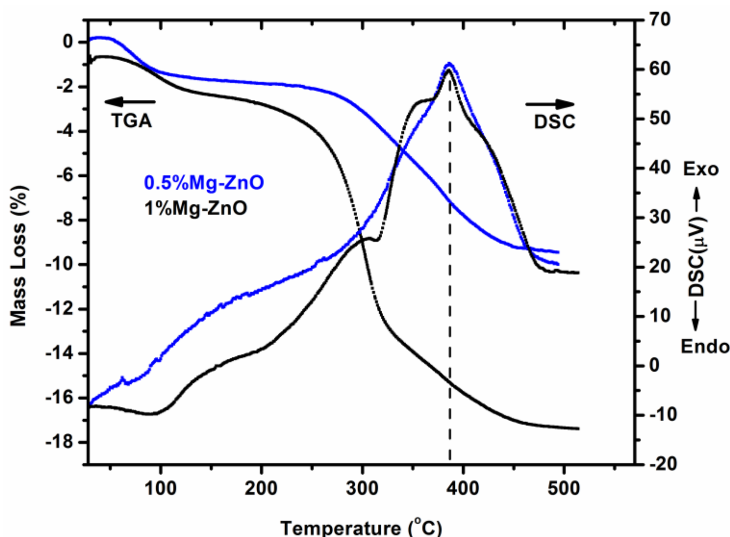

Figure VII-1. Thermal analyses plots of undoped and Mg-ZnO xerogel powders samples: 0.5 % Mg-ZnO cured at 300 °C (blue) and 1 % Mg-ZnO cured at 300 °C (black)

Figure (2 a) shows the FT-IR spectra of Mg-doped ZnO xerogel powders thermally treated at 300 ºC for 10 min compared to the spectrum of the undoped ZnO sample. As discussed in chapter VI, the spectra are dominated by the contribution of MEA and acetate groups but no significant differences can be found between doped and undoped ZnO powders. After annealing at 400 ºC for 4 h (Figure 2 b), the signals corresponding to the organic residuals are reduced but still observable in doped samples together with the peak corresponding to the Zn-O stretching mode (435 cm^{-1}).

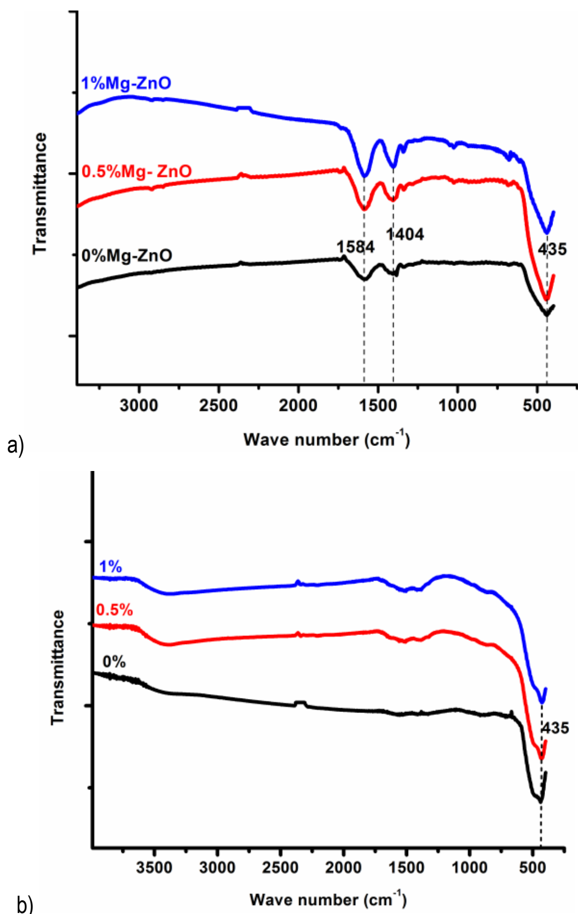

Figure VII-2. FT-IR spectra of undoped, 0.5 and 1% Mg-ZnO powders (a) thermally treated at 300 ºC for 10 min, and (b) annealed at 400 ºC for 4 h

Figure (3 b-c) shows the high magnification FE-SEM images acquired on the 0.5 at % and 1 at % Mg-doped ZnO thin films cured at 250 °C for 1 h. The increase in roughness and inter-grain porosity was observed for the Mg-doped films in comparison with the undoped ZnO films (Figure 3 a).

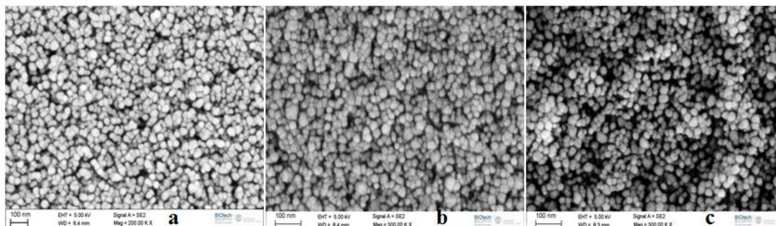

Figure VII-3. FE-SEM images of the Mg-doped ZnO films cured at 250 °C: a) 0% b) 0.5 % c) 1%

A further increase in surface inhomogeneity and roughness is observed for the Mg-doped thin films (Figure 4 b and c) cured at 300 °C in comparison with the undoped sample (Figure 4 a) and with respect to the analogous samples cured at 250 °C (Figure 3 b and c). The presence of large inter-grain surface porosity is particularly evident in the case of 1 % Mg-doped ZnO (Figure 4 c).

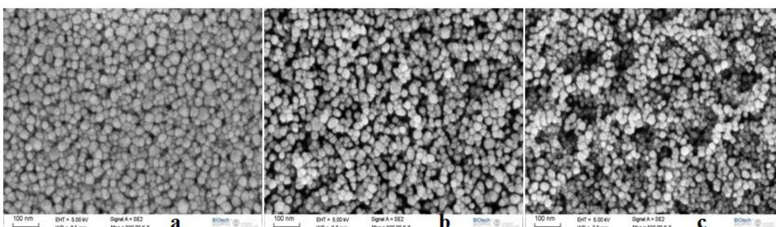

Figure VII-4. FE-SEM images of the Mg-doped ZnO films cured at 300 °C: a) 0 % b) 0.5 % c) 1 %

Figure (5 a-d) shows the AFM images of the Mg-doped ZnO films cured both at 250 °C and 300 °C. The values of the surface roughness and the parameter related to the lateral grain dimension are reported in Table (1), compared to the values obtained for pure ZnO films (Chapter VI).

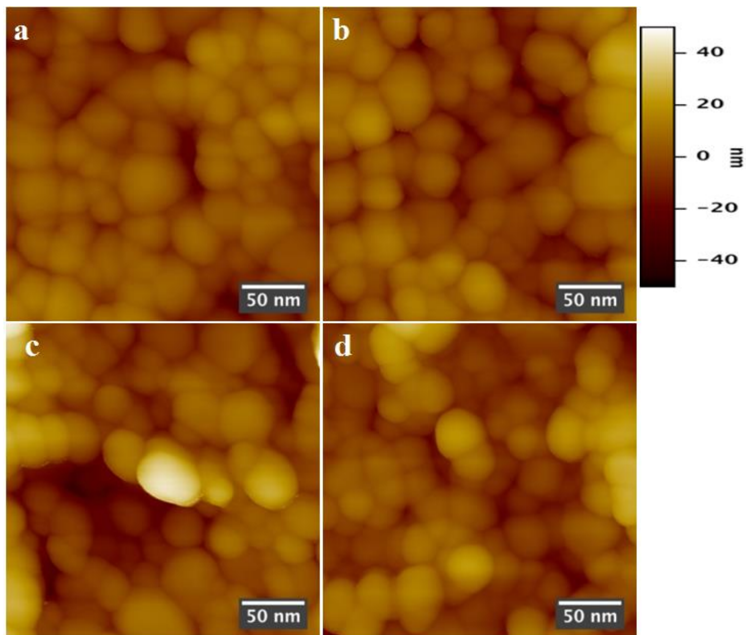

Figure VII-5. AFM image of Mg-doped ZnO films a) 0.5 % and b) 1 % cured at 250 °C; c) 0.5 % and d) 1 % cured at 300°C °C

Table VII-1. Surface roughness, R (nm) and equivalent lateral diameter (nm) of undoped and Mg-doped ZnO thin films cured at different conditions.

Curing T (°C)	Mg (at. %)	R (nm)	Equivalent diam. (nm)
	0	4.9 ± 0.2	42 ± 4
250	0.5	6.5 ± 0.4	45 ± 4
	1	10 ± 1	62 ± 16
	0	4.5 ± 0.2	30.5 ± 0.9
300	0.5	19 ± 5	53 ± 8
	1	10.3 ± 0.6	64 ± 21

Increasing the Mg content leads to a general increase in surface roughness and grain sizes. However, from the results reported in Table (1), it is difficult to assess the trend of the grain size due to high errors reported from the analysis.

In order to have information on the chemical composition of the doped films, the XPS spectra were collected on 0.5 % and 1 at % Mg-doped ZnO films, cured at either 250 °C or 300 °C.

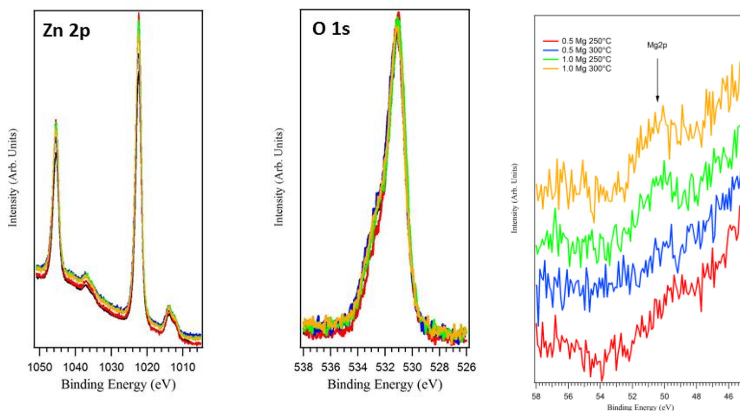

Figure VII-6. XPS Zn2p, O1s and Mg 2p core level spectra

The Zn 2p spectra present two major peaks identified as Zn 2p3/2 and Zn 2p1/2, as shown in Figure (6) and do not show changes with respect to the level of Mg doping for both curing conditions. The same behavior is observed in the case of O 1s spectra (Figure 6). The Mg 2p core levels are detectable in all Mg-doped ZnO films and the corresponding signals show an increase in intensity according to the nominal amount of Mg doping (Figure 6). From the survey spectra no contaminations are detectable except adventitious carbon (C 1s signal).

As reported in chapter I, the band gap of ZnO can be tailored by doping ZnO with Mg considering that the radius of the Mg^{2+} ion (72 pm) matches with the radius of Zn^{2+} ion (74 pm) and makes the incorporation of Mg^{2+} ion into ZnO lattice feasible. Therefore, the UPS spectra were recorded with the aim of calculating the work functions (WF) of the doped samples. The plots are displayed in Figure (7) and the values of the calculated work functions are summarized in Table (2).

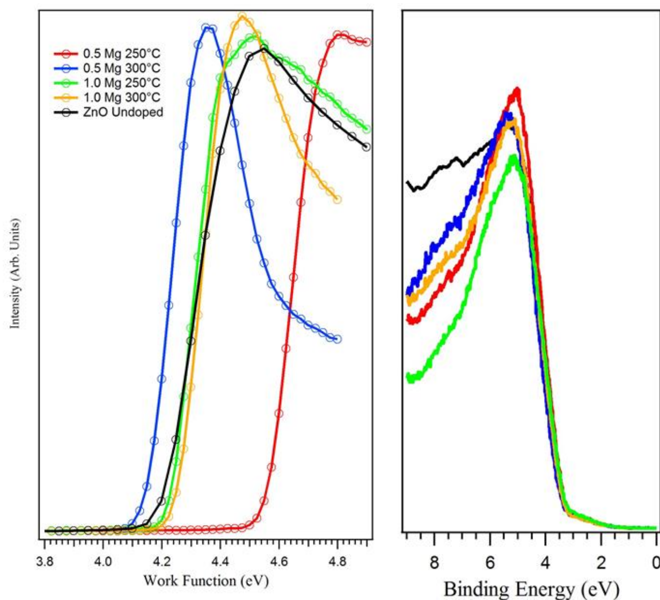

Figure VII-7. Work function (WF) of undoped and Mg-doped ZnO

The shifts in work function with respect to undoped ZnO samples (the WF value is the same for both curing at 300 and 250°C) are found to be incoherent with the Mg dopant atomic percentage. As shown in the figure, the work function shift suggests a p-type doping for the films doped with 0.5 % Mg and cured at 250 °C. On the other hand, the samples cured at 300° seem to induce a small n-type doping. The values of the work function for samples doped with 1 % Mg are not affected indicating that no effective doping was detected regardless of the curing conditions. The inconsistency may be related to the samples, and a further study with different batch of samples is needed to elucidate the Mg effect. No further conclusion can be drawn at this stage. Moreover, all the samples are found to be stoichiometric (Zn/O = 1) regardless of the doping level, as reported in Table (2).

Table VII-2. Work function of undoped and Mg-doped ZnO

Sample	Work Function, WF(eV)	On-Set (eV)	Stoichiometry (Zn/O)
0% - 300	4.20	3.40	~1 ± 2%
0.5% - 250	4.55	3.40	~1 ± 2%
0.5% - 300	4.15	3.40	~1 ± 2%
1% - 250	4.20	3.40	~1 ± 2%
1% - 300	4.25	3.40	~1 ± 2%

Figure (8) shows the XRD patterns recorded on all the undoped and Mg-doped ZnO films deposited on $Pt/Ti/SiO_2$ substrate. XRD data were analyzed using the Maud software, adopting a full-pattern quantitative modeling approach based on the Rietveld method. The XRD patterns of the films displayed no difference regardless of the curing conditions.

As reported in chapter VI, the broad signal of the silica glass (SiO_2) and the strong peaks attributed to platinum are a contribution from the $Pt/Ti/SiO_2$ substrate. All the films were crystalline displaying the ZnO hexagonal wurtzite type phase. Only ZnO-related peaks were observed and no other signals related to MgO or Mg was detected. Thus, the films do not present any phase segregation or secondary phase formation.

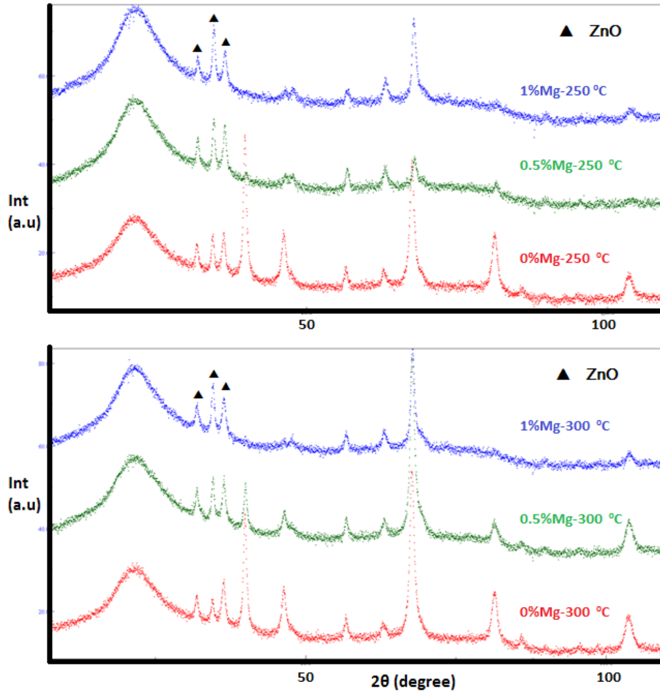

Figure VII-8. XRD patterns of Mg-doped ZnO thin films cured at 250 °C for 1 h (top) and 300 °C for 10 min (bottom)

The average crystalline domain sizes were determined by assuming an isotropic shape and a Lorentzian broadening model (implemented in the Maud software). The crystallite domains for the undoped, 0.5 % and 1 % Mg-doped films cured at 250 ºC are 17.7 nm, 26.1 nm and 29.1 nm, respectively. Likewise, the corresponding crystallite sizes are 15.2 nm, 28.7 nm and 24.6 nm for the undoped, 0.5 % and 1 % Mg-doped films cured at 300 ºC. In both cases, doping with Mg was found to increase the crystallite size.

In summary, FE-SEM and AFM observation together with XRD results display that doping with Mg has a relevant effect on the microstructure of the ZnO films. The grain sizes of the Mg-doped ZnO layers are larger compared to the undoped samples, regardless of the curing conditions and the film surface roughness increases, in particular for the samples cured at 300 ºC. Moreover, the calculated work functions do not point out

a clear effect of Mg doping on the ZnO band gap. These results point out that Mg doping negatively affects the microstructure of the ZnO films, introducing severe restrictions to the fabrication of memristive cells, in particular concerning the electrode deposition onto the layers.

7.2 Al-doped ZnO samples

7.2.1 Effect of dopant precursor

The first Al-doped samples were prepared using aluminum nitrate nonahydrate (Al $(NO_3)_3.9H_2O$) as a dopant precursor. The morphological features of the 0.5 % Al-doped ZnO films deposited on soda lime glass, silica glass, silicon wafer and $Pt/Ti/SiO_2$ substrates, obtained with intermediate curing at 250 °C for 1 h and annealing at 400 °C for 4 h, were analyzed by FE-SEM (Figure 9 a-d).

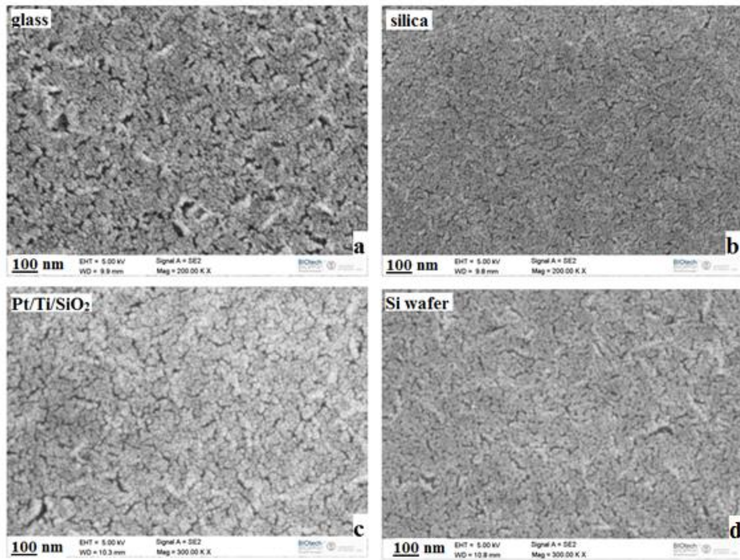

Figure VII-9. FE-SEM images of 0.5 % Al-doped ZnO films deposited on: a) soda-lime glass b) silica glass c) $Pt/Ti/SiO_2$ d) silicon wafer substrate

In general, the film surface appears quite smooth and homogenous, presenting a decrease in grain size upon doping with Al compared to the undoped ZnO films shown in Figure VI-13(a-d).

The FTIR analysis was performed on the corresponding Al-doped ZnO powders (Figure 10). The spectra appear very similar to those acquired on undoped ZnO powders but residual broad peaks in the range 1600-1400 cm^{-1} are still observable at 400 °C, contrariwise to the case of undoped ZnO (Figure VI-10) and similarly to the results obtained with Mg-doped samples, which were also prepared starting from the metal nitrate.

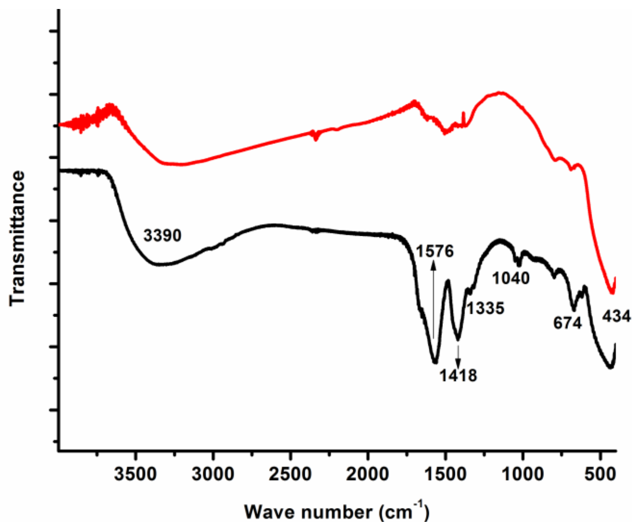

Figure VII-10. FTIR spectra of Al-doped ZnO powders prepared using Al $(NO_3)_3.9H_2O$ as a dopant precursor; thermally treated at 250 °C for 1 h (black) or 400 °C for 4 h (red)

The XRD analysis performed on 0.5 and 1 at % Al-doped ZnO powders treated in air atmosphere at 400 °C for 4 h is shown in Figure (11). The spectra are displayed in the indicated range for comparison with the results for undoped ZnO powders, presented in Figure VI-12.

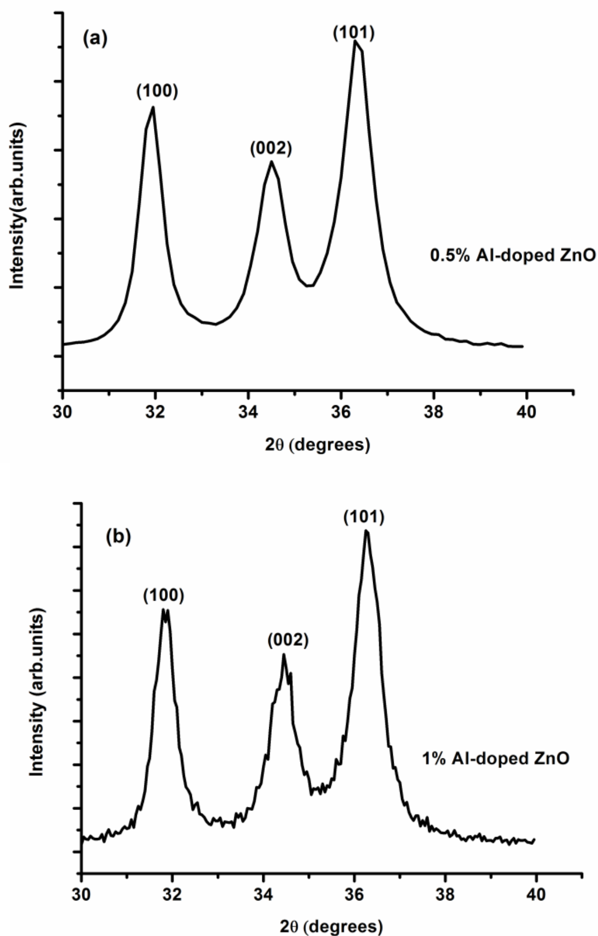

Figure VII-11. XRD traces of a) 0.5 at %; and b) 1 at % Al-doped ZnO powders annealed at 400 ^{o}C for 4 h

In both cases, the signals are consistent with the presence of pure ZnO. The average crystallite sizes were estimated and the results are reported in Table (3). The values reveal that the crystallite sizes (Table 3) are unaffected by increasing Al concentration from 0.5 to 1 at %. However, it is worth of noting that Al-doped ZnO samples display lower crystallite sizes than those of undoped ZnO powders (Table VI-2).

Table VII-3. Crystallite size, D (nm) of Al-doped ZnO powders annealed at 400 °C for 4 h

	D (nm)	
hkl	**0.5 at. %**	**1 at. %**
100	14.8 ± 0.9	15.2 ± 0.8
002	14 ± 2	13 ± 1
101	13 ± 1	12.8 ± 0.9

Despite the good solubility of aluminum nitrate nonahydrate as well as the positive effect observed in modifying the grain size and the morphology of the films, the presence of nitrogen derived from the Al precursor (Al $(NO_3)_3.9H_2O$) could affect the final properties of the films. Indeed, the drawback of using inorganic precursors like nitrates is related to the retention of anionic species after thermal treatment. Nitrogen is among the acceptor impurities that substitute for oxygen [131] in ZnO due to both atomic size and electronic structure and therefore can alter the electrical properties of the final active layer.

Accordingly, a different Al precursor was employed and new Al-doped ZnO samples were prepared from aluminum isopropoxide ($[(CH_3)$ $CHO]_3Al$. The thermal behavior was studied on the 0.5 % Al-doped powders (Figure 12) and appears almost identical to that of the undoped sample. In analogy to the TGA trace of pure ZnO, the TGA plot reveals two weight loss steps leading to total weight loss of about 7 %. The organics decomposition together with the sharp exothermic peak due to the ZnO crystallization is observed from the DTA curve at about 390 °C. As observed for undoped ZnO, changing the curing conditions (from 300 °C to 250 °C) does not substantially affect the thermal behavior.

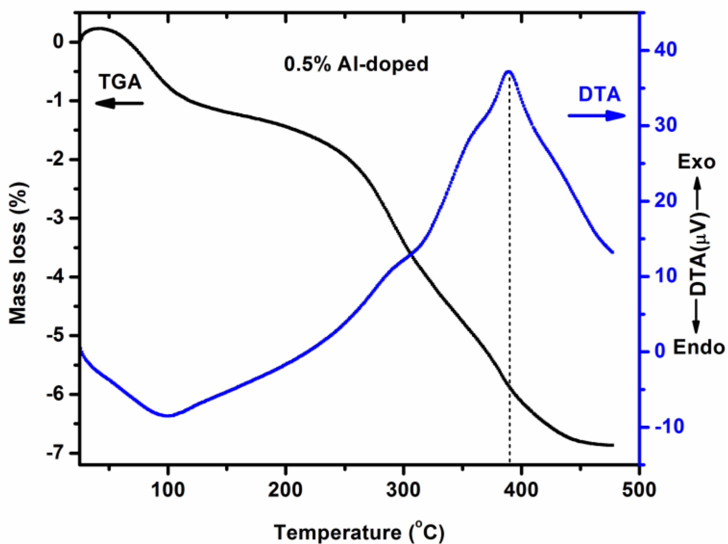

Figure VII-12. TG/DTA plot of 0.5 % Al-doped ZnO powders cured at 300 °C

The FTIR survey (Figure 13) run on the annealed Al-doped ZnO powders, regardless of the curing conditions, showed improved efficiency in removing the residual organics at the final annealing condition, similarly to the case of the undoped ZnO samples.

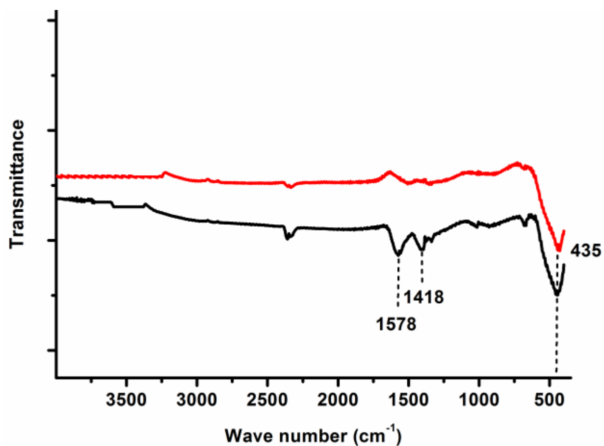

Figure VII-13. FTIR spectra of 0.5 % Al-doped ZnO powders cured at 300 °C for 10 min (black) and annealed at 400 °C for 4 h (red)

According to the results of powder characterization, the curing and annealing conditions used for undoped ZnO can be applied to the Al-doped ZnO samples. The analysis of film morphology was conducted first on 8-layered Al-doped ZnO films deposited on Pt/Ti/SiO_2 substrates, cured at 250 °C for 1 h and annealed at 400 °C for 4 h. Figure (14 a-c) shows the comparison of the FE-SEM image acquired on undoped ZnO with the images of 0.5 at % and 1 at % Al-doped ZnO films (as reported in chapter V, the images were obtained with a different microscope).

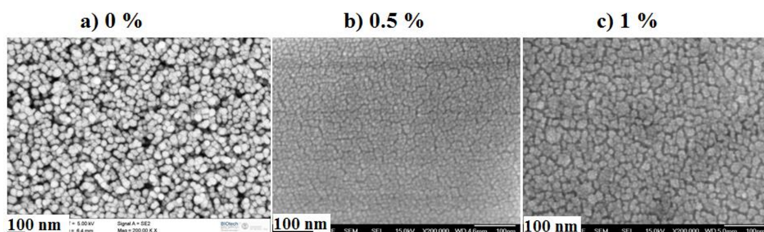

Figure VII-14. FE-SEM images of the undoped, 0.5 % and 1 % Al-doped ZnO films cured at 250 °C and annealed at 400 °C

The effect of Al-doping on the surface morphology is clearly observable in the case of 0.5 % Al addition (Figure 14 b) that leads to a very smooth surface with decrease of inter-grain porosity and grains sizes of about 10 nm. Besides the relative increase in grain size up to approximately 25 nm observed with 1 % Al-doped films (Figure 14 c), compared to the average size of 40 nm detected for undoped ZnO (Figure 14 a), the positive effect of the Al addition on the film surface features is confirmed.

In agreement with the FE-SEM study, the AFM analyses recorded on Al-doped ZnO films cured at 250 °C for 1 h and annealed at 400 °C for 4 h confirm the reduction of the grain size upon doping with 0.5 % Al, compared to the undoped or 1 % doped films (Figure 15 a-c).

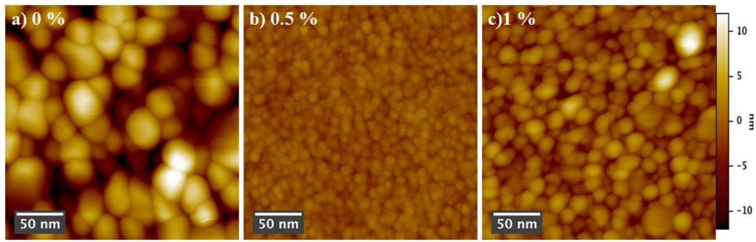

Figure VII-15. AFM images of the undoped, 0.5 % and 1 % Al-doped ZnO films cured at 250 ^{o}C and annealed at 400 ^{o}C for 4 h

The decrease in the grain size with Al doping has been already reported in the literature and ascribed to the role of the dopant element as a microstructural modifier, providing fine and uniform grains [124]. As a consequence, the most relevant effect of Al doping is the achievement of very smooth film surfaces, according to the values of roughness reported in Table (4). Roughness and grain sizes show a dependence on Al load, slightly increasing as the dopant level increases from 0.5 to 1 % Al.

Table VII-4. Roughness and equivalent diameter of undoped, 0.5 % and 1 % Al-doped ZnO films cured at 250 ^{o}C

Al (at. %)	**Roughness (nm)**	**Equivalent diam. (nm)**
0	4.9 ± 0.2	42.4±4.7
0.5	1.0 ± 0.1	11.3±0.6
1	2.3 ± 0.1	17.4±0.6

For a complete comparison of the structural parameters studied on undoped ZnO samples, optical transmission measurements were also performed on the Al-doped samples deposited on silica glass substrates. The transmission spectrum for 0.5 % Al-doped films is presented in Figure (16). By means of the PUMA software (equation 6.1 and 6.3), film thickness, refractive index and porosity were calculated from the transmission spectra (Table 5).

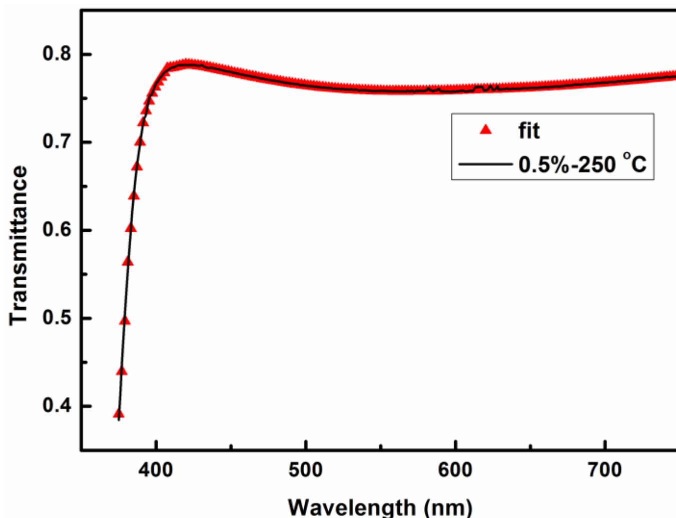

Figure VII-16. Transmittance spectra of the 0.5 % Al-doped ZnO samples cured at 250 °C for 1 h

Al- doped films display thickness from 75 nm to 90 nm, with values of the refractive index higher than the undoped ZnO. Moreover, the overall porosity of the films was reduced for the Al-doped ZnO films, and a significant reduction was observed in particular for 0.5 % doped films, in agreement with the morphological analyses.

Table VII-5. Thickness, refractive index and porosity of the films cured at 250 °C.

Al (at. %)	Thickness (nm)	Ref. index at 632.8 nm	Porosity
0	96	1.85	0.14
0.5	75	1.92	0.06
1	90	1.87	0.12

The XRD patterns recorded on the Al-doped ZnO films and compared to the results obtained for the undoped sample (Figure 17) point out unchanged peak position and the absence of any characteristics of Al related phases.

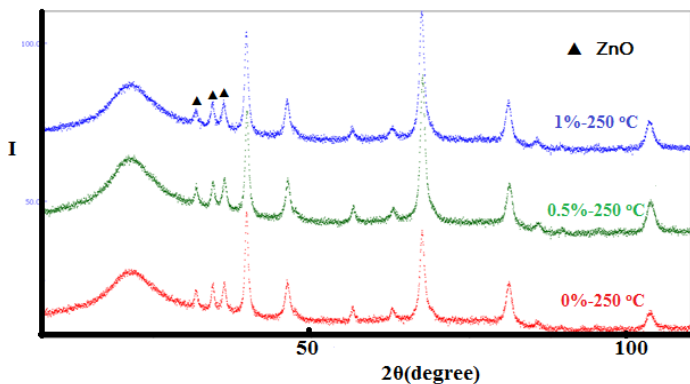

Figure VII-17. XRD patterns of undoped and Al-doped ZnO films cured at 250 °C and annealed at 400°C

The average crystallite dimension, determined by means of Maud software, were 17.7 nm, 14.1 nm and 12.8 nm for undoped, 0.5 % and 1 % Al-doped ZnO films, respectively. The decrease in the crystallite size with Al doping could be attributed to the difference between ionic radii of Zn and Al [125]. Moreover, the decrease of grain size by doping with Al was previously assessed from morphological analyses in agreement with a previous report [54].

Micro-Raman measurements were performed on Al-doped ZnO layers to give additional structural information (Figure 18). The peaks related to ZnO appeared at 324 cm^{-1}, 431 cm^{-1} and 565 cm^{-1}. As reported, the $E_2^{(high)}$ mode at 431 cm^{-1} is characteristic of the wurtzite phase and the peak at 324 cm^{-1} is assigned to $E_2^{(high)}$ - $E_2^{(low)}$ mode. The peak assigned to the longitudinal optical (LO) modes appears shifted to high frequency (564 cm^{-1}) in the doped samples.

Relative peak shift and broadening of the $E_2^{(high)}$ band, with respect to the usual position of the ZnO thin film at 437cm^{-1} [126], were observed, attributed to a slight lattice distortion. Moreover, both the peak shift and increase in the intensity of the longitudinal optical (LO) band at 565 cm^{-1} and the decrease of the $E_2^{(high)}$ band were detected. These evidences can be the result of both the formation of defects, such as oxygen vacancies [127]-[128], and the modification of the ZnO crystalline lattice due to

the dopant inclusion [129]. According to the diffraction analysis reported above, the increase in defects density appears more probably the reason for intensity increase and shift of the LO mode in the Raman spectra.

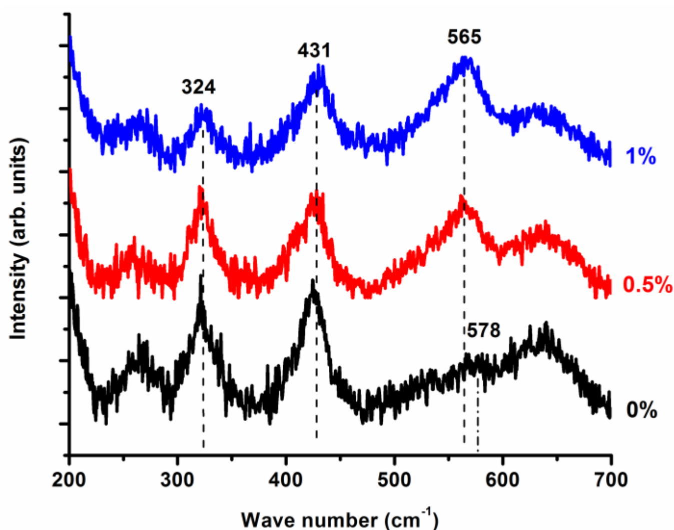

Figure VII-18. Raman spectra of undoped, 0.5 % and 1 % Al-doped ZnO films cured at 250 °C

As in the case of Mg-doped samples, the effect of curing at 300 °C for 10 min after each layer deposition was studied on Al-doped ZnO thin films deposited on Pt/Ti/SiO_2 substrate. The FE-SEM images of the samples are shown in Figure (19 a-c).

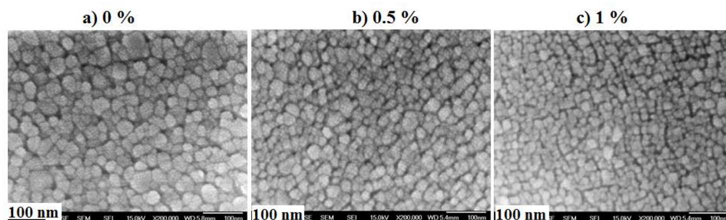

Figure VII-19. FE-SEM images of 0.5 % and 1 % Al-doped ZnO films cured at 300 °C and annealed at 400 °C compared to the undoped film

No significant differences can be observed in FE-SEM micrographs between 0.5 and 1 % Al-doped films (Figure 19 b-c). In addition, FE-SEM images of the samples cured at 300 °C generally display larger grains than those cured at 250 °C discussed in the previous section (Figure 14).

Figure (20) shows the AFM images of the ZnO films cured at 300 °C, partially confirming the trend observed with samples cured at 250 °C. As reported in Table (6), doping with 0.5 % Al gives relatively smooth surface and reduced grain size compared to undoped; the increase in surface roughness is observed upon doping with 1 % Al.

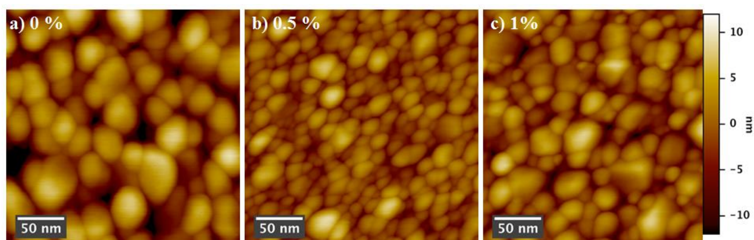

Figure VII-20. AFM images of the undoped, 0.5 % and 1 % Al-doped ZnO films cured at 300 °C and annealed at 400 °C for 4 h

Generally, the grain sizes of the Al-doped ZnO layers cured at 300 °C are larger than those of the samples treated at 250 °C but, contrary to the samples cured at 250 °C (Table 4), the average grain diameter of 1 % Al-doped films was lower than the value measured for 0.5 % Al-doped samples (Table 6).

Table VII-6. Roughness and equivalent diameter of undoped, 0.5 % and 1 % Al-doped ZnO films cured at 300 °C

Al (at. %)	Roughness (nm)	Equivalent diam. (nm)
0	4.5 ± 0.2	30.5 ± 0.9
0.5	2.5 ± 0.2	23 ± 2
1	3.0 ± 0.2	18 ± 1

Doping with Al slightly changed the thickness and refractive index of the films, according to the results of optical spectroscopy (Figure 21 and Table 7). It is worth noticing that Al-doped ZnO films present lower porosity with respect to the undoped one confirming that Al allows modifying the film morphology and grain size as evidenced by morphological analysis. In general, the porosity of the samples cured at 300 °C was relatively reduced also compared to the films cured at 250 °C (reported in Table 5).

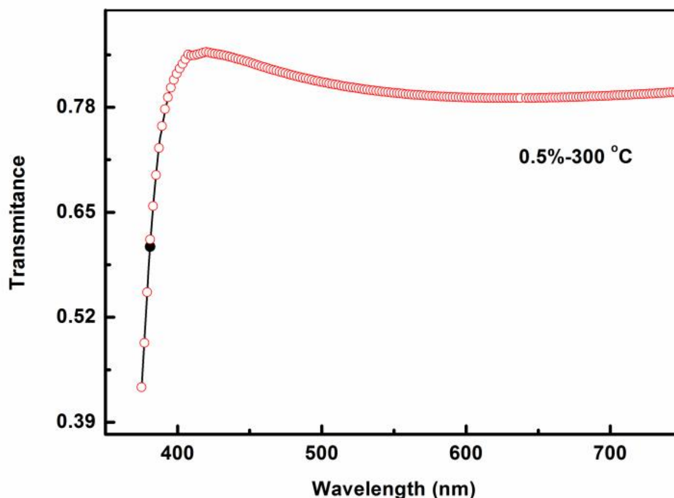

Figure VII-21. Transmittance spectra of the 0.5 % Al-ZnO samples cured at 300 °C for 10 min

Table VII-7. Thickness, refractive index and porosity of the films cured at 300 °C.

Al (at. %)	Thickness (nm)	Ref. index at 632.8 nm	Porosity
0	85	1.88	0.11
0.5	83	1.94	0.05
1	90	1.90	0.08

Figure (22) shows the XPS survey spectra collected from undoped, 0.5 and 1 at % Al-doped ZnO films and cured at 300 °C, where the labels identify the characteristic peaks. The fact that no other peaks appear indicates the samples are contaminant-free except the C 1s signal detected from the survey spectra that derives from the atmosphere.

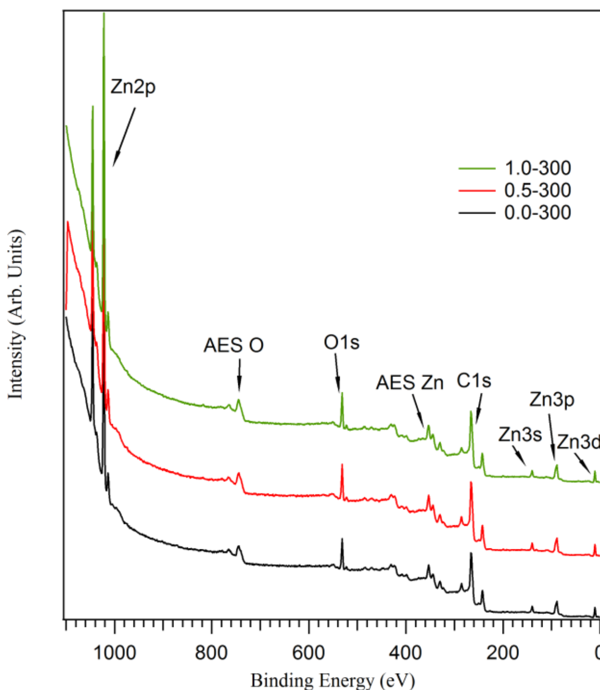

Figure VII-22. XPS survey spectra collected from ZnO films with different dopant level (0 %, 0.5 % and 1 at % Al) cured at 300 °C

The XPS Zn 2p, Al 2p and O 1s core level spectra are shown in Figure (23).

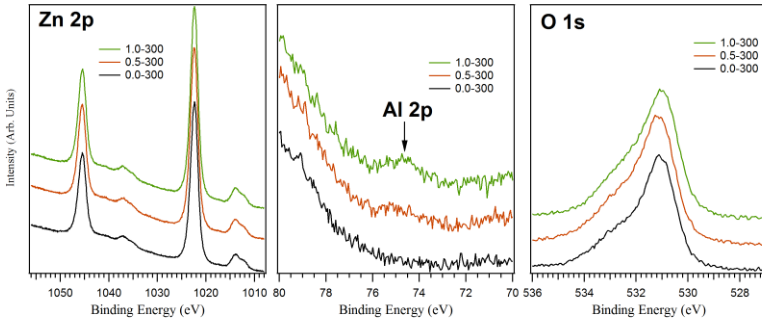

Figure VII-23. XPS Zn 2p, Al 2p and O 1s core level spectra

The Zn 2p signals (Zn 2p3/2 and Zn 2p1/2) show no change with respect to the level of Al doping, most probably as a consequence of the small doping amount. The Al 2p core levels are detectable in all Al-doped ZnO films. The signal corresponding to Al shows an increase in intensity according to the nominal amount of Al doping. The O 1s spectra exhibit the expected line shape with a main peak centered at BE of 531 eV, which can be attributed to the bulk oxygen, and a shoulder at higher BE (i.e. 532.5 eV) related to the oxygen from the surface of the film.

The work functions were calculated from the UPS spectra for undoped, 0.5 and 1 % Al-doped ZnO films cured at 300 °C (Figure 24). The values of the work functions obtained values were 4.20, 4.35 and 4.50 eV, respectively. It is worth of noting that films work function strongly depend on the top surface chemical composition and surface potential of the samples. The increase in work function with Al doping may be related to the modification of the surface features. The observed trend shows that the Al doping seems to induce p-type doping. Therefore, the shift in work functions compared to the undoped sample, are coherent with the Al level indicating the effectiveness of Al-doping.

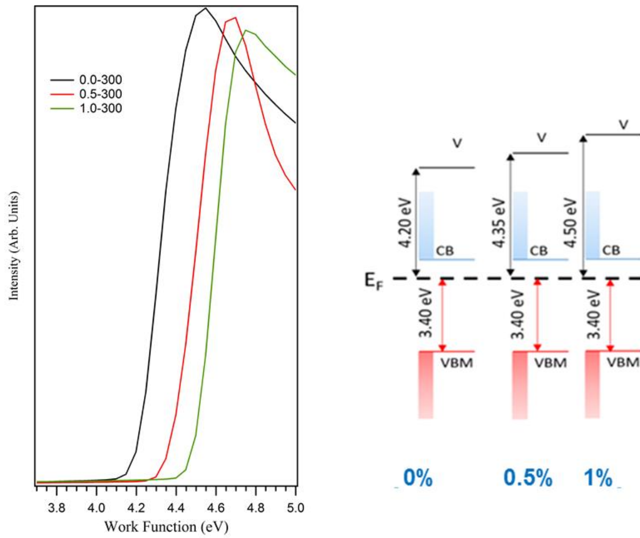

Figure VII-24. Energy level diagrams for undoped, 0.5 % and 1 % Al-doped ZnO films cured at 300 ^{o}C.

Regardless of the different intermediate curing conditions, the XRD patterns of the films (Figure 25) displayed no difference with the films cured at 250 ^{o}C (Figure 18).

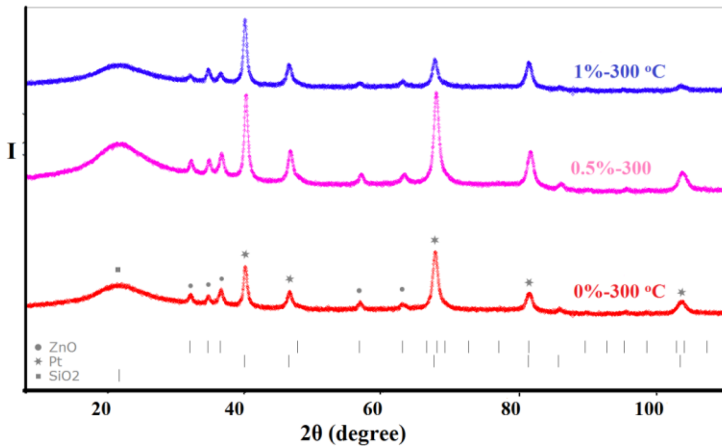

Figure VII-25. XRD patterns of ZnO thin films cured at 300 ^{o}C

The calculated crystallite sizes of the films are quite similar, being 13 nm and 14 nm for 0.5 % and 1 % Al-doped ZnO films, respectively compared to the value of 15 nm displayed by the undoped sample.

As for films cured at 250 °C, the relative peak shift and broadening of the E_2 $^{(high)}$ band, with respect to the usual position of the ZnO thin film at 437 cm^{-1}, were observed in the Micro-Raman spectra with increasing the doping load from 0.5 % to 1 % Al (Figure 26). This effect, related to a decrease in lattice order of the wurtzite phase, could be related both to the addition of dopant and the stress induced by a mismatch of thermal expansion coefficients of the film and the substrate [130]. The signal corresponding to the longitudinal optical (LO) mode is shifted due to the presence of defects. The increase in the intensity of the LO band at 578 cm^{-1} and the decrease of the E_2 $^{(high)}$ band can be probably attributed to the formation of defects such as oxygen vacancies [127]-[128] more than to the modification of the ZnO crystalline lattice upon inclusion of the dopant [129].

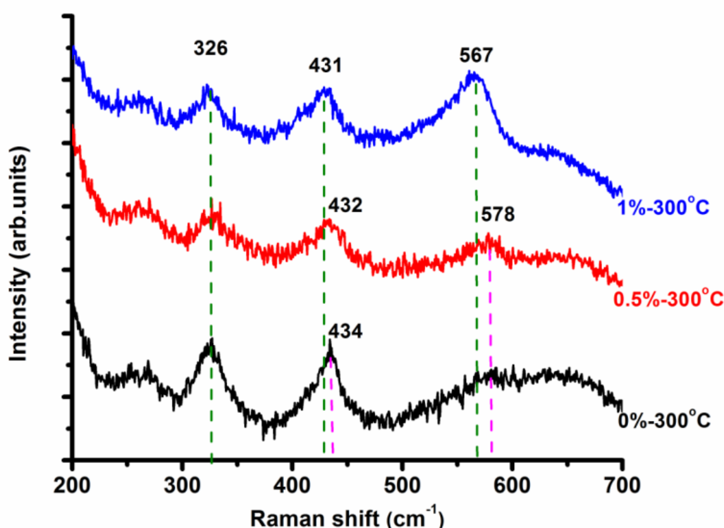

Figure VII-26. Raman spectra of undoped, 0.5 % and 1 % Al-doped ZnO films cured at 300 °C

The results obtained from Al-doped ZnO layers are promising keeping in mind the requirements of the memristive layers in particularly if compared to the Mg-doped ZnO films. The reduction of porosity, surface roughness and grain sizes of the films obtained by Al-doping can be beneficial for the fabrication of dense switching layers and for achieving a good adhesion with the electrodes in the production of the memristive cell.

Despite the fact that the smaller grains with highly reduced surface roughness was obtained from 0.5 % Al-doped ZnO films cured at 250 ^{o}C for 1 h, the sample cured at 300 ^{o}C for 10 min was chosen to fabricate a memristive cell for electrical measurement, taking into consideration the advantage of the short processing time in the clean room and for the possible scaling up. Unfortunately, due to the limited availability of both fabrication and measurement set ups, it was not possible to test the 1 % Al-doped ZnO layer that according to the Raman spectra could present high defects density. The electrical measurements were then performed on a Pt/Al-ZnO/Pt/Ti/SiO_2 building block with 0.5 at % Al-doped ZnO active layer with interlayer curing at 300 ^{o}C for 10 min acquiring the I-V curves on at least ten different points. Both bottom and top electrodes are the same used for the fabrication of the undoped ZnO-based memristive cell discussed in section 6.4.

The measurements were performed under LED light and the I-V curves acquired for ten cycles are shown in Figure (27). The I-V plot indicates that the characteristic switching loop of a unipolar memristor is obtained without a forming step within the sweep voltage between -1.5 V and 3 V, comparable with the values of the undoped ZnO-based memristive cell. On the contrary, a lower compliance current (CC) of 5 mA was applied compared to the undoped ZnO films reported in the previous section (Figure VI-30). The high resistance state (HRS) and the low resistance state (LRS) set at -0.1 V displayed resistance values of 800 Ω and 230 Ω, respectively. Both resistance values at high (HRS) and low (LRS) were reduced in 0.5 % Al-doped ZnO-based devices compared to those obtained from the undoped materials. A stable switching property was observed during the 10 cycles.

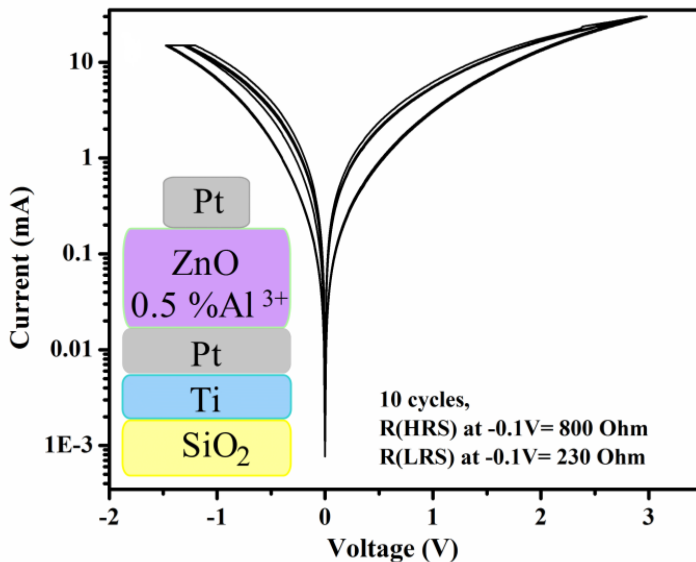

Figure VII-27. Schematic device structure (inset) of 8-layers 0.5 % Al-doped ZnO films with Pt-dishes as top electrode (Pt/0.5% Al-ZnO/Pt/Ti/SiO_2 structure) cured at 300 °C for 10 min and its I-V characteristic curve.

The recorded memristive behavior indicates that the reduction of thickness, porosity, surface roughness and grain size obtained by doping the ZnO layers with Al can be exploited for the fabrication of dense switching layers with improved properties. Moreover, the stable memristive behavior with lower compliance current observed for the Al-doped ZnO layer appears advantageous and suggests its possible application in low power operation devices.

Chapter VIII

Conclusions

The aim of this work was the development by sol-gel processing of ZnO thin films for memristive application. Starting from alcoholic solutions of zinc acetate dihydrate (ZAD) with the addition of monoethanolamine (MEA), the preparation protocol for the fabrication by spin coating technique of undoped and doped-ZnO multi-layer thin films on different substrates, and in particular on the engineered platinum (Pt/Ti/SiO_2) substrate employed as bottom electrode in a memristive cell, was developed. The detailed investigation of the ZnO thin films features was conducted and film curing and annealing conditions were adjusted based on the study performed on the ZnO xerogel powders. For the fabrication of the memristive building blocks, the active layers were deposited on the Pt/Ti/SiO_2 bottom electrode in a clean room, and different top electrodes including Ag wire, Ag-dishes and Pt-dishes were used.

The compositional and morphological features of the films were investigated by FE-SEM, AFM and XPS analysis. The obtained final samples were structurally characterized by XRD, FTIR, and micro-Raman analysis. Furthermore, PUMA software was applied to estimate the thickness and refractive index of the films from the transmission spectra. The electrical measurements were performed on the memristive cells based on undoped and Al-doped ZnO active layers sandwiched between Pt/Ti/SiO_2 bottom electrode and the different top electrodes.

The appropriate curing and annealing conditions, resulting in pure and crystalline ZnO films were established based on the thermal analysis performed on ZnO xerogel powders. The final conditions of the annealing step were selected by taking into account the thermal stability of the bottom electrode in the memristive cells. The performed studies suggested that curing each layer at 250 °C for 1 h and annealing the final film at 400 °C for 4 h is sufficient to produce organic-free and crystalline ZnO thin films. Low magnification SEM analysis demonstrated the effect of ZAD concentration and number of layers on ZnO thin film features, suggesting ZnO films derived from sol concentration of 0.1 M obtained by multi-layer deposition as the most suitable for memristive device fabrication. The FE-SEM study provided the detailed information on the morphology of the films revealing the formation of spherical-shaped grains regardless of the nature of

substrates, but pointing out the dependence of layer quality on substrates and the effect of ZAD to MEA molar ratio on grain size. The XRD study revealed that the films deposited on different substrates were crystalline and presented the hexagonal wurtzite-type phase with different extent of preferential c-axis orientation. It was also noted that relatively higher degree of preferential orientation on the substrates was observed in the case of lower MEA content in ZnO sol (ZAD to MEA molar ratio of 0.5).

Based on the results obtained from morphological, thermal and structural analysis, the electrical measurements were performed on the multi-layer films prepared from fixed ZAD to MEA molar ratio (0.5) in the ZnO sol. The results acquired on 4-layered sol-gel derived ZnO thin films sandwiched between $Pt/Ti/SiO_2$ and Ag-top electrode showed a true memristive response. Yet, some modification approaches were foreseen to improve the resistive switching responses of the ZnO thin layers and the cell stability. The top electrodes constituted by Ag-dishes were replaced by Pt-dishes to make the possible charge carriers more predictable. In addition, a less time-consuming fabrication procedure was adopted changing the intermediate curing conditions (300°C, 10 min duration), thus making feasible the increase in number of layers from four to eight. The electrical measurements obtained from $Pt/ZnO/Pt/Ti/SiO_2$ memristive building blocks showed a stable memristive response with reduced compliance current (15 mA) compared to the four-layered $Ag/ZnO/Pt/Ti/SiO_2$ cells, obtained by intermediate curing of the single layers at 250 °C. Furthermore, doping of ZnO layers was among the modification approaches selected in this thesis work to improve the memristive switching performance of ZnO layers. The AFM analysis clearly indicated that Al-doping was found to modify film’s morphology and grain sizes. In particular, 0.5 at % Al-doping resulted in significant reduction of surface roughness, grain sizes and overall porosity of the films that are desirable features in memristive switching devices. The obtained results from electrical measurements on 0.5 % Al-doped ZnO revealed that stable memristive behavior was obtained. Apparently, the electrical measurement was performed without the requirement of electroforming process, and lower compliance current (5 mA) was applied compared to the undoped ZnO films. It is worth of note that the assessment of the memristive response with low compliance current suggests promising potential applications of these layers in devices that require low power operation. This is a key

point towards the possible coupling of the inorganic memristors with neuronal cells, in order to build up hybrid bio-inorganic devices.

In conclusion, the present thesis points out that the sol-gel route is a suitable technique for the fabrication of dense layers for memristive switching devices, which allows the easy tuning of the processing parameters by inexpensive procedures. In particular, the composition of the metal oxide layers can be changed and, as suggested by Al-doping of ZnO, represents an effective tool for the modification of the memristive switching performance. As reported in this thesis, the memristive response of the fabricated cell with Al-doped ZnO was proved to be stable for 10 cycles operation.

In perspective, the cell stability must be improved, and endurance tests under different measurement conditions are necessary in order for scaling up the production.

List of abbreviation and acronyms

HRS	High resistance state
LRS	Low resistance state
ECM	Electrochemical metallization memory
BE	Bottom electrode
TE	Top electrode
VCM	Valence change memory
RRAM	Resistive random access memories
MBE	Molecular beam epitaxy
PLD	Pulsed laser deposition
ALD	Atomic layer deposition
SEM	Scanning Electron Microscopy
FESEM	Field Emission Scanning Electron Microscopy
AFM	Atomic force microscopy
SPM	Scanning Probe Microscopy
XPS	X-ray photoelectron
UPS	Ultra violet photoelectron spectroscopy
XRD	X-ray diffraction
FTIR	Fourier-Transform Infrared Spectroscopy
PUMA	Point-wise Unconstrained Optimization Approach
TGA	Thermogravimetric analysis
DTA	Differential thermal analysis
DSC	Differential Scanning Calorimetry
ZAD	Zinc acetate dihydrate
MEA	Monoethanolamine
CC	Compliance current

References

[1]. Chua, L. O., *Memristor-the missing circuit element*. IEEE Transactions on Circuit Theory, **1971**. 18(5): p. 507-519.

[2]. Chua, L. O., *Resistance switching memories are memristors*. Applied Physics A, **2011**. 102(4): p. 765-783.

[3]. Strukov, D. B., G. S. Snider, D. R. Stewart, and R. S. Williams, *The missing memristor found*. Nature, **2008**. 453: p. 80-83.

[4]. Meuffels, P., and Soni, R., *Fundamental Issues and Problems in the Realization of Memristors*. **2012**.

[5]. Prakash,A., Jana, D and Maikap, *S, TaO_x-based resistive switching memories: prospective and challenges,* Nanoscale Research Letters, **2013**, 8: p. 418-435.

[6]. Waser R., *Resistive non-volatile memory devices*. Microelectron Engineering, **2009**. 86: p. 1925-1928.

[7]. Li Y. T., S. Long, Q. Liu, H. Lü, S. Liu & M. Liu, *An overview of resistive random access memory devices*. **2011**. Chinese Science Bulletin, 56(28-29): p. 289.

[8]. Yang Y. C., F. Pan, Q Liu, M. Liu, and F. Zeng, *Fully room temperature fabricated nonvolatile resistive memory for ultrafast and high-density memory application*. Nano Letters, **2009**. 9(4): p. 1636-1643.

[9]. Zoolfakar A. S., R. A. Kadir, R. A. Rani, S. Balendhran, X. Liu, E. Kats, S. K. Bhargava, M. Bhaskaran, S. Sriram, S. Zhuiykov, A. P. O'Mullanee and K. Kalantar-zadeh, *Engineering electrodeposited ZnO films and their memristive switching performance*. Physical Chemistry Chemical Physics, **2013.** 15: p. 10376-10384.

[10]. Gorm K. J., *An introduction to the memristor - a valuable circuit element in bioelectricity and bioimpedance*. Journal of Electrical Bioimpedance, **2012**. 3: p. 20-28.

[11]. Chua L., *If it's pinched, it's a memristor.* Semiconductor Science and Technology, 2014. 29(104001): p. 42.

[12]. Duarte, J. C., Ernesto V. M., and Luis N. A., *Frequency characterization of memristive devices.* Circuit Theory and Design (ECCTD), 2013. European Conference on. IEEE.

[13]. Waser, R. & Aono, M., *Nanoionics-based resistive switching memories*. Nature Materials, **2007**. 6: p. 833-840.

[14]. Lee M-J et al., *A fast, high-endurance and scalable nonvolatile memory device made from asymmetric Ta_2O_5/ TaO_{2-x} bilayer structures*. Nature Materials, **2011**. 10: p. 625.

[15]. Wong, P., H. Y. Lee, S. Yu, Y. S. Chen, Y. Wu, P. S. Chen, B. Lee, F. T. Chen, and M. J. Tsai, *Metal Oxide RRAM.* Proceedings of the IEEE, **2012**. 100(6): p. 1951.

[16]. Akinaga, H., and H. Shima, *Resistive random access memory (ReRAM) based on metal oxides*. Proceedings of the IEEE, **2010**. 98(12): p. 2237-2251.

[17]. Lee S., H. Kim, D.J. Yun, S.W. Rhee and K. Yong, *Resistive switching characteristics of ZnO thin film grown on stainless steel for flexible nonvolatile memory devices*. Applied Physics Letters, **2009**. 95(262113): p. 1-4.

[18]. Muhammad N. M., D. Navaneethan, R. Khalid, W. D. Hyun, J. Jeongdae, and H. C. Kyung, *Fabrication of printed memory device havin zinc-oxide active nano-layer and investigation of resistive switching*. Current Applied Physics, **2013**. 13, pp. 90-96, 2013.

[19]. Chang W.Y., Lai Yen-C., Wu Tai-B., Wang Sea-F., Chen F., and Tsai Ming-J., *Unipolar resistive switching characteristics of ZnO thin films for nonvolatile memory applications*. Applied Physics Letters, **2008**. 92, p. 1-3.

[20]. Radzimska A. K., and T. Jesionowski, *Zinc oxide-from synthesis to application: a review*. Materials, **2014**. 7: p. 2833-2881.

[21]. Janotti A., and C.G. Van de Walle*, Fundamentals of zinc oxide as a semiconductor*. Reports on Progress in Physics, **2009**. 72: p. 1-29.

[22]. Liu Y., Y. Li, and H. Zeng, *ZnO-based transparent conductive thin films: doping, performance, and processing*. Journal of Nanomaterials, **2013.** 2013: p. 1-9.

[23]. Bagnall D.M., Y.F. Chen, Z. Zhu, T. Yao, S. Koyama, M.Y. Shen, and T. Goto, *Optically pumped lasing of ZnO at room temperature*. Applied Physics Letters, **1997**. 70(17): p. 2230-2232.

[24]. Cao H., Y.G. Zhao, H.C. Ong, S.T. Ho, J.Y. Dai, J.Y.Wu, and R.P.H. Chang, *Ultraviolet lasing in resonators formed by scattering in semiconductor polycrystalline films*. Applied Physics Letters, **1998**. 73(25): p. 3656-3658.

[25]. Ma X., P. Chen, D. Li, Y. Zhang, and D. Yang, *Electrically pumped ZnO film ultraviolet random lasers on silicon substrate*. Applied Physics Letters, **2007**. 91: p. 1-3.

[26]. Chu S., M. Olmedo, Z. Yang, J. Kong, and J. Liu, *Electrically pumped ultraviolet ZnO diode lasers on Si*. Applied Physics Letters, **2008**. 93: p. 1-3.

[27]. Molarius J., J. Kaitila, T. Pensala, and M. Ylilammi, *Piezoelectric ZnO films by r.f sputtering*. Journal of Materials Science: Materials in Electronics, **2003**. 14: p. 431-435.

[28]. Hwang D.-K., M.S. Oh, J.-H. Lim, and S.J. Park, *ZnO thin films and light-emitting diodes*. Journal of Physics D: A Physics, **2007**. 40: p. R387-R412.

[29]. Du X.Y., Y.Q. Fu, S.C. Tan, J.K. Luo, A.J. Flewitt, S. Maeng, S.H. Kim, Y.J. Choi, D.S. Lee, N.M. Park, J. Park, and W.I. Milne, *ZnO film for application in surface acoustic wave device*. Journal of Physics: Conference Series 76, **2007**. P. 1- 6.

[30]. Park H.J., K.H. Lee, B. Kumar, K.S. Shin, S.-W. Jeong, and S.W. Kim, *Inverted organic solar cells with ZnO thin films prepared by sol-gel method*. Journal of Nanoelectronics and Optoelectronics, **2010**. 5(1-4): p. 135-138.

[31]. Ma A.M., M. Gupta, F.R. Chowdhury, M. Shen, K. Bothe, K. Shankar, Y. Tsui, and D.W. Barlage, *Zinc oxide thin film transistors with Schottky source barriers.* Solid State Electron, **2012**. 76: p. 104-108.

[32]. Musat V., A.M. Rego, R. Monteiro, and E. Fortunato, *Microstructure and gas-sensin properties of sol-gel ZnO thin films*. Thin Solid Films, **2008**. 516: p. 1512-1515.

[33]. Arya S.K., S. Saha, J.E. Ramirez-Vick, V. Gupta, S. Bhansali, and S.P. Singh, *Recent advances in ZnO nanostructures and thin films for biosensor applications: review*. Analytica Chimica Acta, **2012**. 737: p. 1-21.

[34]. Mang A, K Reimann and St. Rubenacke, *Band gaps, crystal-field splitting, spin-orbit coupling, and exciton binding energies in zno under hydrostatic pressure*. Solid State Communications, **1995**. 94(4): p. 251-254.

[35]. Norton, D.P., Y.W. Heo, M.P. Ivill, K. Ip, S.J. Pearton, M.F. Chisholm, T. Steiner, *ZnO: growth, doping and processing*. materialstoday, **2004**. P. 34-40.

[36]. Brauer G., J. Kuriplach, C. C Ling and A. B. Djurišić, *Activities towards p-type doping of ZnO*. Journal of Physics: Conference Series, **2011**. 265: p. 1-14.

[37]. Look D. C., G. C. Farlow, Pakpoom Reunchan, Sukit Limpijumnong, S. B. Zhang and K. Nordlund, *Evidence for Native-Defect Donors in n-Type ZnO*. Physical Review Letters, **2005**. 95: p. 1-4.

[38]. Janotti A. and C. G. Van deWalle, *Fundamentals of zinc oxide as a semiconductor*. Reports on Progress in Physics, **2009**. 72: p. 1-29.

[39]. Morkoc H., and U. Ozgur, *Zinc Oxide. Fundamentals, Materials and Device Technology*. **2009**, WILEY-VCH Verlag GmbH & Co. KGaA.

[40]. Ashrafi A. and C. Jagadish, *Review of zincblende ZnO: Stability of metastable ZnO phases*. Journal of Applied Physics, **2007**. 102: p. 1-12.

[41]. Peng H. Y., G. P. Li, J. Y. Ye, Z. P. Wei, Z. Zhang, D. D. Wang, G. Z. Xing, and T. Wu., *Electrode dependence of resistive switching in Mn-doped ZnO: Filamentary versus interfacial mechanisms.* Applied Physics Letters, 2010. 96: p. 1-3.

[42]. Lee S., H. Kim, D. J. Yun, S. W. Rhee, and K. Yong., *Resistive switching characteristics of ZnO thin film grown on stainless steel for flexible nonvolatile memory devices*. Applied Physics Letters, 2009. 95: p. 1-3.

[43]. Xu N., Lifeng L., Xiao S., Xiaoyan L., Dedong H., Yi W., Ruqi H., Jinfeng K., and Bin Y., *Characteristics and mechanism of conduction/set process in TiN/ZnO/Pt resistance switching random-access memories*. Applied Physics Letters, **2008**. 92: p. 1-3.

[44]. Zhang F., X. Li, X. Gao, L. Wu, F. Zhuge, Q. Wang, X. Liu, R. Yang, Y He, *Effect of defect content on the unipolar resistive switching characteristics of ZnO thin film memory devices*. Solid State Communications, **2012**. 152: p. 1630-1634.

[45]. Huang C. H., J. S. Huang, C. C. Lai, H. W. Huang, S. J. Lin, and Y. L. Chueh, *Manipulated Transformation of Filamentary and Homogeneous Resistive Switching on ZnO Thin Film Memristor with Controllable Multistate*. ACS Applied Materials & Interfaces, **2013**. 5: p. 6017-6023.

[46]. Huang1 H. W., C. F. Kang, F. I. Lai, J. H. He, Su-Jien Lin1 and Yu-Lun Chueh, *Stability scheme of ZnO-thin film resistive switching memory: influence of defects by controllable oxygen pressure ratio*. Nanoscale Research Letters, **2013**. 8:483, p. 1-7.

[47]. Chang K. C., T. C. Chang, T. M. Tsai, R. Zhang, Y. C. Hung, Y. E. Syu, Y. F. Chang, M. C. Chen, T. J. Chu, H. L. Chen, C. H. Pan, C. C. Shih, J. C. Zheng and S. M Sze, *Physical and chemical mechanisms in oxide-based resistance random access memory*. Nanoscale Research Letters, **2015**, p. 1-27.

[48]. Shi L., D. S. Shang, Y. S. Chen, J. Wang, J. R. Sun and B. G. Shen, *Improved resistance switching in ZnO-based devices decorated with Ag nanoparticles*, Journal of Physics D: Applied Physics, **2011**. 44: p. 1-5.

[49]. Kumar A. and M.S. Baghini, *Experimental study for selection of electrode material for ZnO-based memristors*. Electronics Letters, **2014**. 50(21), p. 1547-1549.

[50]. Xu N., L. F. Liu, X. Sun, C. Chen, Y. Wang, D. D. Han, X. Y. Liu, R. Q. Han, J. F. Kang and B. Yu, *Bipolar switching behavior in TiN/ZnO/Pt resistive nonvolatile memory with fast switching and long retention*. Semiconductor Science and Technology, **2008**. 23: p. 1-4.

[51]. Jing S., A. Younis, D. Chu and S. Li, *Resistive Switching Characteristics in Electrochemically Synthesized ZnO Films*. AIMS Materials Science, **2015**. 2(2): p. 28-36.

[52]. Lee H. Y., P. S. Chen, T. Y. Wu, Y. S. Chen, C. C. Wang, P. J. Tzeng, C. H. Lin, F. Chen, C. H. Lien, and M.-J. Tsai, *Low Power and High Speed Bipolar Switching with A Thin Reactive Ti Buffer Layer in Robust HfO2 Based RRAM*, p. 1-4.

[53]. Nunes P., Fortunato E., Tonello P., Fernandes F. B., Vilarinho P. and Martins R., *Effect of different dopant elements on the properties of ZnO thin films*. Vacuum, **2002**. 64: p. 281-285.

[54]. Salam S., Islam V., and Akram A., *Sol-gel synthesis of intrinsic and aluminum-doped zinc oxide thin films as transparent conducting oxides for thin film solar cells*. Thin Solid Films, **2013**. 529: p. 242-247.

[55]. Rezaee M., M. Behdani, H. Arabshahi and N. Hosseini, *Indium-doped Zinc Oxide Thin Films by Sol-Gel Method*. International Review of Physics, **2009**. 12(3): p. 103-106.

[56]. Rydzek M., M. Reidinger, M. Arduini-Schuster and J. Manara, *Comparative study of sol–gel derived tin-doped indium- and aluminum-doped zinc-oxide coatings for electrical conducting and low-emitting surfaces*. Progress in Organic Coatings, **2011**. 70: p. 369-375.

[57]. Chen X., Wu G., and Bao D., *Resistive switching behavior of Pt / Mg 0.2 Zn 0.8 O / Pt devices for nonvolatile memory applications*. Applied Physics Letters, **2008**. 93: p. 1-3.

[58]. Yang S., Y. Liu, Y. Zhang, and D. Mo, *Spectroscopic ellipsometry studies of Mg-doped ZnO thin films prepared by the sol-gel method*. Physics Status Solidi A 206, **2009**. 7: p. 1488-1493.

[59]. Singh J., P. Kumar, K. S. Hui, K. N. Hui, K. Ramam, R. S. Tiwaria and O. N. Srivastavaa, *Synthesis, band-gap tuning, structural and optical investigations of Mg doped ZnO nanowires*. CrystEngComm, **2012**. 14: p. 5898-5904.

[60]. McKenna K. and A. Shluger, *The interaction of oxygen vacancies with grain boundaries in monoclinic HfO2*. Applied Physics Letters, **2009**. 95: p. 1-3.

[61]. Lee D., D. K. Hwang, M. Chang, Y. Son, D. Seong, D. Choi and H. Hwang, *Resistance switching of Al doped ZnO for Non Volatile Memory applications*. IEEE 2006 International Electron Devices, p. 1-2.

[62]. Lu W. and C. M. Lieber, *Nanoelectronics from the bottom up*. Nature Materials, **2007**. 6: 11, p. 841-850.

[63]. Opel M., S. Geprags, M. Althammer, T. Brenninger, and R. Gross, *Laser molecular beam epitaxy of ZnO thin films and heterostructures*. Journal of Physics D: Applied Physics, **2014**. 47: p. 1-17.

[64]. Zhao K., S. Wang, and A. Shen, *ZnO Grown on (111) ZnS Substrates by Plasma-Assisted Molecular Beam Epitaxy*. Journal of Electronic Materials, **2012**. 41(8): p. 2151-2154.

[65]. Wang W., R. Dong, X. Yan and B. Yang, *Memristive characteristics in semiconductor/metal contacts tested by conductive atomic force microscopy*. Journal of Physics D: Applied Physics, **2011**. 44: p. 1-5.

[66]. Chiou W. T., W. Y. Wu, and J. M. Ting, *Growth of single crystal ZnO nanowires using sputter deposition*. Diamond and Related Materials, **2003**. 12: p. 1841-1844.

[67]. Dang W.L., Y.Q. Fu, J.K. Luo, A.J. Flewitt, and W.I. Milne, *Deposition and characterization of sputtered ZnO films Superlattice*. Superlattices and Microstructures, **2007**. 42: p. 89-93.

[68]. Hosseinnejad M. T., M Shirazi, M. Ghoranneviss, M. R. Hantehzadeh, and E. Darabi, *Preparation of Nanostructured ZnO Thin Films Using Magnetron Sputtering for the Gas Sensors Applications*. J Inorg Organomet Polym, **2016**. 26: p. 405-412.

[69]. Schaaf P., *Laser Processing of Materials: Fundamentals, Applications and Developments*. Springer Science & Business Media, 2010-Technology & Engineering-234 pages.

[70]. Ohnishi T., H. Koinuma, and M. Lippmaa, *Pulsed laser deposition of oxide thin films*. Applied Surface Science, **2006**. 252: p. 2466-2471.

[71]. Novotný M., J. Čížek, R. Kužel, J. Bulíř, J. Lančok, J. Connolly, E. McCarthy, S. Krishnamurthy, J.-P. Mosnier, W. Anwand, and G. Brauer, *Structural characterization of ZnO thin films grown on various substrates by pulsed laser deposition*. Journal of Physics D: Applied Physics, **2012**. 45: p. 1-12.

[72]. Franklin J. B., B. Zou, P. Petrov, D. W. McComb, M. P. Ryan and M. A. McLachlan, *Optimised pulsed laser deposition of ZnO thin films on transparent conducting substrates*, Materials Chemistry, **2011**. 21: p. 8178-8182.

[73]. Kukreja L. M., A. K. Das and P. Misra, *Studies on nonvolatile resistance memory switching in ZnO thin films*. Bulletin of Materials Science, **2009**. 32(3): p. 247-252.

[74]. Macaluso R., M. Mosca, V. Costanza, A. D’Angelo, G. Lullo, F. Caruso, C. Calì, F. Di Franco, M. Santamaria and F. Di Quarto, *Resistive switching behaviour in ZnO and VO_2 memristors grown by pulsed laser deposition*. Electronics Letters, **2014**. 50(4): p. 262-263.

[75]. Punugupati S., N. K. Temizer, J. Narayan, and F. Hunte, *Structural and resistance switching properties of epitaxial Pt/ZnO/TiN/Si(001) heterostructures*. Journal of Applied Physics, **2014**. 115: p. 1-6.

[76]. Ponraj J. S., G. Attolini, and M. Bosi, *Review on Atomic Layer Deposition and Applications of Oxide Thin Films*. Critical Reviews in Solid State and Materials Sciences, **2013**. 38: p. 203-233.

[77]. Johnson1 R. W., A. Hultqvist and S. F. Bent, *A brief review of atomic layer deposition: from fundamentals to applications*. Materials Today, **2014**. 17(5): p. 236-246.

[78]. Lim J. and C. Lee, *Effects of substrate temperature on the microstructure and photoluminescence properties of ZnO thin films prepared by atomic layer deposition*. Thin Solid Films, **2007**. 515: p. 3335-3338.

[79]. Zhang J., H. Yang, Q. Zhang, S. Dong, and J. K. Luo, *Bipolar resistive switching characteristics of low temperature grown ZnO thin films by plasma-enhanced atomic layer deposition*, Applied Physics Letters, **2013**. 102: p. 1-4.

[80]. Lee W., E. Kim, and S. Yoon, *Effect of Al incorporation amount upon the resistive-switching characteristics for nonvolatile memory devices using Al-doped ZnO semiconductors*. Journal of Vacuum Science & Technology B, **2015**. 33(5): p. 1-7.

[81]. Perednis D. & L. J. Gauckler, *Thin Film Deposition Using Spray Pyrolysis*. Journal of Electroceramics, **2005**. 14: p. 103-111, 2005.

[82]. Lehraki N., M.S. Aida, S. Abed, N. Attaf, A. Attaf, and M. Poulain, *ZnO thin films deposition by spray pyrolysis: Influence of precursor solution properties*. Current Applied Physics, **2012**. 12: p. 1283-1287.

[83]. Dongale T. D., S. V. Mohite, A. A. Bagade, P. K. Gaikwad, P. S. Patil, R. K. Kamat, and K. Y. Rajpure, *Development of Ag/WO3/ITO Thin Film Memristor Using Spray Pyrolysis Method*. Electronic Materials Letters, **2015**. 11(6): p. 944-948.

[84]. Brinker C. J. and G. W. Scherer, *Sol-gel science: the physics and chemistry of sol-gel processing*. **1990**, San Diego, CA, USA: vol. 8, academic Inc. Press.

[85]. Dislich H., *Sol-gel: science, processes and products*. Journal of Non-Crystalline Solids, **1986**. 80: p. 115-121.

[86]. Yang C.Y, Pan F, Zeng F, and Liu M, *Switching mechanism transition induced by annealing treatment in nonvolatile Cu/ZnO/Cu/ZnO/Pt resistive memory: From carrier trapping/detrapping to electrochemical metallization.* J. Appl. Phys., **2009**, 106: p. 1-4.

[87]. Danks A. E., S. R. Hall and Z. Schnepp, *The evolution of sol-gel chemistry as a technique for materials synthesis*, Mater. Horiz., **2016**. 3: p. 91.

[88]. L. Znaidi, *Sol-gel-deposited ZnO thin films: A review*. Materials Science and Engineering, **2010**. B 174: p. 18-30.

[89]. H. Bahadur, A. K. Srivastava, R. K. Sharma and S. Chandra, *Morphologies of Sol-Gel Derived Thin Films of ZnO Using Different Precursor Materials and their Nanostructures*. Nanoscale Res Lett., **2007**. 2: p. 469-475

[90]. K.R. Murali, *Properties of sol-gel dip-coated zinc oxide thin films*. Journal of Physics and Chemistry of Solids, **2007**. 68: p. 2293-2296.

[91]. M. Sahal , B. Hartiti , A. Ridah, M. Mollar, B. Marı´, *Structural, electrical and optical properties of ZnO thin films deposited by sol-gel method*. Microelectronics Journal, **2008**. 39: p. 1425-1428.

[92]. James B. Miller, Hsin-Jung H., Bret H. Howard, Esteban B., *Microstructural evolution of sol-gel derived ZnO thin films*. Thin Solid Films, **2010**. 518: p. 6792-6798.

[93]. Detlef W. Bahnemann., Claudius Kormann, and Michael R. Hoffmann, *Preparation and Characterization of Quantum Size Zinc Oxide: A Detailed Spectroscopic Study*. J. Phys. Chem., **1987**. 91: p. 3789-3798.

[94]. L. Znaidi, *Elaboration of ZnO Thin Films with Preferential Orientation by a Soft Chemistry Route*. Journal of Sol-Gel Science and Technology, **2003**. 26: p. 817-821.

[95]. L. Armelao, M. Fabrizio, S. Gialanella, F. Zordan, *Sol-gel synthesis and characterisation of ZnO-based nanosystems*. Thin Solid Films, 2001. 394: p. 90-96.

[96]. C.J. Brinker, A.J. Hurd, G. C. Frye, P. R. Schunk and C. S. Ahley, *Sol-gel Thin films*. Journal of the ceramic society of Japan, **1991**. 99 (10): p. 862-877.

[97]. P. Hosseini Vajargah, H. Abdizadeha, R. Ebrahimifard, M.R. Golobostanfard, *Sol-gel derived ZnO thin films: Effect of amino-additives*. Applied Surface Science, **2013**. 285P: p. 732-743.

[98]. H. Li, J. Wang, H. Liu, Ch. Yang, H. Xu, X. Li and H. Cui, *Sol-gel preparation of transparent zinc oxide films with highly preferential crystal orientation*. Vacuum, **2004**. 77: p. 57-62.

[99]. L. Znaidi, G.J.A.A. Soler-Illia, R. Le Guennic, A. Kanaev, C. Sanchez, *Elaboration of ZnO Thin Films with Preferential Orientation by a Soft Chemistry Route*. J. Sol-Gel Sci. Tech., **2003**. 26: p. 817-821.

[100]. L. Znaidia, G.J.A.A. Soler Illia, S. Benyahia, C. Sanchez, A.V. Kanaev, *Oriented ZnO thin films synthesis by sol-gel process for laser application.* Thin Solid Films, **2003**. 428: p. 257-262.

[101]. R.E. Marotti et al., *Characterization of ZnO and ZnO:Al thin films deposited by the sol-gel dip-coating technique*. Thin Solid Films, **2008**. 517: p. 1077-1080

[102]. K. Norrman, A. Ghanbari-Siahkali and N. B. Larsen, *Studies of spin-coated polymer films: Riview*, Annu. Rep. Prog. Chem., Sect. C, **2005**. 101: p. 174-201.

[103]. Y. Kim , W. Tai, S. Shu, *Effect of preheating temperature on structural and optical properties of ZnO thin films by sol-gel process*. Thin Solid Films, **2005**. 491: p. 153 -160.

[104]. Y. Natsume, H. Sakata, *Zinc oxide films prepared by sol-gel spin-coating*. Thin in Solid Films, **2000**. 372: p. 30-36.

[105]. Z.Q. Xu et al., *Characteristics of Al-doped c-axis orientation ZnO thin films prepared by the sol-gel method.* Materials Research Bulletin, **2006**. 41: p. 354-358.

[106]. M. Smirnov et al., *Structural and optical characteristics of spin-coated ZnO thin film.* Applied Surface Science, **2010**. 256: p. 2405-2408.

[107]. H. Chin, L. Chao and K. Kao, *Study of structural and optical properties of ZnO thin films produced by sol-gel methods*. Sensors and Materials, **2016**. 28(5): p. 523-530

[108]. V. Prusakova, C. Armellini, A. Carpentiero, A. Chiappini, C. Collini, S. Dirè, M. Ferrari, L. Lorenzelli, M. Nardello, S. Normani, A. Vaccari, A. Chiasera, *Morphologic, structural, and optical characterization of sol-gel derived TiO_2 thin films for memristive devices*. Phys. Status Solidi, **2015**. C.12: p. 192-196.

[109]. S. M. M. Kasim, N. A. A. Shaari, R. A. Bakar, Z. Aznilinda, Z. Mohamad, S. H. Herman, *Influence of Different Sol-gel Spin Coating Speed on Memristive Behaviour of Pt/TiO_2/ZnO/ITO Device*. in 4th International Conference on Electronic Devices, Systems and Applications (ICEDSA). **2015.** Selangor**,** Malaysia**.**

[110]. N. A. A. Shaari, N.S. M. Sauki and S. H. Herman, *Effect of Annealing Time on Memristive Behavior of Sol-Gel Spin-coated ZnO-Based Memristive Device*. in AIP Conference Proceedings. **2016**. Kuala Lumpur, Malaysia.

[111]. N.A.A.Shaari, S.M.M. Kasim, N.S.M.Sauki, and S.H. Herman, *The Effect of the Sol-gel Spincoating Deposition Technique on the Memristive Behaviour of ZnO-based Memristive Device*. in IOP Conf. Series: Materials Science and Engineering. **2015**. Kuala Lumpur, Malaysia.

[112]. S. Kim, H. Moon, D. Gupta, S. Yoo, and Y. Choi, *Resistive Switching Characteristics of Sol-Gel Zinc Oxide Films for Flexible Memory Applications*. IEEE Transactions On Electron Devices, **2009**. 56(4): P. 696-699

[113]. Sh. Paul , Paul G. Harris , Ch. Pal , Ashwani K. Sharma and Asim K. Ray, *Low cost zinc oxide for memristors with high On-Off ratios*. Materials Letters, **2014**. 130: p. 40-42.

[114]. Y. Waseda, E. Matsubara, K. Shinoda, *X-Ray Diffraction Crystallography*, ch 4 Diffraction from Polycrystalline Samples and Determination of Crystal Structure, **2011**, Springer Heidelberg Dordrecht: London New York, p. 107-167.

[115]. E. G. Birgin, I. Chambouleyron and J. M. Martinez, *Estimation of the optical constants and the thickness of thin films using unconstrained optimization*. Journal of Computational Physics 151, **2006**. 862(1999): p. 1-28.

[116]. S. Fujihara, C. Sasaki, T. Kimura, *Crystallization behavior and origin of c-axis orientation in sol-gel-derived ZnO:Li thin films on glass substrates*. Appl. Surf. Sci., **2001**. 180(3-4): p. 341-350.

[117]. T. Ivanova, A. Harizanova, T. Koutzarova, B. Vertruyen, *Study of ZnO sol-gel films: effect of annealing*. Mater. Lett, **2010**. 64(10): p.1147-1149.

[118]. G. Socrates, *Infrared and Raman Characteristic Group Frequencies: Tables and Charts*, **2004**. John Wiley & Sons, Chichester.

[119]. L. Chua, *If it's pinched it's a memristor*, Semicond. Sci. Technol., **2014**. 29(104001): p. 1-42.

[120]. Y. Kang, T. Liu, T. Potnis, M. K. Orlowski, *Composite Cu/VO and VO/Cu Nanofilaments in Cu/Ta2O5/Pt Devices*. ECS Solid State Letters, **2013**. 2(7): p. 54-57.

[121]. L. L. Wei, J. Wang, Y. S. Chen, D. S. Shang, Z. G. Sun, B. G. Shen, J. R. Sun, *Pulse-induced alternation from bipolar resistive switching to unipolar resistive switching in the Ag/AgOx/Mg0.2Zn0.8O/Pt device*. J. Phys. D: Appl. Phys, **2012**. 45(42): p.1-5.

[122]. R. Waser, R. Dittmann, G. Staikov, K. Szot, *Redox-based resistive switching memories-nanoionic mechanisms, prospects, and challenges*. Adv. Mater, **2009**. 21(25-26): p. 2632-2663.

[123]. S.P. Heluani , G. Braunstein , M. Villafuerte, G. Simonelli and S. Duhalde, *Electrical conductivity mechanisms in zinc oxide thin films deposited by pulsed laser deposition using different growth environments*. Thin Solid Films, **2006**. 515(4): p. 2379-2386.

[124]. Shahzad S., Mohammad I. and Aftab A., *Sol-gel synthesis of intrinsic and aluminum-doped zinc oxide thin films as transparent conducting oxides for thin film solar cells*. Thin Solid Films, **2012**. 529(2013): p. 242-24.

[125]. P. Nunes, E. Fortunato, P. Tonello, F. B. Fernandes, P. Vilarinho and R. Martins, *Effect of different dopant elements on the properties of ZnO thin films. Vacuum*, **2002**. 64(3): p. 281-285.

[126]. Russo, M. Ghidelli, P. Gondoni, C. S. Casari, and A. Li Bassi, *Multi-wavelength Raman scattering of nanostructured Al-doped zinc oxide*. Journal Of Applied Physics, **2014**. 115(073508): p. 1-10.

[127]. Ben Yahia, L. Znaidi, A. Kanaev and J.P. Petitet, *Raman study of oriented ZnO thin films deposited by sol-gel method*. Spectrochimica Acta, **2008**. 71(4): p.1234-1238.

[128]. Sang-Hun J., Jae-keun K. and Byung-Teak L., *Effects of growth conditions on the emission properties of ZnO films prepared on Si (100) by rf magnetron sputtering*, J. Phys. D: Appl. Phys. **2016**. 36(2006): p. 2017-2020.

[129]. M. F. Cerqueira et al, *Raman study of insulating and conductive ZnO:(Al, Mn) thin films*, Phys. Status Solidi. **2015**, A212(10): p. 2345-2354.

[130]. Yanqiu H., Meidong L., Zhen L., Yike Z., Shaobo L., *Raman spectroscopy study of ZnO-based ceramic films fabricated by novel sol-gel process*. Materials Science and Engineering, **2003**. B97(2003): p. 111-116

[131]. Wu G.M, Chen Y. F and Lu H. C, *Aluminium-Doped Zinc Oxide Thin Films prepared by Sol-Gel and RF Magnetron Sputtering*, Acta Physica Polonica A, **2010**, 120, p. 149-152.

Scientific Production

Dawit G. Ayana, Valentina Prusakova, Cristian Collini, Marco V. Nardi, Roberta Tatti, Mauro Bortolotti, Leandro Lorenzelli, Andrea Chiappini, Alessandro Chiasera, Maurizio Ferrari, Lorenzo Lunelli, Sandra Dirè, *"Sol-gel synthesis and characterization of undoped and Al-doped ZnO thin films for memristive application*'', AIP Advances 6, 111306 (2016)

Dawit G. Ayana, Riccardo Ceccato, Cristian Collini, Leandro Lorenzelli, Valentina Prusakova , Sandra Dirè, "*Sol-gel derived oriented multilayer ZnO thin films with memristive response*, Thin Solid Films 615(2016) p: 427-436

Dawit G. Ayana, Valentina Prusakova, Riccardo Ceccato, Sandra Dire, "*Structural Characterization of Sol-Gel ZnO Thin Films on Different Substrates for Memristive Application*", 2015 XVIII AISEM Annual Conference, 2015 IEEE Xplore Digital Library

Participation to congresses, Schools and Workshops

Congresses

''Sol-Gel Synthesis and Characterization of Undoped and Al-doped ZnO Thin Films for Memristive Application'' **Oral presentation** on **E-MRS 2016 spring meeting**, May 2-6, 2016 Lille, France

"Sol-Gel Synthesis and Characterization of ZnO Thin Films for Memristive Application", **Oral presentation** on **ITFCP 15: 7th International Conference on Innovations in Thin Film processing and Characterization**, 16-20 November 2015, Nancy, France

"Structural Characterization of Sol-Gel ZnO Thin Films on Different Substrates for Memristive Application", **Poster presentation** at **XVIII AISEM 2015**, 3-5 February 2015, FBK-Trento-Italy

Schools and Workshops

Work shop nano, University of Trento, Trento (Italy), March 19 2014

MAUD2015: International School on “Materials Characterization by the Combined Analysis”, October 19-23, 2015 Trento-Italy

SHORT COURSES prior the 7th International Conference on Innovation in Thin Films Processing and Characterization, 16th November-2015, Nancy (France)

Engineering Trends and Business Opportunities for Smart Cities (ASSO2016-TN), Sept. 13-14,2016 Trento-Italy

State of the art and Challenges in Thermal and Mechanical Modeling of Ceramic Materials, March 20, 2015 Trento(Italy)

School on Scientific writing and reading, September 5-6, 2016 Trento-Italy

Acknowledgements

Foremost, I would like to express my sincerest gratitude to my supervisor Prof. Sandra Dirè for her continuous support and critical guidance during my PhD study. Her patience, endless motivation and priceless advice had helped me to make progress in my research career. Her encouragement and kind support throughout my PhD period was enormous.

I am deeply grateful to Prof. Gian Domenico Soraru for his guidance starting from my M.Sc. study and showing me this wonderful chance to develop my research career. It was a great pleasure to work and discuss with him.

I would like to extend my thanks to Dr. Valentina Prusakova for her guidance that enabled me to develop a better understanding of the subject and her continuous support in laboratory; Prof. Riccardo Ceccato for the training of XRD measurements and valuable discussions. I am thankful to Dr. Emanuela Callone, Dr. Marco Ischia, Livio Zottele; and all Professors and colleagues in the department for their help and kind support.

Prof. Luca Lutterotti and Dr. Mauro Bortolotti (University of Trento, Department of Industrial Engineering) are acknowledged for the acquisition of X-ray diffraction and for the helpful discussion. I would like to thank Dr. Mario Barozzi (CMM-MNF) and Mr. Lorenzo Moschini (BIOtech, University of Trento) for the acquisition of FE-SEM images.

This research work has been supported by Province of Trento in a framework of ''Grandi Progetti 2012 PAT'': Developing and Studying novel intelligent nano-Materials and Devices towards Adaptive Electronics and Neuroscience Applications-MaDEleNA project''. I am thankful to Dr. Salvatore Iannotta (IMEM-CNR), Dr. Maurizio Ferrari (CNR-IFN), Dr. Leandro Lorenzelli (FBK-CMM), Dr. Roberto Verucchi (IMEM-CNR) and Dr. Alessandro Chiasera (CNR-IFN) for making the collaboration in this framework very fruitful. Indeed, it was a pleasure for me to work and discuss with colleagues in the network. In particular, I would like to thank Dr. Andrea Chiappini (CNR-IFN), Dr. Marco V. Nardi (CNR-IMEM, DII), Dr. Cristian Collini (FBK-CMM) and Dr. Lorenzo Lunelli (FBK-LABSSAH) for their friendly and kind support in experimental works and data analyses. I

am very pleased to thank all of them individually, and highly acknowledge their effort for helping me in materials characterization.

My special thanks goes to my colleagues and best friends; and all the PhD fellows of the department of Industrial Engineering of University of Trento for the memorable time and valuable discussions.

Certainly, special thanks are going to the rest of the University of Trento (UNITN) community in particular and to the amazing Trentino people, in general.

I am deeply grateful and would like to acknowledge the support of my family who were always behind me and have been a source of support in many forms.

Finally and most important of all, I wish to thank with love, to my one and only beloved Kebene. She has been the reason for every single step in the past three years. Her love and continuous support was simply amazing.